

**EXPERIMENTAL STUDY OF PRESSURE FLUCTUATION IN PNEUMATIC
CONVEYING BY VARIOUS METHODS OF ANALYSIS**

by

Jae Bum Pahk

B.S. in Mechanics and design, Kookmin University, 1995

M.S. in Mechanical Engineering, University of Pittsburgh, 1998

M.S. in Mechanical Engineering, Carnegie Mellon University, 2002

Submitted to the Graduate Faculty of
the School of Engineering in partial fulfillment
of the requirements for the degree of
Doctor of Philosophy

University of Pittsburgh

2006

UNIVERSITY OF PITTSBURGH

SCHOOL OF ENGINEERING

This dissertation was presented

by

Jae Bum Pahk

It was defended on

October 4th, 2006

and approved by

Anne M. Robertson, Ph.D., Associate Professor,
Department of Mechanical Engineering and Materials Science

Ching-Chung Li, Ph.D., Professor, Department of Electrical and computer Engineering

Giovanni P. Galdi, Ph.D., Professor,
Department of Mechanical Engineering and Material Science

Dissertation Director: George E. Klinzing, Ph.D., Professor,
Department of Chemical and Petroleum Engineering

Copyright © by Jae Bum Pahk

2006

EXPERIMENTAL STUDY OF PRESSURE FLUCTUATION IN PNEUMATIC CONVEYING BY VARIOUS METHODS OF ANALYSIS

Jae Bum Pahk, Ph.D

University of Pittsburgh, 2006

Pneumatic transport of solids is widely used due to many of its advantages. Many studies have been carried out to explore the details of the transport of solids with pneumatic conveying with the aim to develop enhanced operations. The flow pattern seen in pneumatic conveying can vary widely depending on the gas velocity, the solid feed rate and the characteristics of the solid. In this study a deeper understanding of the interactions of the parameters has been explored using classical signal analysis of pressure fluctuations.

Experiments on dilute phase pneumatic transport were performed using polyester, polystyrene, and polyolefin pellets. Material properties such as mean diameter of polymer pellets and density of each polymer have been determined. The parameters of gas velocity and the solid loading ratio were varied producing the distinct pressure gradients which were measured at three different locations: vertical, lower and upper horizontal sections of the piping arrangement. Using these data, a phase space analysis, a power spectral density (PSD) analysis, a fractal dimension analysis, and a rescaled range analysis with Hurst's exponents were carried out to try to develop means to identify the flow conditions using simple pressure transducers. By taking a high speed video of the flow process through the transparent section in the pipe, the flow pattern was visually observed and unique dynamics were seen for the polyolefin particles. Furthermore, by using a wavelet analysis to decompose the original signal, noting the

contributions due to the blower and feeder, the flow - pressure fluctuation yielded information about details of the particle-gas interaction.

DESCRIPTORS

Bulk material

Hurst's exponent

Pneumatic conveying

Wavelet

Dilute phase

Phase space

Power spectrum

TABLE OF CONTENTS

ACKNOWLEDGEMENT	XIII
1.0 INTRODUCTION	1
1.1 PNEUMATIC CONVEYING, GENERAL	1
1.2 PHASE SPACE DIAGRAM ANALYSIS	3
1.3 POWER SPECTRAL DENSITY (PSD) METHOD	4
1.4 RESCALED RANGE ANALYSIS AND HURST'S COEFFICIENT	4
1.5 WAVELET ANALYSIS	5
2.0 EXPERIMENTAL SETUP	7
2.1 OVERALL SYSTEM DESCRIPTION	7
2.2 SYSTEM DEVICES	9
2.3 MEASURING DEVICES	10
2.4 CALIBRATION	11
2.4.1 Air velocity	11
2.4.2 Air temperature	14
2.4.3 Pressure transducer	15
2.4.4 Mass flow rate of solid	15
2.5 MATERIALS	16
2.5.1 Geldart's classification of materials	16

2.5.2	Materials used in this research.....	17
2.6	DATA ACQUISITION.....	19
3.0	ANALYSIS METHOD.....	22
3.1	PHASE SPACE DIAGRAM.....	22
3.2	POWER SPECTRAL DENSITY (PSD) ANALYSIS.....	24
3.3	RESCALED RANGE ANALYSIS.....	26
3.4	WAVELET ANALYSIS.....	27
3.5	FLOW PATTERN.....	31
3.6	FRACTAL DIMENSION	33
4.0	RESULTS AND DISCUSSION.....	36
4.1	PHASE SPACE DIAGRAM.....	36
4.1.1	Gas flow only	36
4.1.2	Effect of solid loading	41
4.2	POWER SPECTRAL DENSITY ANALYSIS.....	46
4.2.1	Gas flow only	46
4.2.2	Effect of solid loading	51
4.3	RESCALED RANGE ANALYSIS AND HURST'S EXPONENT.....	56
4.3.1	Gas flow only	57
4.3.2	Effect of solid loading	58
4.4	FRACTAL DIMENSION ANALYSIS	62
4.5	WAVELET ANALYSIS.....	66
4.6	HIGH SPEED VIDEO OBSERVATION.....	81
5.0	CONCLUSION.....	83

6.0 FUTURE WORK.....	85
BIBLIOGRAPHY	87

LIST OF TABLES

Table 1. Material properties of pellets	18
Table 2. Characteristic of decomposed signal for polyester and polystyrene.....	69
Table 3. Characteristic of decomposed signal for polyolefin	71

LIST OF FIGURES

Figure 1	Example of general state diagram	3
Figure 2	Schematic of pneumatic conveying system.....	8
Figure 3	Schematic of rotary feeder.....	10
Figure 4	Blower's rotational frequency Vs air velocity with different measuring instruments ..	14
Figure 5	Geldart's classification of materials	17
Figure 6	Materials used for this study (polyester, polystyrene, and polyolefin from left)	19
Figure 7	PSD graph for Blower's frequency = 100 Hz, gas flow only.....	21
Figure 8	Example of a phase space diagram.....	23
Figure 9	Typical plot of PSD.....	25
Figure 10	Example of the continuous wavelet transform of a signal $f(t)$, the horizontal axis denotes the position shift and the vertical axis denotes the scale	28
Figure 11	Daubechies 4 wavelet (left) and its scaling function (right).....	29
Figure 12	Decomposing procedure of the signal	30
Figure 13	Homogeneous flow.....	31
Figure 14	Dilute pulsating flow	31
Figure 15	Pulsating-Homogeneous flow	32
Figure 16	Homogeneous-Pulsating flow	32
Figure 17	Two phase homogeneous flow	33

Figure 18	An example of the component parts to determine the fractal dimension (M=2, N=4)	34
Figure 19	Phase space diagram at lower horizontal section (Gas Only), with different air velocity.....	38
Figure 20	Phase space diagram at upper horizontal section (Gas Only), with different air velocity.....	39
Figure 21	Phase space diagram at vertical section (Gas Only), with different air velocity.....	40
Figure 22	Phase space diagram for polyester with fixed mass flow rate of solid (0.14 kg/sec) and different blower frequency measured at lower horizontal section	43
Figure 23	Phase space diagram for polyester with different measuring locations, Blower frequency = 88 Hz (left) and 128 Hz(right), mass flow rate of solid = 0.14 kg/s.....	44
Figure 24	Phase space diagram for polyester with different solid loading ratios.....	45
Figure 25	Power spectral density graph at lower horizontal section (Gas Only), with different air velocity.....	48
Figure 26	Power spectral density graph at upper horizontal section (Gas Only), with different air velocity.....	49
Figure 27	Power spectral density graph at vertical section (Gas Only), with different air velocity.....	50
Figure 28	PSD graphs for different sections along the pipe with blower frequency = 100 Hz, air only (left graphs) and solid loading ratio, $\mu = 1.4$ (right graphs), polyester.....	52
Figure 29	Comparison of PSD graph of polyester (left) to polystyrene (right) for the differential pressure measured on the lower horizontal section.....	54
Figure 30	PSD graph of polyolefin for Blower = 56.7 Hz, $\mu = 2.3$ (Left),.....	55
Figure 31	Relationship between R/S, τ , and Hurst's exponent.....	56
Figure 32	Hurst's exponents for different measurement locations and different blower frequencies, gas flow only	57
Figure 33	Hurst Exponents for polyester (left) and polystyrene (right) with different solid loading ratio	60
Figure 34	Hurst Exponents for polyolefin with different solid loading ratio	61

Figure 35 Fractal Dimension for different materials and solid loading ratio measured in the vertical section	63
Figure 36 Fractal Dimension for different materials, and solid loading ratio measured in the lower horizontal section	64
Figure 37 Fractal Dimension for different materials, and solid loading ratio measured in the upper horizontal section	65
Figure 38 Decomposed signals, Polyester, blower = 88 Hz, $\mu = 6.0$, measured in the upper horizontal section	67
Figure 39 Standard deviation of wavelet coefficient of each decomposed signals,	72
Figure 40 Standard deviation of wavelet coefficient of each decomposed signals, polyester, upper horizontal section, blower = 72 Hz (top), 88 Hz (bottom)	73
Figure 41 Standard deviation of wavelet coefficient of each decomposed signals,	74
Figure 42 Standard deviation of wavelet coefficient of each decomposed signals,	75
Figure 43 Standard deviation of wavelet coefficient of each decomposed signals,	76
Figure 44 Standard deviation of wavelet coefficient of each decomposed signals,	77
Figure 45 Standard deviation of wavelet coefficient of each decomposed signals,	78
Figure 46 Standard deviation of wavelet coefficient of each decomposed signals,	79
Figure 47 Standard deviation of wavelet coefficient of each decomposed signals, polyolefin, vertical section, Blower = 57 Hz (top), 74 Hz (bottom)	80
Figure 48 Particle movement behavior, polyester	81
Figure 49 Particle movement behavior, polyolefin	82

ACKNOWLEDGEMENT

Many people supported me during the completion of this thesis with helpful criticism, assistance and references. First of all, I would like to express my deepest sense of gratitude to my advisor, Dr. George E. Klinzing for his patient guidance, encouragement and excellent advice throughout this study. My sincere thanks will also extend to other members of my committee, Dr. Anne M. Robertson, Dr. G. P. Galdi, and Dr. C. C. Li.

I am thankful to Dr. Mark C. Miller, Dr. S. C. Yao, Dr. Kenji Shimada, Dr. Chul Kim, and Dr. Hwa Taek Han who encouraged me constantly. Without their concern and love, I might not write this thesis.

I am also thankful to my colleagues Dr. Pruk Aggarangsi, Mitchell Rutkowski, Dr. Yosef Alyosef, Dr. Kyun Hee Koh and other Korean graduate students for sharing experiences and knowledge during the time of study.

Finally, I would like to express my deepest gratitude for the constant support, understanding and love that I received from my parents, Young Soo Pahk and Hoo Ja Sung, my uncles and aunts, and brothers and sister. I also would like to convey my special thanks to my fiancée, Min Jeong Lee. This work would not be possible without their love and encouragement

1.0 INTRODUCTION

Many experimental and analytical studies have been done to understand the flow characteristic of different particles in dilute phase pneumatic conveying system by applying different methods of analysis. In this chapter, the basic concept of pneumatic conveying, and the previous work that has been done for these analyzing methods will be reviewed. All theoretical descriptions of these methods will be discussed in chapter 3.

1.1 PNEUMATIC CONVEYING, GENERAL

The definition of pneumatic conveying is the transport of solid materials from one place to another using a transporting gas. The materials can be moved through the pipe with air, mainly used to transport these materials, but sometimes nitrogen is used for materials that could cause a chemical reaction with the air.

All powders and granular materials are conveyed⁽¹⁾ in this manner. The pneumatic conveying is widely used in the different industries such as the coal industry (transport of coal from mine to transportation vehicles and from vehicles to factories that utilize the coal), the food industries (transport wheat, rice etc.), the chemical industries (transport of plastic pellets), etc.

The advantages of pneumatic conveying are as follows:

1. Since materials are transported through the pipe, dust is not released in the atmosphere from the pneumatic conveying system.
2. Typical conveying belts cannot move materials vertically, but by pneumatic conveying, it is possible to move materials vertically by simply installing a vertical section of pipe with sufficiently high velocity of the gas to transport the solids.
3. By using pneumatic conveying, one can reduce the maintenance and manpower cost.
4. Pneumatic conveying enables us to transport materials that are poisonous and hazardous.

On the other hand, high power consumption, wear and abrasion of materials and equipment, and the limited conveying distance (1km maximum due to the economical purpose) are the disadvantages of the pneumatic conveying. Considerable research has been carried out to overcome these disadvantages.

One of the most important issues in pneumatic conveying is how to transport the materials with the lowest pressure drop and thus least amount of energy. The pressure drop behavior can be observed by preparing a state diagram. A state diagram is a plot of pressure difference versus the transport gas velocity at a fixed solid flow rate. Figure 1 is an example of a general state diagram.

In Figure 1, each curve shows how the pressure drop changes with the gas velocity at a fixed solid flow rate. Each curve shows a concave downward behavior. One notes that there is a minimum pressure drop that occurs for each solid flow rate, if the velocity becomes too low, saltation may take place often near the minimum pressure difference range. Care needs to be taken when operating in this minimum pressure range.

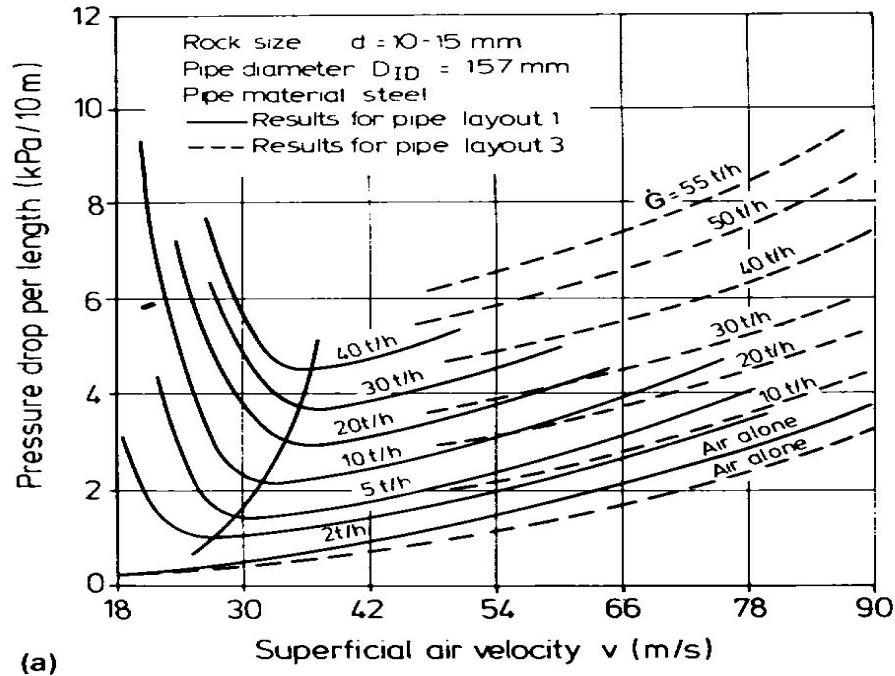


Figure 1 Example of general state diagram⁽²⁾

1.2 PHASE SPACE DIAGRAM ANALYSIS

Cabrejos⁽³⁾ utilized phase space diagram analysis in his Ph.D. dissertation. He measured absolute and differential pressures for dilute phase pneumatic conveying in horizontal pipe with different loading. The shape of the phase space diagram of gas flow only has low eccentricity, but it has higher eccentricity when solid particles are being transported. Also, he found that the velocity of the air contributes to the area of the plots. For higher air velocity, the range of the plot disperse more.

1.3 POWER SPECTRAL DENSITY (PSD) METHOD

The power spectral density method is an attractive method to characterize the flow pattern. Dhodapkar⁽⁴⁾ applied the PSD method to classify flow pattern with different solid loadings. He found that distinguishing PSD graph for the various flow regimes. He used a compressed air supply to supply the air into the system. The material used in his study was 450 μ m and 55 μ m glass beads, 400 μ m alumina, and PVC. In the present study, an air blower was used as an air supply and three different kinds of polymer pellets were transported with different solid loading. Dhodapkar also used a screw feeder while present study employed a rotary feeder. On the PSD figure in the later chapter, one can see the power peaks due to the blower and feeder's rotation. These frequencies should not be considered when one analyzes the pure signals due to the gas – particle interaction.

1.4 RESCALED RANGE ANALYSIS AND HURST'S COEFFICIENT

Rescaled range analysis was developed by Hurst⁽⁵⁾, an English hydrologist. He developed this analysis method to investigate the overflow behavior of the Nile River using an ancient overflow record for 847 years. By using this method with Hurst's exponent, one can predict the future trend of the data from the past time series of data. Nowadays, this method is widely used in various fields of studies such as economics, and medical sciences etc. The Hurst exponent calculated from rescaled range analysis is related to fractal dimension. It is the fractal dimension of the time series and formulated as follows.

$$D = 2 - H \quad (1)$$

Where D is the Fractal dimension calculated by the rescaled range and H is the Hurst's exponent. Fractal dimension is commonly used to investigate random behavior data especially for medical science such as physiology. For example, Vikram K Yeragani et. al.⁽⁶⁾ quantified the heart rate time series using fractal dimension.

The rescaled range analysis with Hurst exponent can be applied to pressure fluctuations in pneumatic conveying. Cabrejos et. al.⁽⁷⁾ measured absolute and differential wall pressure fluctuating signals. They applied rescaled range analysis to these signals and found that the difference between the maximum and minimum value of the Hurst's exponent increases when the gas-solid flow approaches saltation conditions and then tails off. They also found that for all the signals, there is a linear relationship between rescaled range (R/S) and time lag (τ). This will be discussed in detail in chapter 3.

Cabrejos adapted 400 Hz as a sampling frequency and collected 4096 data points for each case, while this study used 1000 Hz as a sampling frequency and 65536 data points have been obtained to increase the accuracy of the experiment. The sampling frequency of 1000 Hz is reasonable sampling frequency based on the Nyquist's sampling frequency theorem.

1.5 WAVELET ANALYSIS

Recently, wavelet analysis is utilized to analyze the time series transient signal analysis. For the field related to this study, the wavelet analysis is used to analyze the dynamic behavior such as pressure fluctuation, cluster size variation, bubble frequencies in fluidized beds, etc.

Ren et. al.⁽⁸⁾ used wavelet analysis for studying dynamic behavior of a fluidized bed. As a result of their research, wavelet analysis enables them to identify the transition moment from

dense phase to dilute phase by decomposing the signal into three scales of component: micro-scale (particle size), meso-scale (cluster size) and macro-scale (unit-size).

Lu et. al.⁽⁹⁾ measured and decomposed the pressure fluctuation signals in a bubbling fluidized bed using discrete wavelet analysis. After decomposing the signal, they found that at the scale 4 detailed signals could represent the behavior of bubbles in a fluidized bed such as the frequency of bubbling and the peak amplitude for the bubble size.

Many studies continue on fluidized bed analysis using wavelet analysis. There are very few researches currently performing in pneumatic conveying. This study applies wavelet analysis to the pneumatic conveying. First, using wavelet analysis, the signal will be decomposed into the few different frequencies of the signal. Then, the variance of each decomposed signal is determined and the relationship between the variance of decomposed signal and flow characteristic will be studied.

2.0 EXPERIMENTAL SETUP

2.1 OVERALL SYSTEM DESCRIPTION

The experimental system is located in a two story room. On the first floor, the lower section of system, is the blower, the lower hopper, the feeder and initial horizontal pipe. At the end of the horizontal pipe, a vertical pipe was connected to deliver the flow to the upper level. A T-bend was used to connect the horizontal and vertical pipes.

At the end of vertical pipe, an upper horizontal pipe was connected by T-bend. The upper horizontal pipe was located on the second floor and the upper hopper was located on the end of second horizontal pipe.

The entire length of pipe, from pipe entrance (right after blower exit) to pipe exit (right before the hopper entrance) is 27.4m. The length of horizontal first floor (from the location of solid particle entrance to tee band), vertical, and horizontal second floor of the pipe are 10.2m, 4.8m and 10.2m respectively.

Transparent sections of pipes were inserted on the middle of the lower and upper horizontal pipes so the movements of particles could be visually observed. Velocities of individual particles can be measured by using high speed camera on these sections, but this study it did not perform.

2.2 SYSTEM DEVICES

Blower: A rotary lobe blower from Dresser Roots Blower and Vacuum Pump Division, Compressor Industries Inc. was used to transport the air into the pipe. The motor used for this blower is US-Electronic Motor with maximum revolution per minute is 3470rpm.

Hopper: Immediately above the feeder, the lower hopper was located. The hopper contained pellets that were fed into the feeder by gravity. After the pellets were transported to the end of the pipe on the second floor, the pellets flow into the upper hopper (Collecting bin)

Valve: A slide gate valve was attached at the bottom of the upper hopper. The valve was closed when the mass flow rate of solid was measured, and the valve was opened when transporting the pellets from upper hopper to lower hopper.

Feeder: Rotary feeder from Young Industry Inc., 6 MODEL HC, was used to inject pellets into the pipe at a constant mass flow rate. The maximum revolution per minute of feeder was approximately 15.5 rpm.

Blower rotation frequency: Blower rotation frequency was measured and will be used in the power spectral density (PSD) analysis (This will be discussed later). A strobotac type 1531-A from General Radio Company was used to measure the blower's rotational speed (RPM). The blower rotational frequency is determined by dividing this rotational speed by 15 since there are four strokes of air pumped into the pipe for every single rotation of the blower motor.

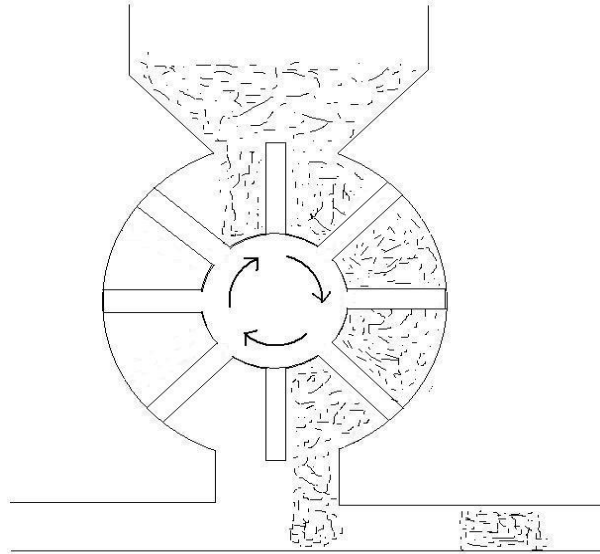


Figure 3 Schematic of rotary feeder

2.3 MEASURING DEVICES

Air velocity: A hot wire anemometer with air velocity transducer, TSI 8455-12 from TSI Inc., was inserted 0.95m after the blower exit to measure the air velocity sending an electronic signal to the data acquisition card.

Air temperature: A J-type(Iron-Constantan) thermocouple from Omega Inc. was inserted after 0.08m of hot wire anemometer. With a digital thermometer, 2168A from Omega Inc., the air temperature was measured. The air temperature will be used to calculate the actual air velocity.

Pressure transducer: There were two pressure taps each on vertical, lower and upper horizontal pipe and these pressure taps were connected to the pressure transducer to measure the pressure drop between two pressure taps. Differential pressure transducers, 162PC01D from Omega Engineering Inc., were used and each transducer is connected to data acquisition card.

Mass flow rate of solid: Three load cells, U35B from BLH electronics Ltd., with the capacity of 1000 lb each were attached on the upper hopper to determine the mass flow rate of pellets.

Data acquisition card and software: A hot wire anemometer, pressure transducers, and load cells were connected to the data acquisition card, SCB-68 from National Instruments (NI). The SCB-68 collected the electrical signals from each measuring devices and using LABVIEW software from National Instruments (NI) and a Pentium III computer, these signals were transformed to data for the experiments.

2.4 CALIBRATION

Before each experiment was carried out, calibration for each device should be performed. The following section describes how individual devices were calibrated. Calibration showed $\pm 5\%$ reproducibility for each device.

2.4.1 Air velocity

The velocity of the air obtained from the hot wire anemometer is reported in standard meter per second (SMS) and standard air conditions are 15 °C, 101.3 kPa, 1.23 kg/m³ for

temperature, atmospheric pressure, and density of air respectively, but the actual experimental condition is different from standard condition. Air temperature may be higher than 15 °C and also the atmospheric pressure and density of the air will be higher or lower than standard condition. The velocity of the air in the actual condition is a function of these parameters. So, after air velocity of stand atmospheric condition was obtained, the actual air velocity has to be determined. One can determine the actual velocity⁽¹⁰⁾ of the air using the formula

$$ACFM = \frac{SCFM \times P_{std}}{(P_1 - P_{sat1}) \times \phi_1} \times \frac{T_1}{T_{std}} \quad (2)$$

where, ACFM: Actual volumetric flow rate

SCFM: Standard volumetric flow rate

P_{std} : Pressure at standard condition

P_1 : Actual pressure

P_{sat1} : Saturation pressure at actual condition

T_1 : Actual temperature

T_{std} : Standard temperature

Φ_1 : Relative humidity

The velocity measured had a range of values from 3 to 20 m/s. At these conditions the flow can be considered as incompressible and for incompressible flow, the volumetric flow rate, Q, is given as:

$$Q = \bar{V}A \quad (3)$$

where \bar{V} : Average velocity of fluid

A: Cross sectional area of pipe

Since the area A is constant, this expression can be used to determine the actual air velocity as follows

$$V_{actual} = \frac{V_{Std} \times P_{std}}{(P_1 - P_{sat1}) \times \phi_1} \times \frac{T_1}{T_{std}} \quad (4)$$

Also, by neglecting the humidity term, this equation is simplified to

$$V_{actual} = V_{std} \times \frac{T_1}{T_{std}} \quad (5)$$

To calibrate the hot wire anemometer, a Pitot tube has been used. The static pressure and stagnation pressure were measured from the Pitot tube with a pressure transducer and the air temperature is measured by thermocouple. To determine the velocity of air from these data, first, define the relationship between static, stagnation and dynamic pressure as follows⁽¹¹⁾;

$$P_{Stagnation} = P_{Static} + P_{Dynamic} \quad (6)$$

Also the dynamic pressure is defined as follow

$$P_{Dynamic} = \frac{1}{2} \rho V^2 \quad (7)$$

Where ρ : air density

V : air velocity

Using the measured temperature, static pressure, stagnation pressure, and the density of the air, the actual velocity of the air from the hot wire anemometer with air velocity transducer, and Pitot tube can be determined by equation (5) and (7). The following figure shows the relationship between air velocity and blower rotation.

Both the Pitot tube and the hot wire anemometer have a linear relationship with the blower's rotational frequency. After linear fitting for these plots has been done, the value of the velocity from hotwire anemometer is reliable to within 5%.

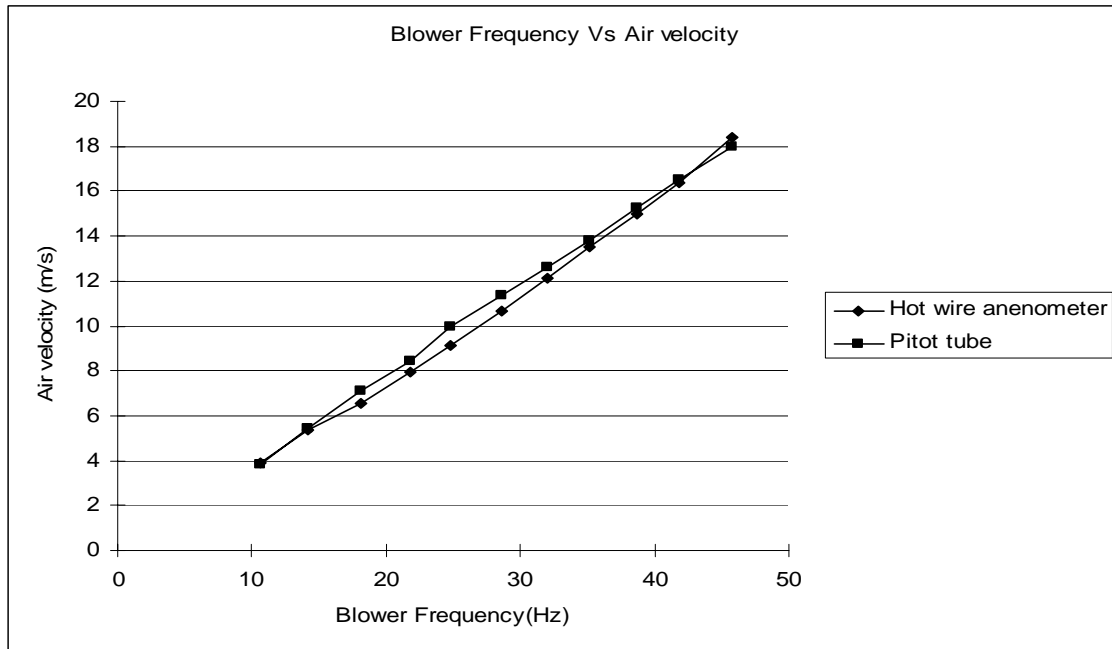


Figure 4 Blower's rotational frequency Vs air velocity with different measuring instruments

2.4.2 Air temperature

A J-type thermocouple (Iron-Constantan) with digital thermometer was employed in this study. For calibration, ice water (with the temperature of 0 °C) and water with room temperature was used as a reference temperature. Besides a thermocouple, a mercury thermometer was used to measure these temperatures and compare the values from the thermocouple for calibration.

2.4.3 Pressure transducer

Three pressure transducers were used in this study. Two of them were brand new and were calibrated from the manufacturer. To calibrate the third transducer, the differential pressure was measured at the same velocity of the air for several times and then averaged. This transducer was then replaced with a factory calibrated pressure transducer which measured the differential pressure again with the same condition, and the output signal difference between transducers was reproducible to $\pm 5\%$.

Note that the distance between pressure taps are 0.99 m, 2.49 m, and 3.15 m for the vertical, the lower horizontal and upper horizontal respectively. The distance between pressure taps were different, but according to Dhodapkar, et. al.⁽⁴⁾ the spacing between pressure taps didn't influence the spectra generated from pressure fluctuation signal.

2.4.4 Mass flow rate of solid

Three load cells attached on the upper hopper were used to measure the weight of the particles. The load cells were located at a fixed radius from the center of the hopper with a spacing of 120° between them. The method for measuring the mass flow rate of solids is as follows. First, run the machine and wait for steady state. After steady state is achieved, collect the weight data for more than one minute. Then plot time versus weight, do linear fitting and find the linear relationship (equation) between weight and time. The slope of this relationship will be the mass flow rate of solid.

For calibration purposes, the particles were collected in a container for 180 seconds the container's weight was measured with a scale. The mass flow rate for solid can then be

determined by dividing weight by 180 sec. Also, 3 iron weights were placed on the upper hopper to measure their weight with the load cells and the result obtained gave less than 2% of error.

2.5 MATERIALS

2.5.1 Geldart's classification of materials

In pneumatic conveying, many different kinds of materials can be transported. The properties of these materials are different from one to another but the materials can be classified in a few groups. Geldart⁽¹²⁾ found that materials can be classified by four characterized groups (called Geldart A, B, C, and D) by the size and density difference between particle and gas. Each material group has its own characteristic property⁽¹³⁾ as follows:

Group A : Powders, ideal for fluidization, the non-bubbling fluidization occurs at the minimum fluidization gas velocity and bubbling occurs as fluidization gas velocity increases.

Group B : Start bubbling at minimum fluidization velocity.

Group C : Very fine and cohesive material, very hard to be fluidized.

Group D : Coarse solids

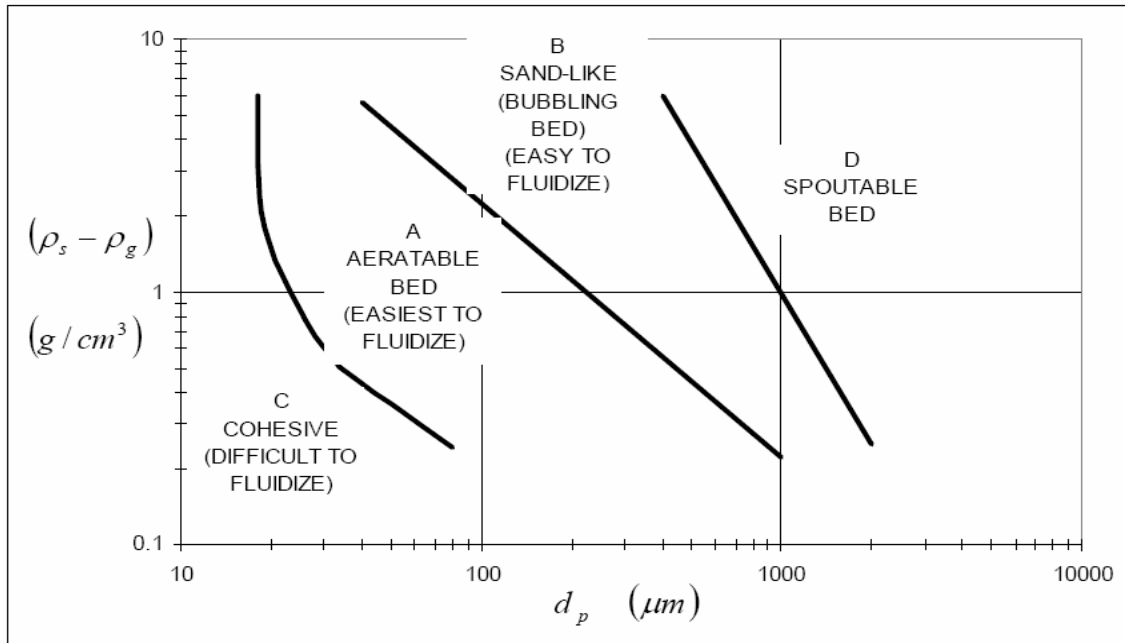


Figure 5 Geldart's classification of materials⁽¹⁴⁾

2.5.2 Materials used in this research

Polyester, polystyrene and polyolefin pellets from Dow Chemical LTD. were used for this experiment. All materials are Geldart's D type materials. Polyester is a green, rectangular parallelepiped shaped particle. Polystyrene is cylindroids shape and the color is white, and transparent. Both polyester and polystyrene are hard materials and they are easy to break while transported. Polyolefin is comparatively soft and it sticks together if it is not in motion for a while. The shape of this particle is elliptical and it has white and semi transparent color.

The density of polyester and polystyrene was obtained from Luis Sanchez⁽¹⁵⁾. The density of Polyolefin was measured as follows. Put pellets into the cylinder with the volume of 500 ml and measure its mass. Put water into the cylinder until water reaches 500 ml scale, so the gap between particles will be filled with water. Collect the water in the cylinder with another cylinder and measure its mass. The actual volume of pellets will be calculated by subtracting the volume of water from the total (Pellets and water) volume. Then the density of the pellets can be determined from the mass of pellets divide by the volume of the pellets.

The size of the particles was obtained as follows. First, take a picture of particles using digital camera and saved a picture image on the personal computer. Then by using Scion Image software the picture image was analyzed and the mean size of particles was determined. The following table shows the material properties of polyester, polystyrene, and polyolefin.

Table 1. Material properties of pellets

	Polyester	Polystyrene	Polyolefin
Particle shape	Cube	Cylinder	Elliptic
Mean particle size (mm)	3.3	3.9	4.6
Particle density (kg/m ³)	1400	1045	870-940
Bulk density (kg/m ³)	892	735	N/A



Figure 6 Materials used for this study (polyester, polystyrene, and polyolefin from left)

2.6 DATA ACQUISITION

The hot wire anemometer, the pressure transducers, and the load cells were connected to the SCB-68 data acquisition card. As mentioned before, this card was connected to the computer and by using LABVIEW software the electronic signals from each device were converted to the air velocity, differential pressures, and the weight of upper hopper respectively.

When acquiring data, choose the “optimized” sampling frequency, the number of data points to be acquired is very important. By increasing the number of data points, the time to collect and analyze the data and the amount of data storage space will also increase. To decrease the sampling frequency and the number of data points, one will less accurately obtain the true signal.

The optimized (minimum) sampling frequency required is given by Nyquist’s sampling frequency theorem⁽¹⁶⁾, which states that the maximum frequency capable in the spectrum is equal

to half of the sampling frequency if aliasing is to be avoided. In this study a 1000 Hz of sampling frequency is more than enough for the analysis based on the Nyquist's sampling frequency theorem. Figure 7 is an example of the power spectral density (PSD) graph to determine the sampling frequency. The power spectral density method will be discussed in detail later.

As one can see, after 300 Hz the signal was negligible except for a few sudden peaks. By neglecting these peaks, since they represent the blower components of the signal, the minimum sampling frequency in terms of the Nyquist's criterion would be $300 * 2 = 600$ Hz. Thus a sampling frequency of 1000 Hz was sufficiently high for the experiments performed.

The number of data points acquired in this experiment was 65536, which is 2^{16} . There are 2 reasons to choose the number of data points as 2^n . The first reason was due to the PSD analysis. The number of data as 2^n converges faster than the other data sets. The second reason was because there is a need for 2^n data points for rescaled data analysis. This will be discussed in a later chapter.

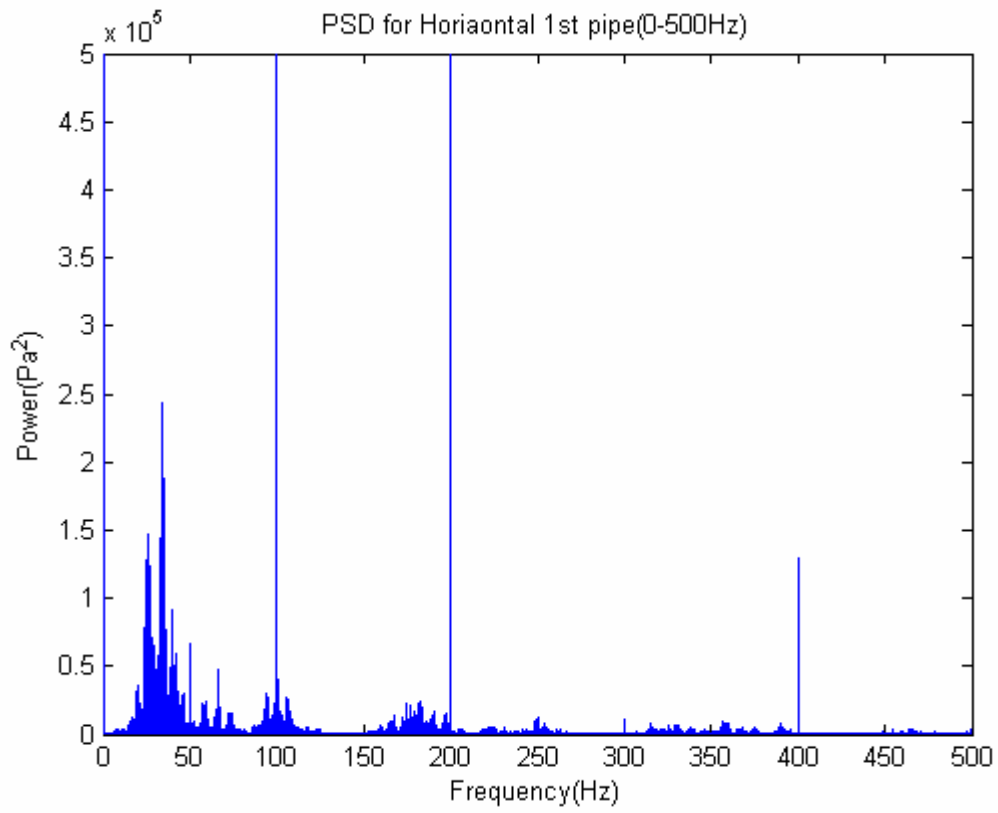


Figure 7 PSD graph for Blower's frequency = 100 Hz, gas flow only

3.0 ANALYSIS METHOD

3.1 PHASE SPACE DIAGRAM

Phase space is defined as the space where all possible states of a system are represented, with each possible state of the system corresponding to one unique point in the phase space⁽¹⁷⁾. In a mechanical system, phase space consists of position and momentum variables as a function of time and it is often called as a phase diagram. Phase space diagrams represent the explanation of the differences with the other diagrams. One can see the differences clearly for different system setups with these diagrams. Example of a phase space diagram is shown in Figure 8.

In this study, the phase space diagram is represented in two different ways. The first way is plot the normalized value of pressure drop per unit length at a certain time t versus the normalized value of pressure drop per unit length at $t+dt$, where dt represents the time step between the collection of two data points.

The normalized pressure drop per unit length was determined from the raw data as follows. First, the pressure difference between two pressure taps was divided by the distance between the two pressure taps. The distance between two pressure taps was 0.99 m, 2.49 m, and 3.15 m for vertical pipe, the lower section of horizontal pipe, and the upper section of horizontal pipe respectively. After that, the mean (average) value of pressure drop per unit length was determined (divide the sum of the pressure differences per unit length by number of data, 65536

in this study). Finally, the normalized pressure drop per unit length was determined by subtracting the mean value of pressure difference per unit length from each pressure difference per unit length. Since the sampling frequency in this study was 1000 Hz, the value of dt is equal to 0.001 sec.

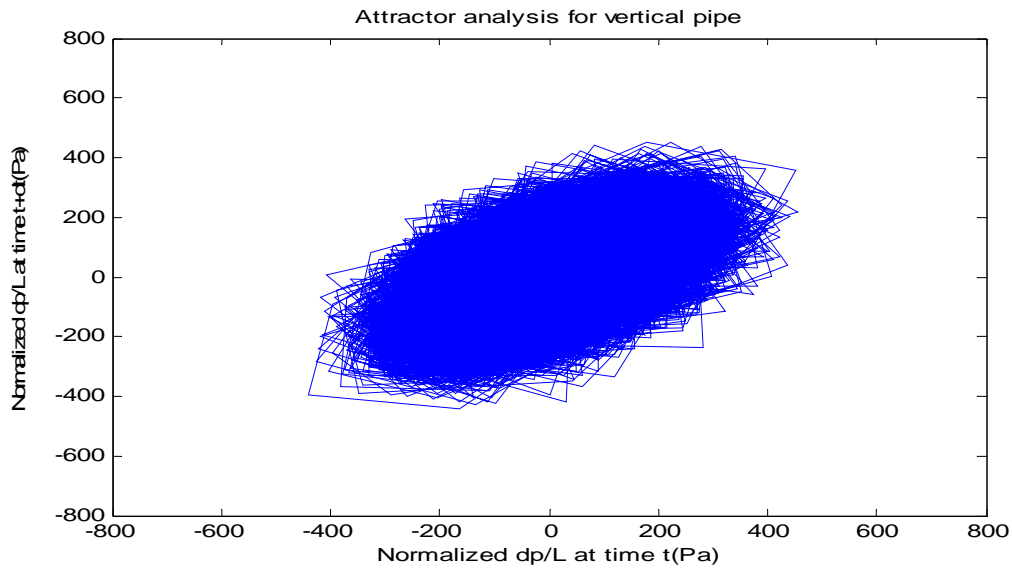


Figure 8 Example of a phase space diagram

Another way to plot the phase space diagram is to plot the normalized pressure at time t and its time derivative (dp/dt) at the same time. dp/dt is defined as follows.

$$\frac{dp}{dt} = \frac{P(t + \Delta t) - P(t)}{\Delta t} \quad (8)$$

Where $P(t)$ is a normalized pressure at time t , $P(t+\Delta t)$ is a normalized pressure at time $t+\Delta t$, and Δt is time to collect one datum to another (since our sampling frequency is 1 kHz, Δt will be 0.001 sec).

3.2 POWER SPECTRAL DENSITY (PSD) ANALYSIS

The PSD describes how the power (or variance) of a time series is distributed with frequency.⁽¹⁸⁾ This method was used to determine the dominant characteristic frequency (the frequency where the maximum power occurs) of flows with different velocity of the air and feed rate for the materials.

The Fourier Transform of a continuous time dependent function⁽¹⁹⁾ is defined as

$$X(f) \equiv \int_{-\infty}^{\infty} x(t)e^{-2\pi ift} dt \quad (9)$$

where $x(t)$ is a time dependent function, for this study, pressure fluctuation with time, f is an arbitrary frequency between two sided domain, $(-\infty, \infty)$.

The Discrete Fourier Transform (DFT) is defined as

$$X(n) = \sum_{k=0}^{N-1} x(k)e^{-ik2\pi n/N} \quad \text{for } n=0, 1, \dots, N-1 \quad (10)$$

In this study, $x(k)$ is pressure at time t . The disadvantage of DFT is there are a lot of redundant calculations while $X(n)$ is being calculated. The Fast Fourier Transform allows reducing the number of calculations from $2N^2$ to $2N\log N$ and that is defined as follows

$$X(n) = \sum_{k=0}^{N-1} x(k)e^{-\frac{2\pi i}{N}nk} \quad \text{for } n=0, 1, \dots, N-1 \quad (11)$$

PSD function is the magnitude of the FFT square divided by the time period. Also, in this study, one side PSD was used (its unit is Pa^2/Hz) and defined as follows

$$PSD(f) \equiv \frac{2|X(n)|^2}{t_2 - t_1} \quad (12)$$

The following figure is an example of a PSD plot.

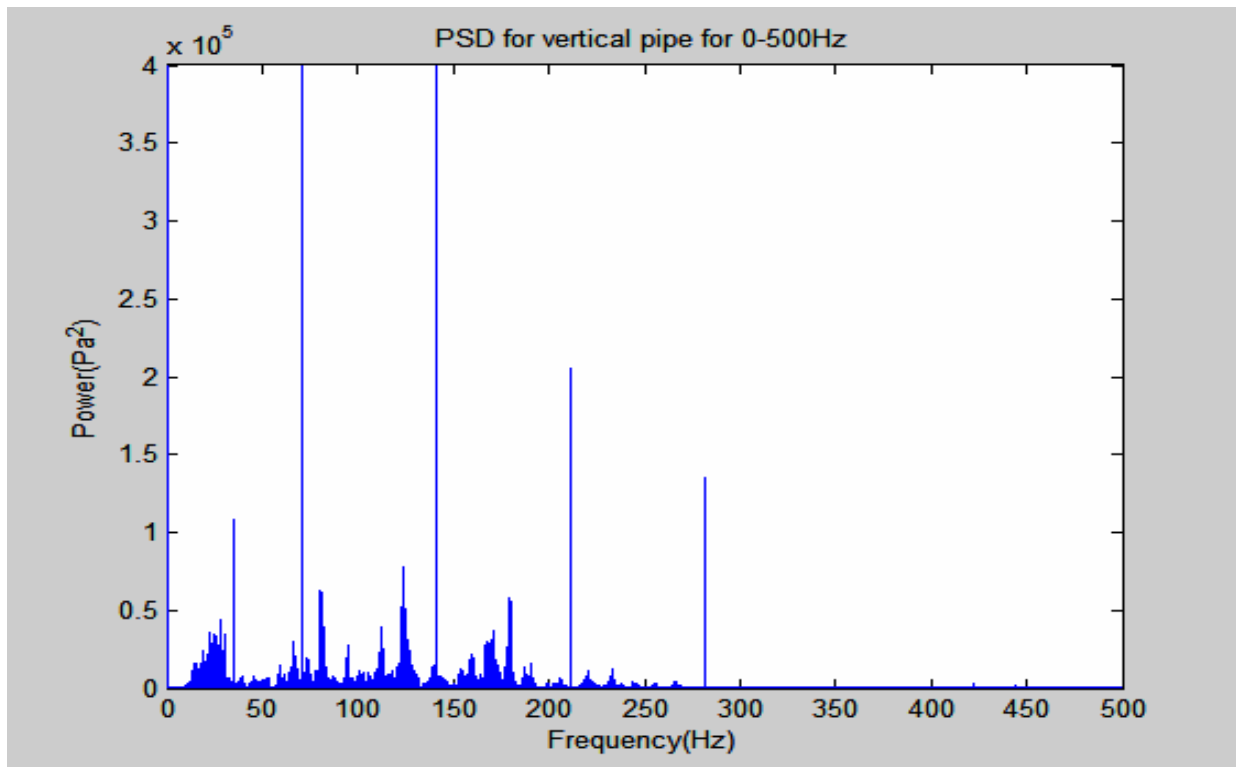


Figure 9 Typical plot of PSD

From the figure above, the dominant frequency of a certain case can easily be determined.

3.3 RESCALED RANGE ANALYSIS

Rescaled range analysis was developed by Hurst in 1965. This method is a statistical method to analyze long term records of natural phenomena such as weather changes, in and out flow from a reservoir, price change of stocks, etc.

The value of R (Rescaled range) and S (Standard deviation) are defined as follows;

$$R(\tau) = \max_{1 \leq t \leq \tau} X(t, \tau) - \min_{1 \leq t \leq \tau} X(t, \tau) \quad (13)$$

$$S = \left(\frac{1}{\tau} \sum_{t=1}^{\tau} \{ \xi(t) - \langle \xi \rangle_{\tau} \}^2 \right)^{\frac{1}{2}} \quad (14)$$

Where $\xi(t)$ is a sum of individual influx at a given time, and $\langle \xi \rangle_{\tau}$ is an average of influx at a time period

$$\langle \xi \rangle_{\tau} = \frac{1}{\tau} \sum_{t=1}^{\tau} \xi(t) \quad (15)$$

$X(t, \tau)$ is the sum of $\xi(t) - \langle \xi \rangle_{\tau}$

$$X(t, \tau) = \sum_{u=1}^t \{ \xi(u) - \langle \xi \rangle_{\tau} \} \quad (16)$$

Finally R/S is defined as,

$$\frac{R}{S} = (\alpha \tau)^H \quad (17)$$

The coefficient, α was chosen to be 0.5 by Hurst⁽²⁰⁾ and H is called ‘‘Hurst exponent’’. The Hurst exponent has a range of $0 < H < 1$. If $H > 0.5$ then it is called ‘‘persistence’’ meaning that

the trend (increasing or decreasing for certain data) in the past will be the same in the future (keep increase or decrease respectively). On the other hand, $H < 0.5$ is called “anti-persistence” meaning that trend in the past (increase or decrease) will be reversed (decrease or increase respectively) in the future. For the case of H equal to 0.5, the trend or behavior for the past record is random, so prediction of the future trend can not be estimated. Using MATLAB code (.m file) provided by Leontitsis,⁽²¹⁾ the Hurst exponent was determined.

3.4 WAVELET ANALYSIS

A wavelet is defined as follows,⁽²²⁾ a wavelet is a small wave which has its energy concentrated in time to give a tool for the analysis of transient state. The continuous wavelet transform (CWT) of a function $f(t)$ is defined as follows

$$C(a,b) = \int_{-\infty}^{\infty} f(t)\psi\left(\frac{t-b}{a}\right)dt \quad (18)$$

where C : wavelet transform at scale a and position shift b

ψ : wavelet function

a : scale of time

b : position

The wavelet transform, $C(a,b)$ represents how closely correlated the original signal, $f(t)$ is to the wavelet, $\psi = \frac{(t-b)}{a}$. The higher value of C means more similarity between the chosen wavelet and the original signal. The time scale of the wavelet means expansion or compression of the mother wavelet (originally chosen). A position constant means the amount of shifting of

the wavelet from its original position. For a discrete time signal $\{f(k)\}$, the discrete wavelet transform (DWT) gives wavelet coefficient $\{d(m,n)\}$ where $a=2^m$, $b=n2^m$.

MATLAB software with the wavelet toolbox is used for wavelet analysis. The following figure shows an example of continuous wavelet analysis with MATLAB. The horizontal axis represents the time, and the vertical axis represents the time scale of a chosen wavelet. A number of mother wavelets have been constructed. Among them, Daubechies4 wavelet was chosen to analyze signals in this study. The intensity of the graph represents the magnitude of wavelet coefficients. The higher value of the wavelet coefficient, the brighter the plot is.

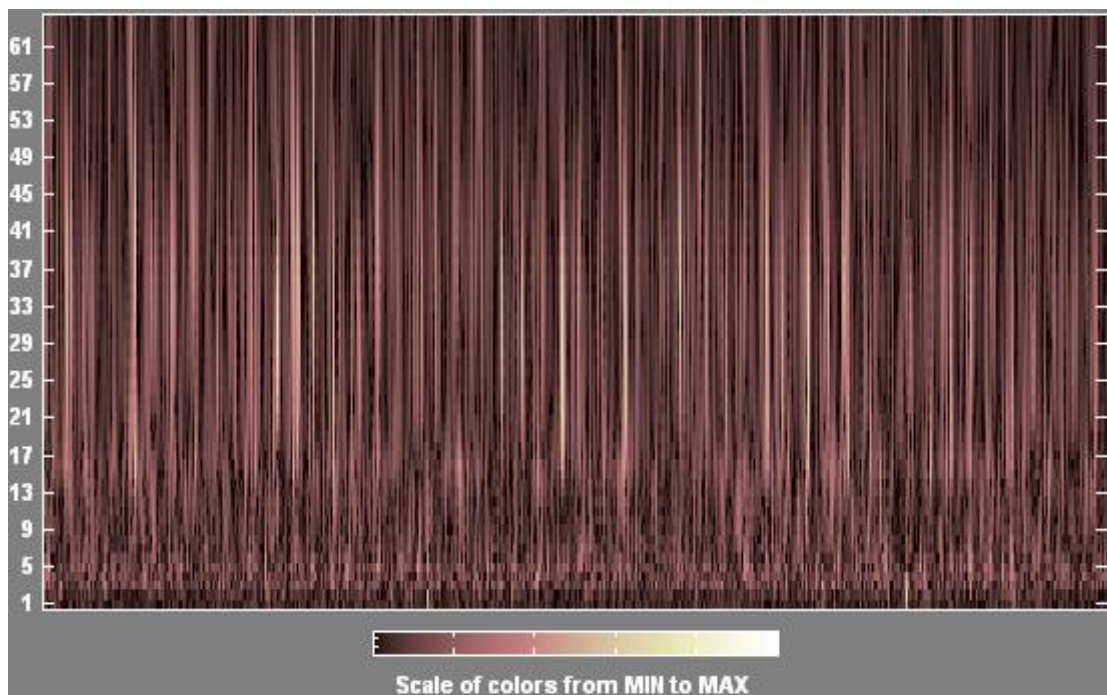


Figure 10 Example of the continuous wavelet transform of a signal $f(t)$, the horizontal axis denotes the position shift and the vertical axis denotes the scale

The wavelet transform can be used for de-noising of signals, identifying pure signals, and detecting self similarities, etc. For this study, the discrete wavelet transform is used to decompose signals, and to determine the pure signals for different system setups without the effect of blower and feeder.

Figure 11 shows the Daubechies4 wavelet $\psi(t)$ and its corresponding scale function $\phi(t)$.

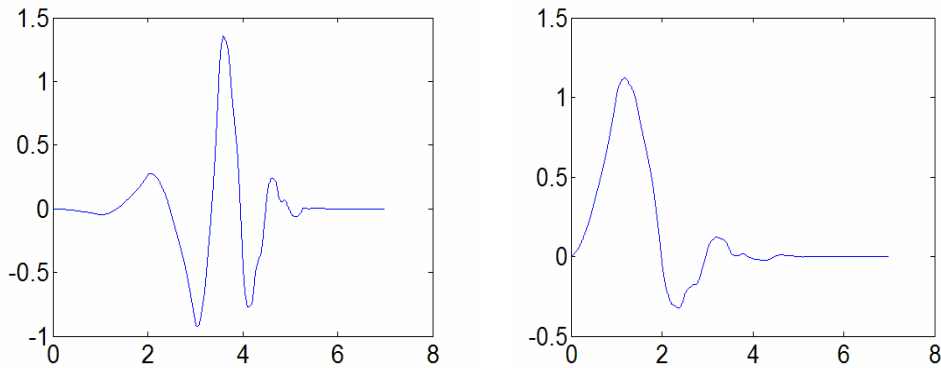


Figure 11 Daubechies 4 wavelet (left) and its scaling function (right)

To decompose the signal, a high pass filter and low pass filter are used. The signal component that passed through the high pass filter is called “details”, and the signal component that passed through the low pass filter is called “approximations”. Thus the “details” signal contains high frequency components while the “approximations” signal has low frequency components. When the signal has been decomposed once, the “approximations” can be decomposed again and it breaks into another “details” and “approximations” set at a lower scale

level, and this can be repeated again to further lower scales as desired. Figure 12 illustrate the principle of decomposing signals.

From Figure 12, $x[n]$ is the original input signal and this signal passes through the high and low pass filters and is then decomposed to details, “ d_n ”, and approximations, “ a_n ”. Then the signal is down sampled with a factor of two, so the number of samples in each signal component reduces to 1/2. The approximation is decomposed again, generating a new (level two) approximation and details and so on. In this study, signals were decomposed for five levels, so as a result, five levels of detailed wavelet coefficients and the approximation scaling coefficients at level five were obtained for each system configuration.

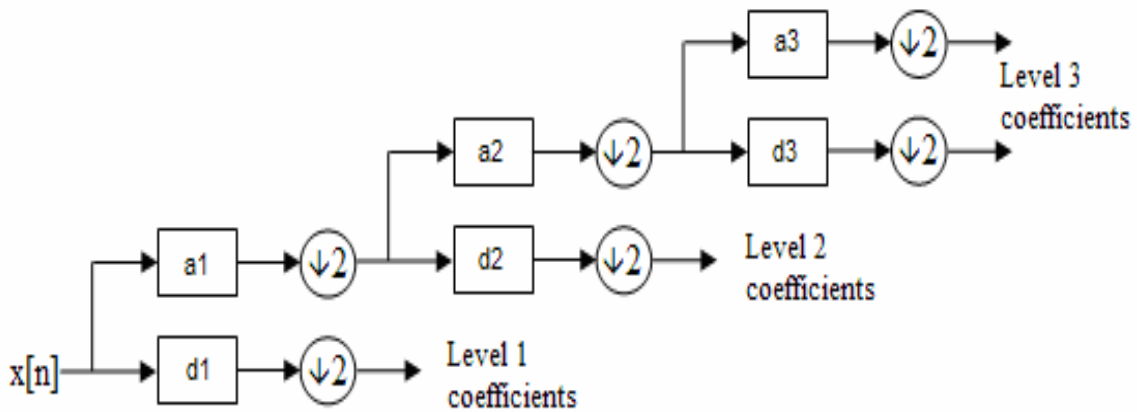


Figure 12 Decomposing procedure of the signal⁽²³⁾

3.5 FLOW PATTERN

This study deals only with the dilute phase, and four different flow patterns were defined by taking video through the transparent section of the pipe.

Homogeneous flow : particles in the pipe are evenly distributed along the cross section of pipe

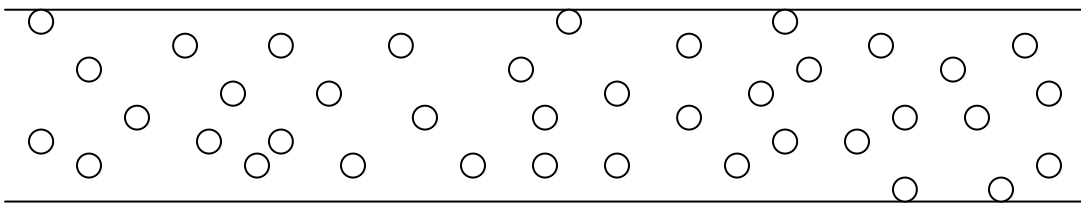


Figure 13 Homogeneous flow

Dilute Pulsating flow : appears to similar to pulsating flow in dense phase flow, but unlike pulsating flow, the gap between particles was observed in the pulse of the particle flow.

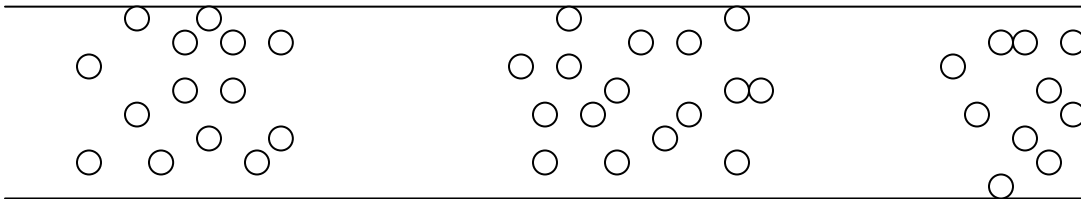


Figure 14 Dilute pulsating flow

Pulsating-Homogeneous flow : pulses were observed dominantly, but flow remains homogeneous between pulses.

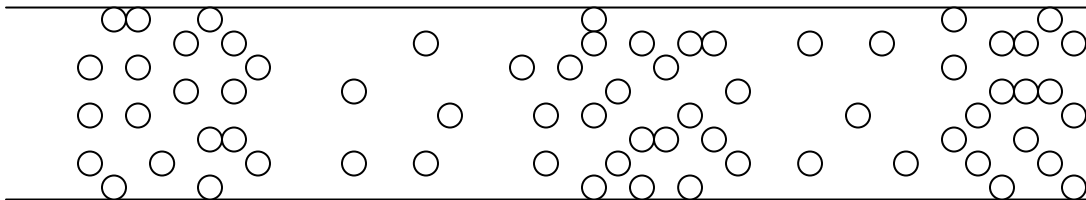


Figure 15 Pulsating-Homogeneous flow

Homogeneous-Pulsating flow : Homogeneous flow was observed dominantly, but small pulses were also observed in the flow.

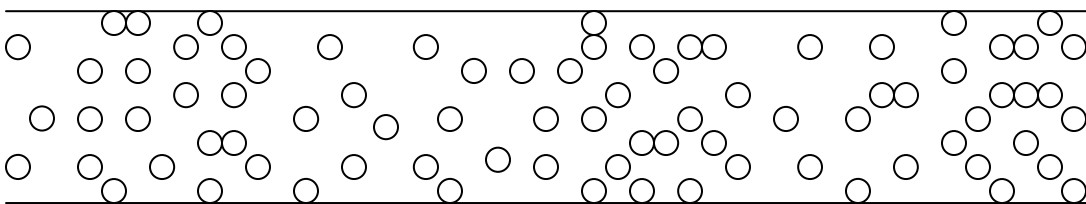


Figure 16 Homogeneous-Pulsating flow

Two phase homogeneous flow : A heavier concentration of particles was seen moving in layers located on the bottom of the pipe, but above this layer, flow remains homogeneous.

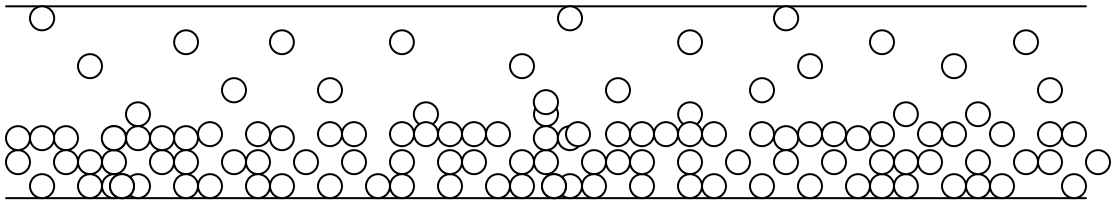


Figure 17 Two phase homogeneous flow

In the Homogeneous-Pulsating flow and Pulsating-Homogeneous flow, one can clearly see the differences by observing the flow pattern video file in the attached DVD-rom. Also, these flow patterns occur when the flow pattern changes from pulsating to homogeneous in either direction except for two phase homogeneous flow.

3.6 FRACTAL DIMENSION

A dimension is defined as the number of degrees of freedom that describes the motion of an object. So, a point has a zero dimension since it can not move. A line has one dimension because an object can move on that line only in one direction. A plane has two dimensions because an object that moves on the plane with two degrees of freedom. These dimensions have integer number, but fractal dimension can have non - integral values.

There are several different methods to determine the fractal dimension. As mentioned before, the Hurst's exponent is one way to determine fractal dimension (the Hurst exponent is

sometimes defined as the fractal dimension of a time series). In this study, a box counting method has been adapted to determine the fractal dimension. For this case, the fractal dimension is defined as follows⁽²⁵⁾;

$$Fd = \frac{\log(N)}{\log(M)} \quad (19)$$

where Fd is Fractal dimension, N is the number of self-similar boxes (component parts), and M is the magnification factor.

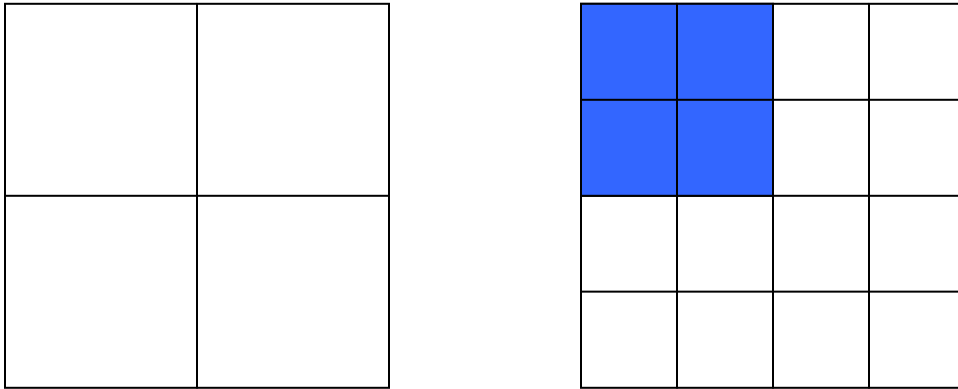


Figure 18 An example of the component parts to determine the fractal dimension (M=2, N=4)

To explain how to determine the fractal dimension clearly, consider the two geometries shown above. The left rectangle is divided into four small rectangles and the right one is divided into sixteen small rectangles. Starting with the biggest rectangle, when the length of each edge divided into two, one can make four small rectangles that can cover the entire geometry (biggest rectangle). Again, when one of the four small rectangle's edge is divide by a factor of two, one

produces another four small rectangles in that geometry (small rectangle of the upper left hand side geometry). In this case, the magnitude factor, M , is equal to 2 since the edge of the small geometry is divided into two. Also, the number of self similar components that cover one small geometry is four. Thus the fractal dimension of this geometry would be

$$Fd = \frac{\text{Log}(N)}{\text{Log}(M)} = \frac{\text{Log}4}{\text{Log}2} = 2 \quad (20)$$

4.0 RESULTS AND DISCUSSION

The experimental results and analysis of these results by phase space diagram, power spectral density analysis, and rescaled range analysis will be discussed in this chapter.

4.1 PHASE SPACE DIAGRAM

The phase space diagrams of the normalized differential pressure fluctuations obtained are presented showing that the shape of these diagrams is affected by the air velocity, solid loading ratio, material property, and the location of the pressure measurement.

The horizontal length of phase space diagram shows the difference between maximum and minimum differential pressure. The longer the horizontal length of the phase space diagram is, the larger the difference of the differential pressure is expected to be. Also, the vertical length of phase space diagram represents how fast the differential pressure changes from one time to next measuring time.

4.1.1 Gas flow only

The “gas flow only” means that gas is the only material that flows along the pipe. Since no pellets were transported, the solid loading ratio will be equal to zero. For this case, the

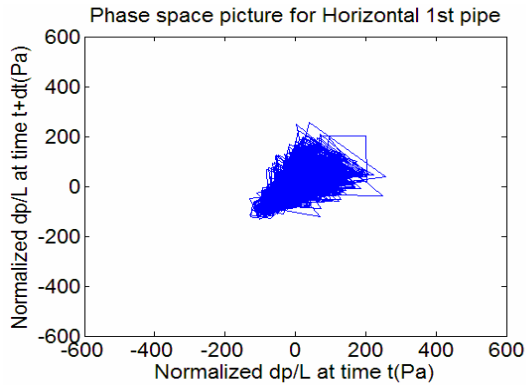
velocity of the air and the location of the pressure measurements are the major factors that contribute to the shape of the phase space diagram. Note that for gas flows only, the phase space has only one attractor point.

The differential pressure data were obtained from lower horizontal section, upper horizontal section, and vertical section of piping system with five different blower frequencies (air velocities). For each case, the number of data obtained was 65536. Figure 19, 20, and 21 show the phase space diagrams at the lower horizontal section, upper horizontal section, and vertical section respectively with different velocity of the air.

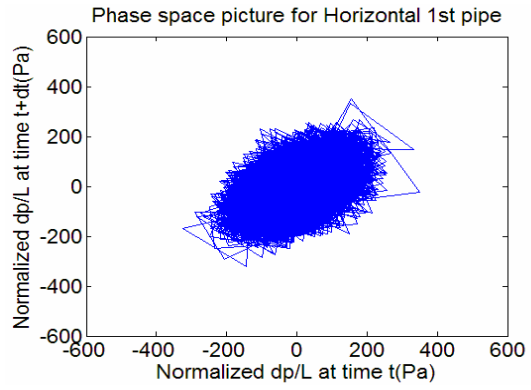
As seen on the figures, when the velocity of the gas increases, both horizontal and vertical length of the phase space diagrams also increases. This means that the more differential pressure is expected and the differential pressure changes faster as one increases the gas velocity. This phenomenon was clearly seen in every section of pipe. Note that on the horizontal section, the shape of diagram at the lower velocity of the air was triangular, and it becomes elliptical shape as velocity of the air is increased.

The location of measuring differential pressure also affected the length along horizontal and vertical direction of the phase space diagram. For the case of the same air velocity, it was clear that the length, along both horizontal and vertical directions of the phase space diagram, at the vertical section is the largest. Also note that the one at the lower horizontal section is next largest and the upper horizontal section has the smallest area. Thus, in the vertical section, more signal fluctuation is present than the other two sections. The differential pressure fluctuation at the lower horizontal section was higher than the one at the upper horizontal section since this section is located near the blower and feeder, so, the differential pressure fluctuation would be affected more by these devices. The shape of the phase space diagrams for the gas flow only was

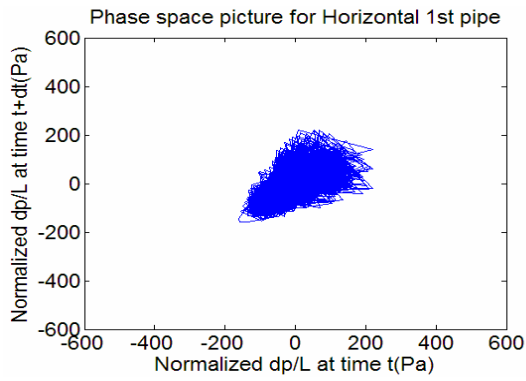
generally elliptic except for a few cases. The ellipticity of these ellipses increases when the solid loading ratio increases.



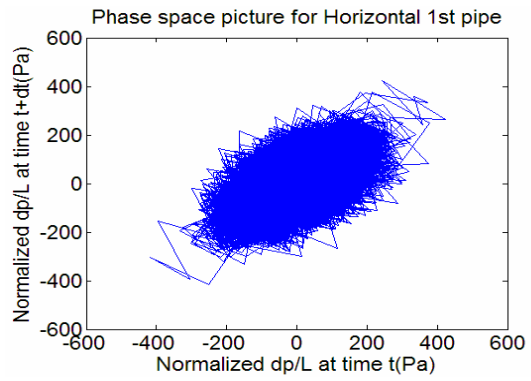
Vair = 20.2 m/s



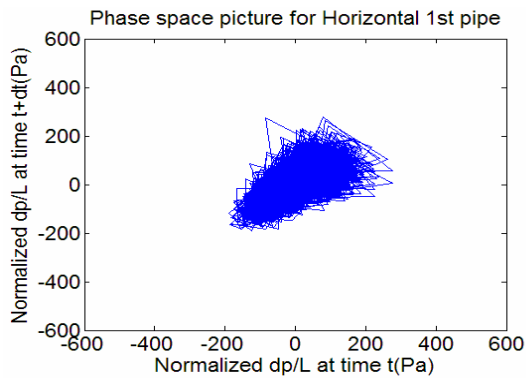
Vair = 38.9 m/s



Vair = 25.2 m/s

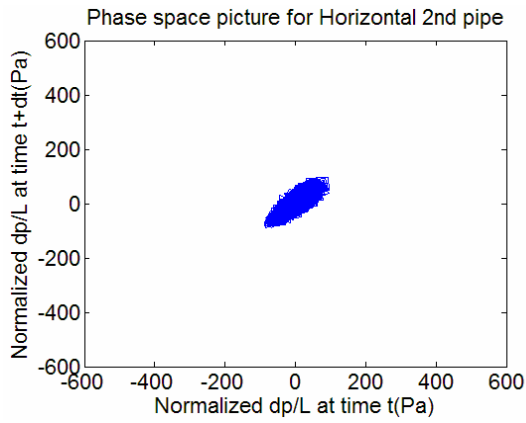


Vair = 50.0 m/s

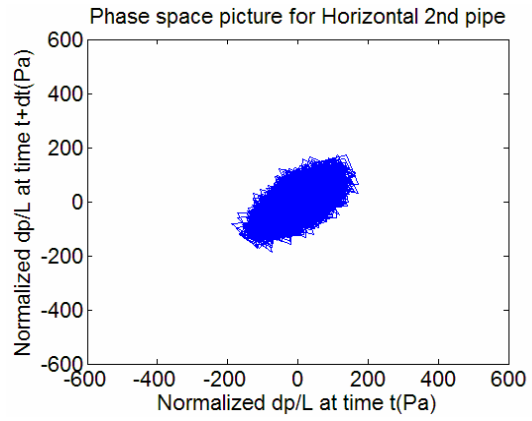


Vair = 28.9 m/s

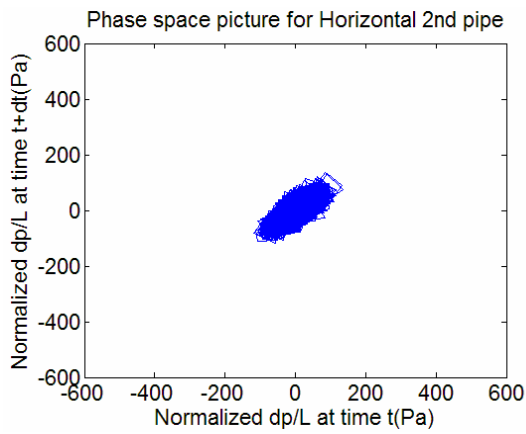
Figure 19 Phase space diagram at lower horizontal section (Gas Only), with different air velocity



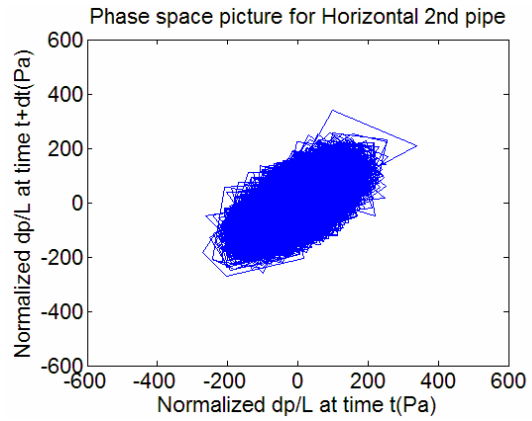
Vair = 20.2 m/s



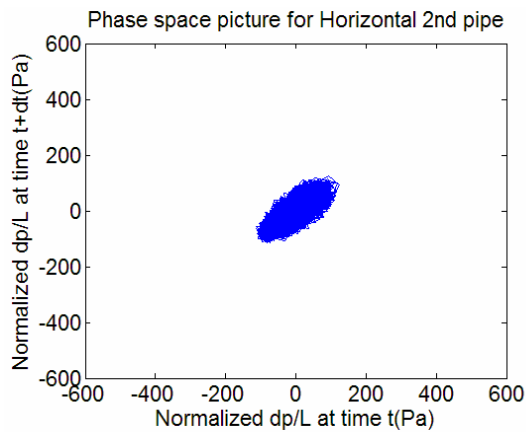
Vair = 38.9 m/s



Vair = 25.2 m/s



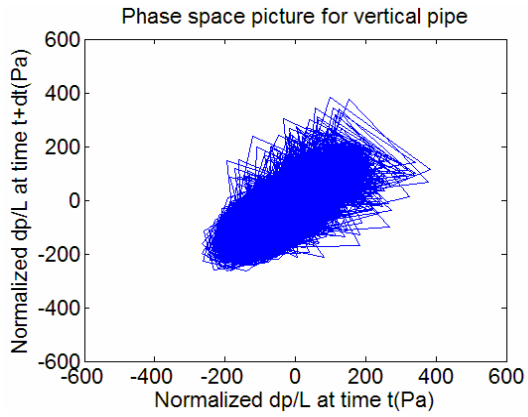
Vair = 50.0 m/s



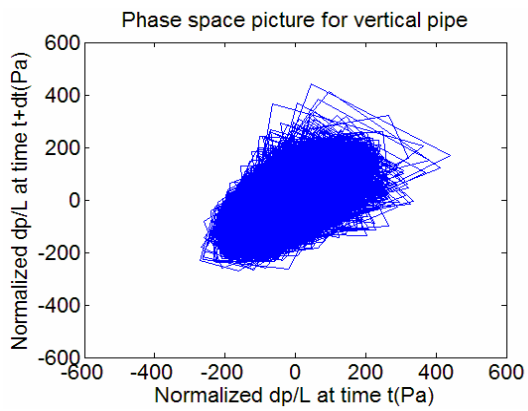
Vair = 28.9 m/s

Vair

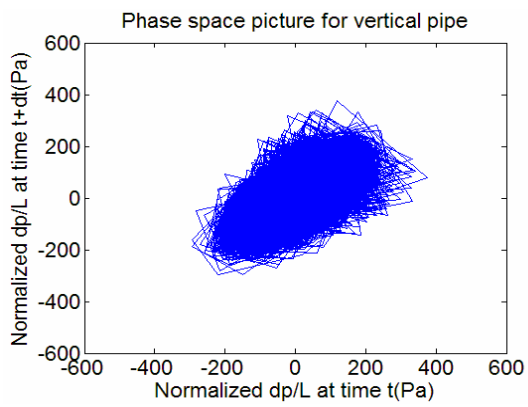
Figure 20 Phase space diagram at upper horizontal section (Gas Only), with different air velocity



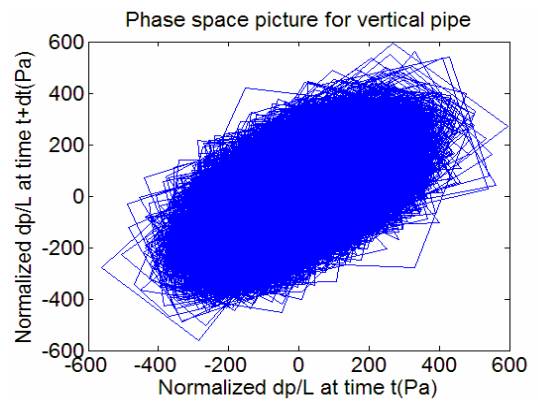
Vair = 20.2 m/s



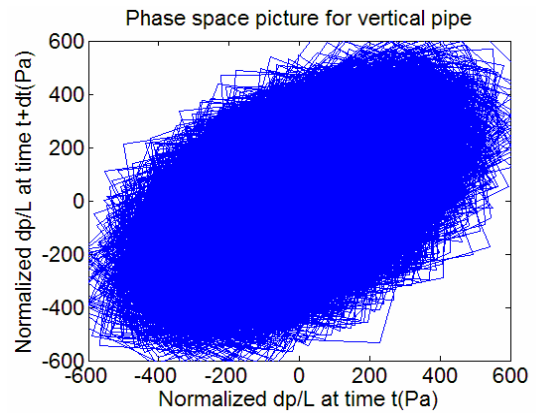
Vair = 25.2 m/s



Vair = 28.9 m/s



Vair = 38.9 m/s



Vair = 50.0 m/s

Figure 21 Phase space diagram at vertical section (Gas Only), with different air velocity

4.1.2 Effect of solid loading

As mentioned before, when the solid loading ratio, μ , is not zero, the shape of the phase space diagram was changed. The ellipticity of the ellipse was larger than for gas flow only. The shape is cigar-like and two or more attractor points were observed.

For polyester and polystyrene, data of thirty seven different cases (combinations of blower's rotational frequency in the range of 72 Hz to 160 Hz and feeder's rotational frequency in the range of 0.37 Hz to 2.06 Hz) were acquired from three different locations.

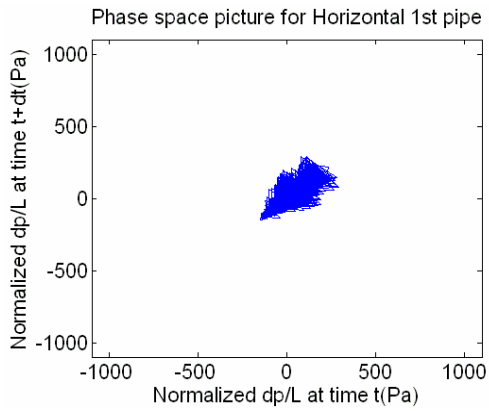
On the other hand, for polyolefin, only 11 cases of data could be obtained because of its material properties. The density of polyolefin is lower (see Table 1) than the other materials. In other words, polyolefin is a light material, so, at the high velocity of the air, the air prevents this material dropping down into the pipe and the material is getting fluidized at the feeding pipe (pipe between the main pipe and feeder). Also, this material sometimes sticks to each other and high surface friction causes a feeding problem. It was very hard to achieve the constant solid loading ratio. By using a rotary airlock feeder, one may obtain constant solid loading ratio, but this study was only able to analyze 11 cases.

When the solid loading ratio is not zero, it was clear to see that the phase space diagram was expanded in the horizontal direction but they do not change much for the vertical direction when the blower frequency increased with a fixed mass flow rate of solid. This phenomenon was observed at all measurement locations. Thus, when solid loading exists, increasing air velocity will increase the difference between the maximum and minimum differential pressure, but it does not affect much for variation of differential pressure from one time to next time step.

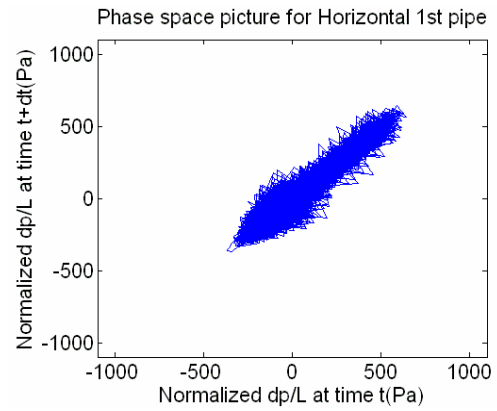
Figure 22 is phase space diagrams for different blower frequencies (different air velocities) with a fixed solid loading ratio measured at the lower horizontal section.

The effect of measurement location (Figure 23) was similar to the one without solid loading (gas flow only). The expansion in the horizontal and vertical direction of the phase space diagram for the vertical section was the biggest, and lower horizontal section was next, and upper horizontal section has the smallest expansion.

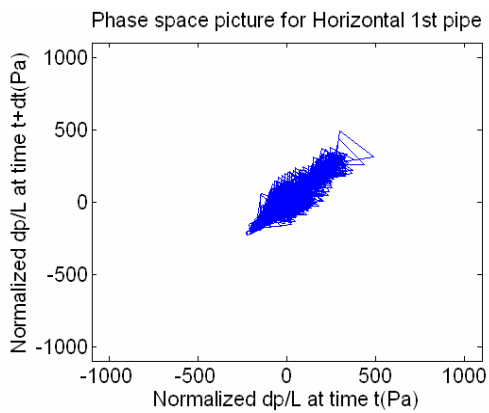
The effect of increasing the solid loading ratio is a bit complicated to analyze. As seen on Figure 24, the area of the phase space diagram is increasing when the solid loading ratio is increased at the lower range of the loading ratio, then a sudden decrease and increase at the middle range and a decrease again at the higher range. These phenomena (increasing or decreasing of area as the solid loading ratio changes) does not seem to have a pattern, but in general, the area was decreased when the solid loading ratio increases. The particles being transported worked as a damper for pressure fluctuation, so increasing the solid loading ratio decreases the pressure fluctuation.



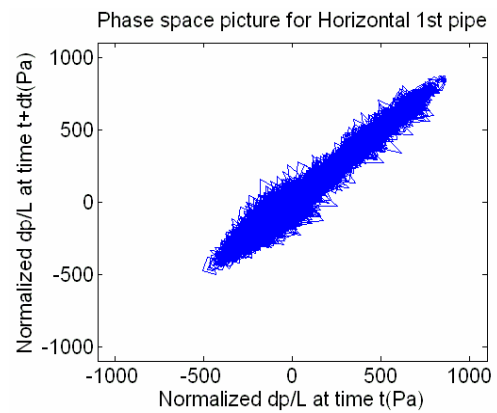
Blower = 72 Hz, loading = 1.5



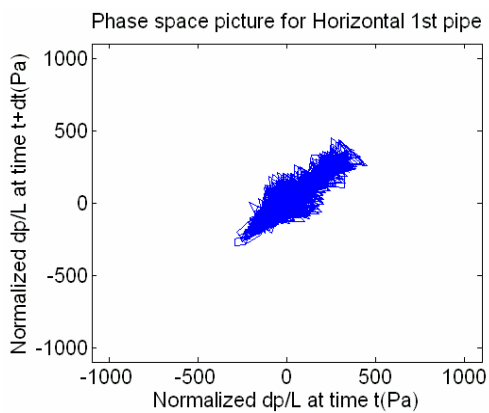
Blower = 128 Hz, loading = 1.5



Blower = 88 Hz, loading = 1.4

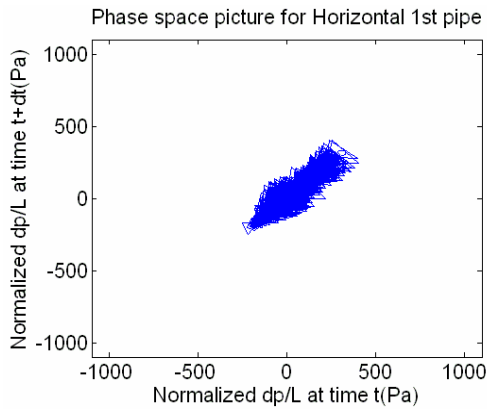


Blower = 160 Hz, loading = 1.5

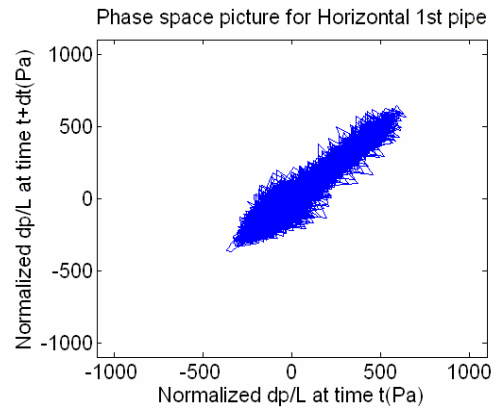


Blower = 100 Hz, loading = 1.4

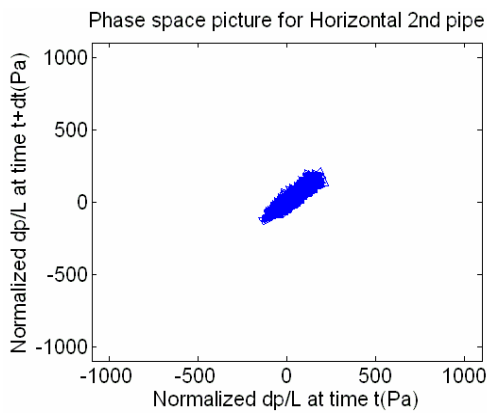
Figure 22 Phase space diagram for polyester with fixed mass flow rate of solid (0.14 kg/sec) and different blower frequency measured at lower horizontal section



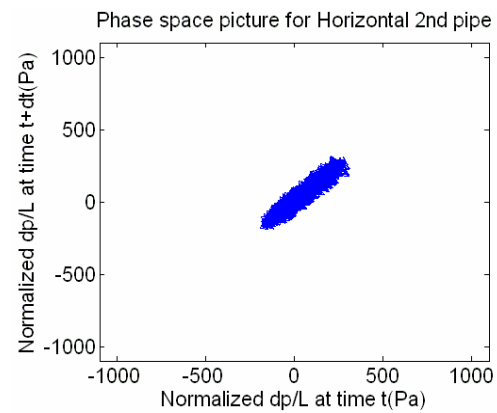
Lower horizontal



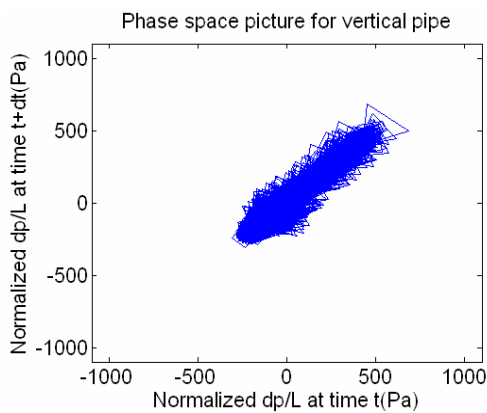
Lower horizontal



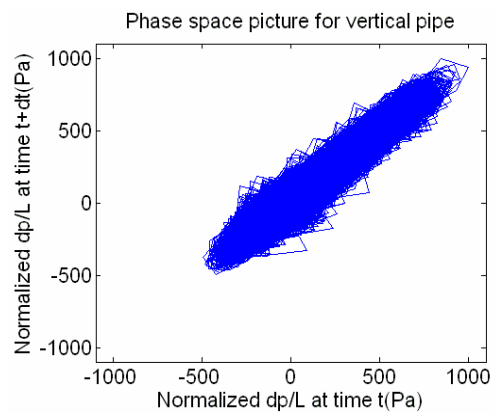
Upper horizontal



Upper horizontal

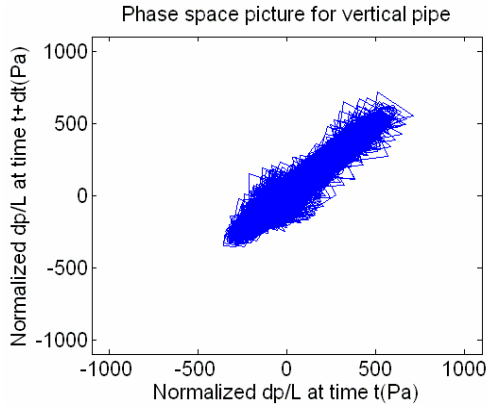


Vertical

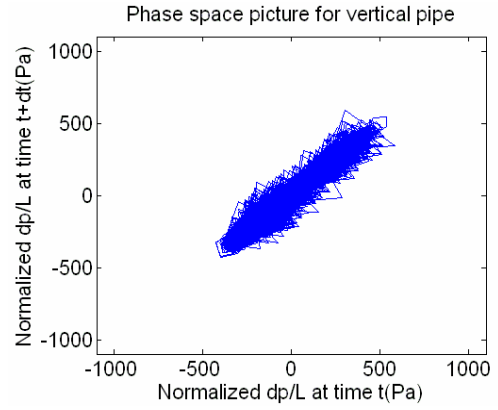


Vertical

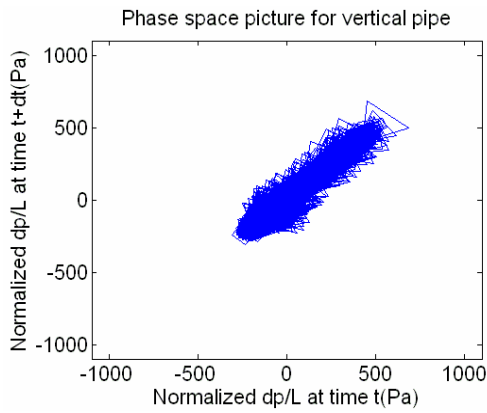
Figure 23 Phase space diagram for polyester with different measuring locations, Blower frequency = 88 Hz (left) and 128 Hz(right), mass flow rate of solid = 0.14 kg/s



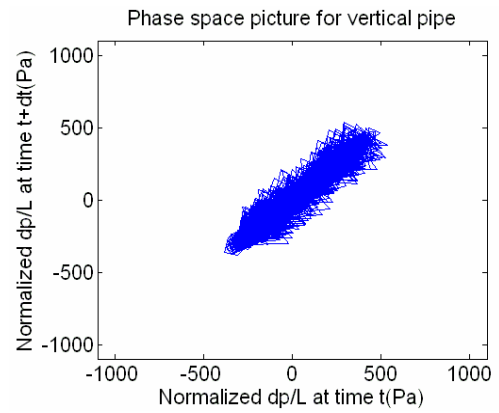
$$\mu = 1.4$$



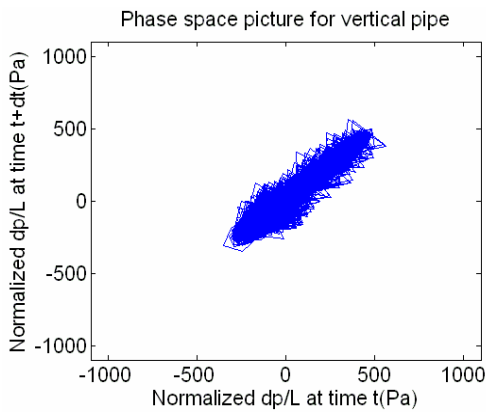
$$\mu = 3.0$$



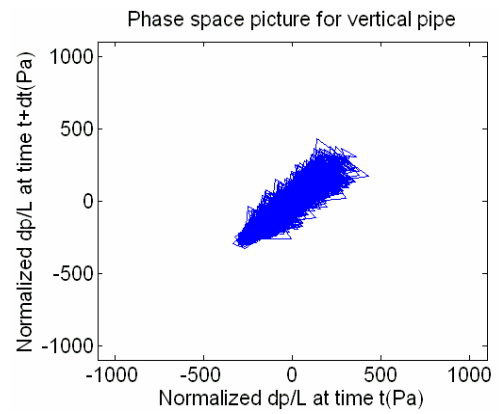
$$\mu = 2.1$$



$$\mu = 3.6$$



$$\mu = 2.6$$



$$\mu = 4.2$$

Figure 24 Phase space diagram for polyester with different solid loading ratios.
Blower frequency = 100 Hz, measured at vertical section

4.2 POWER SPECTRAL DENSITY ANALYSIS

The power spectral density (PSD) graphs for different system setups will be presented in this chapter. It was found that the power spectral density of the differential pressure signals was complex of blower, feeder, gas-particle interaction and turbulent fluctuation. By plotting the power spectral density graph, the effect of those components will be clearly seen and the flow characteristics for different system set up and materials will be determined.

4.2.1 Gas flow only

For the case of gas flow only, since the feeder did not operate, the power due to the feeder was not shown in the PSD figure. Only the power due to the blower frequency and the turbulent fluctuation will be shown in the PSD graph. Figure 25, 26, and 27 are the PSD graphs with different blower frequencies at the lower horizontal, upper horizontal, and vertical section respectively.

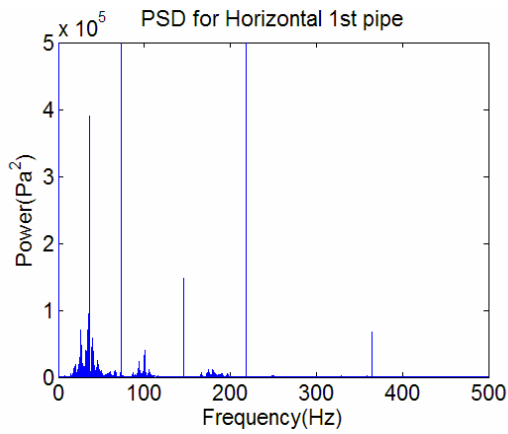
As seen on Figure 25, 26, and 27, there are several sudden jumps (peaks) for the magnitude of power. And the relevant frequencies of these peaks coincided to the frequency of the blower. For example, on blower = 128 Hz, $V_{air} = 38.9$ m/s of Figure 25 (The top right graph of Figure 25) there is a power peak at the frequency of 128 Hz. It is clear that this power peak occurs due to the blower. And another power peak was occurs near 256 Hz, and 384 Hz. These frequencies are the multiple of the blower frequency, 128 Hz, and it might be a resonance frequency of the blower. It was shown that the magnitude of the power due to the resonance frequencies was smaller than the original blower frequency, but generally higher than the power due to the gas – particle interaction. The original and resonance frequencies due to the blower do

not help to understand the flow characteristics. The pure gas – particle interactions are the only interesting things to analyze. So the signal due to the blower and feeder should be disregarded when the signal is being analyzed.

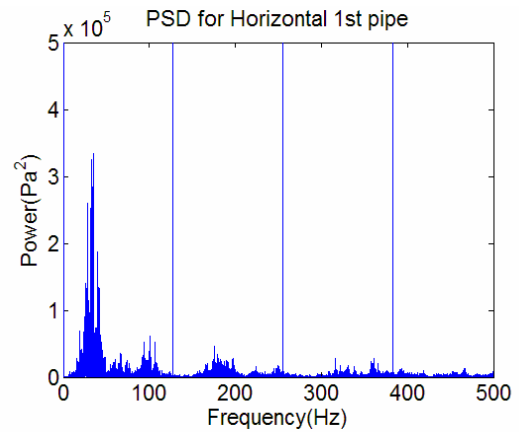
Note that another power peak occasionally occurred at the half of the blower frequency (36 Hz – upper left graph of Figure 25, 36 Hz, 44 Hz, and 50 Hz – left hand graphs of Figure 26, and 36 Hz – upper left graph of Figure 27). This peak was not shown at the blower frequency of 128 Hz and 160 Hz. This power is ambiguous. It might be due to the blower (power due to another resonance frequency) or power due to the gas – particle interactions. Further study is needed to find out the characteristic of this power.

For the lower and upper horizontal pipe section, the power concentrations due to the gas – particle interaction occur at a frequency lower than 250 Hz (See Figure 25 and 26). In each case, there were four significant power concentrations and their magnitudes increase when frequency of blower increases. For the lower horizontal section, these concentrations occur at the frequencies of 20 Hz - 45 Hz, 55 Hz - 65 Hz, 90 Hz - 110 Hz, and 170 - 190 Hz. The largest magnitude of power occurs at 30 Hz - 40 Hz. In the case of the upper horizontal section, the power concentration occurs at slightly lower frequencies (about 5 Hz - 10 Hz lower) than the one for lower horizontal pipe section. The magnitude of power due to the gas – particle interaction at the lower horizontal section was higher than the one at the upper horizontal section for the entire frequency domain.

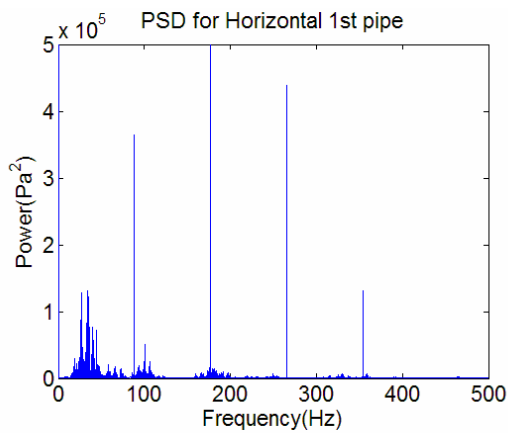
For the vertical section, the magnitude of power was much higher than the other two sections and more than five power concentrated regions were found. Also those power concentrations were dispersed in the lower frequency domain (0 to 300Hz).



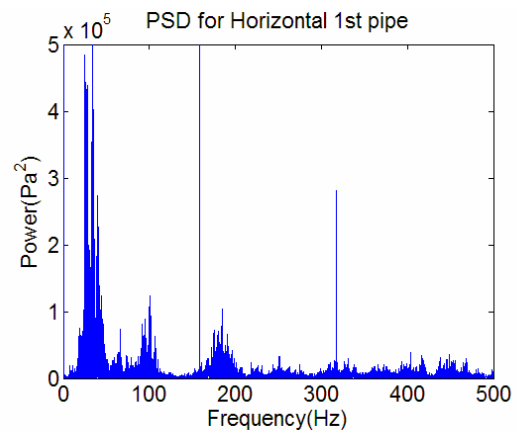
Blower = 72 Hz, Vair = 20.2 m/s



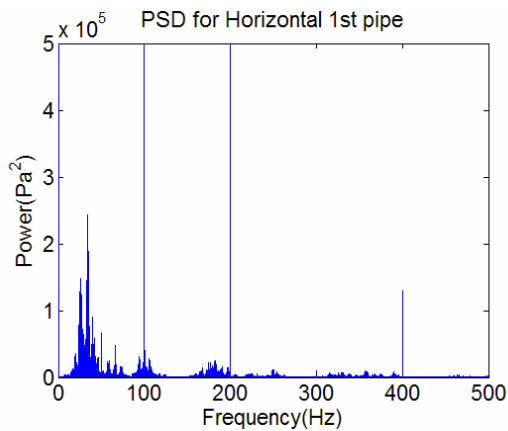
Blower = 128 Hz, Vair = 38.9 m/s



Blower = 88 Hz, Vair = 25.2 m/s

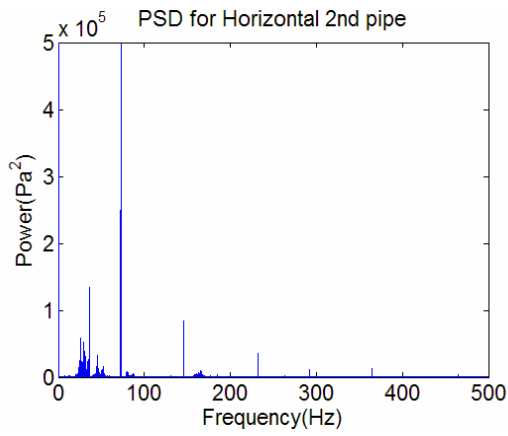


Blower = 160 Hz, Vair = 50.0 m/s

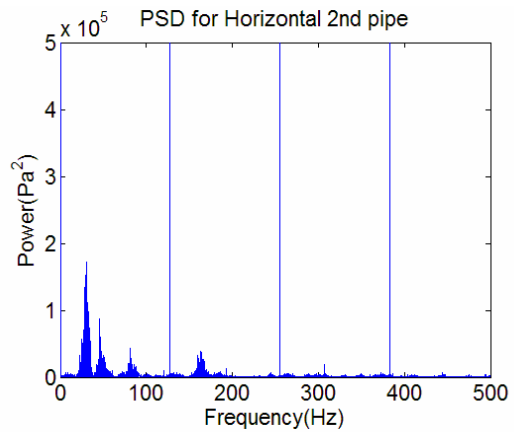


Blower = 100 Hz, Vair = 28.9 m/s

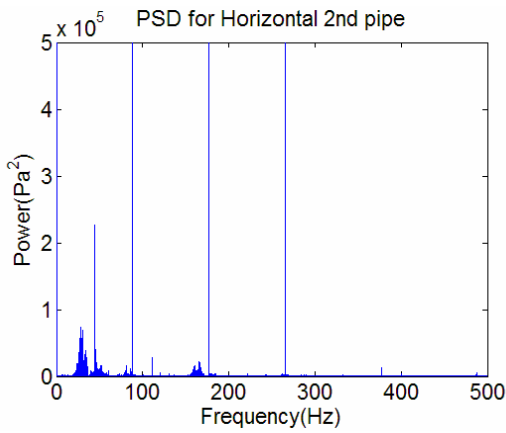
Figure 25 Power spectral density graph at lower horizontal section (Gas Only), with different air velocity



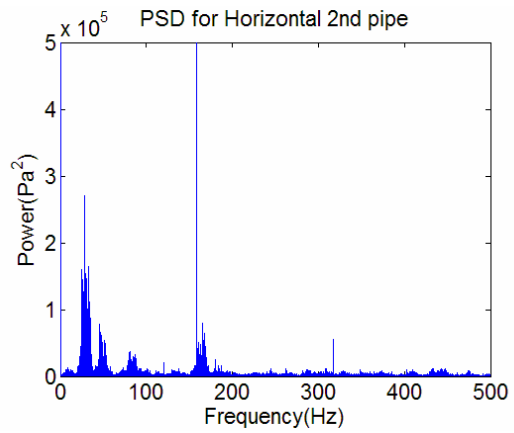
Blower = 72 Hz, Vair = 20.2 m/s



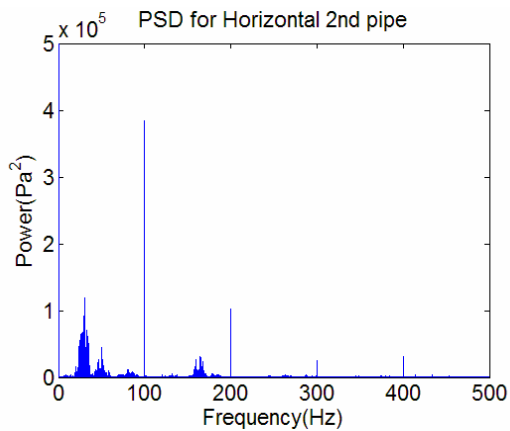
Blower = 128 Hz, Vair = 38.9 m/s



Blower = 88 Hz, Vair = 25.2 m/s

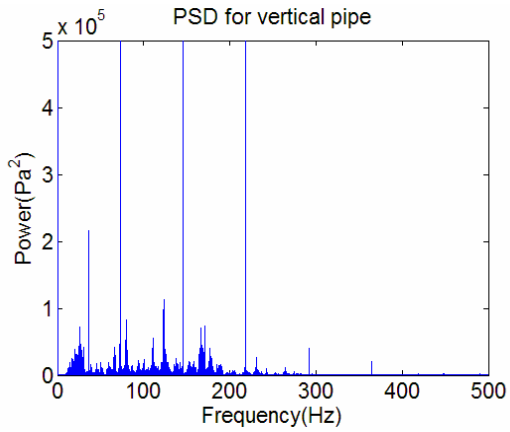


Blower = 160 Hz, Vair = 50.0 m/s

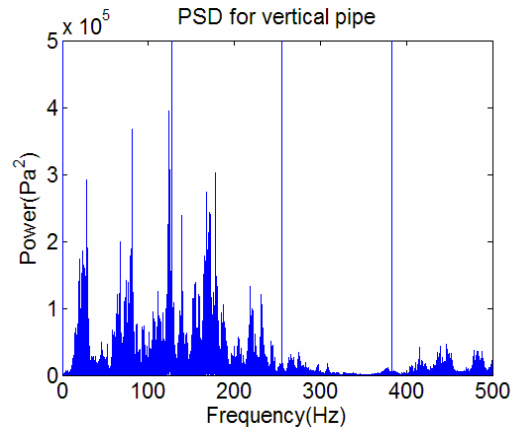


Blower = 100 Hz, Vair = 28.9 m/s

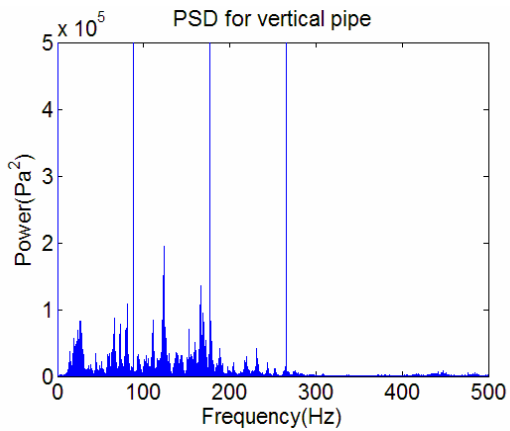
Figure 26 Power spectral density graph at upper horizontal section (Gas Only), with different air velocity



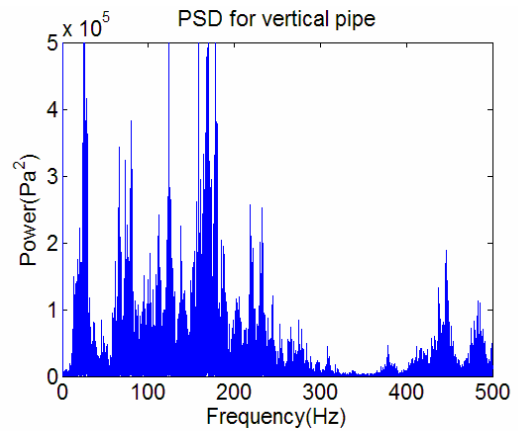
Blower = 72 Hz, Vair = 20.2 m/s



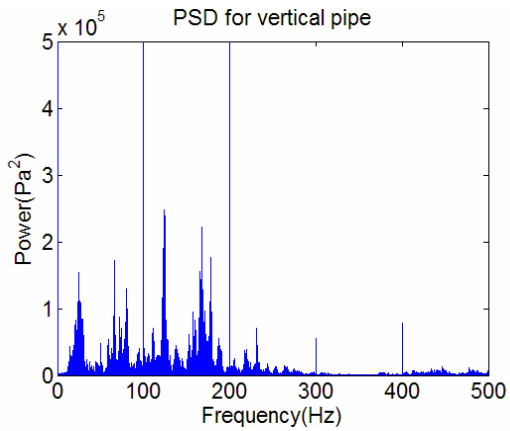
Blower = 128 Hz, Vair = 38.9 m/s



Blower = 88 Hz, Vair = 25.2 m/s



Blower = 160 Hz, Vair = 50.0 m/s



Blower = 100 Hz, Vair = 28.9 m/s

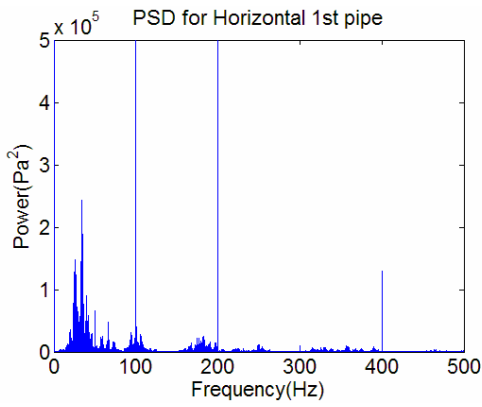
Figure 27 Power spectral density graph at vertical section (Gas Only), with different air velocity

Another interesting phenomenon was found at the higher frequency of blower operation (at the blower frequency of 128 Hz and 160 Hz, see right hand side of pictures in Figure 27). The power is increasing again after a frequency of 400 Hz.

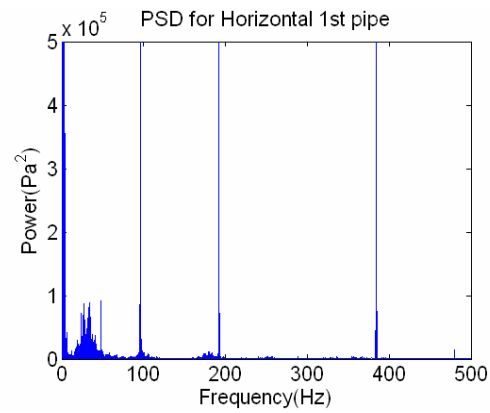
4.2.2 Effect of solid loading

When the solid loading ratio, μ , is not zero, the magnitude of power on the PSD graph was much smaller than the case of gas flow only ($\mu = 0$). These were observed with all three different materials and at different measuring locations (Figure 28). Also, when μ is not zero, one can see the power peaks near the zero frequency regions. These peaks are due to the rotational frequency of the feeder. For example, the case of Figure 28, the rotational speed of the feeder was 4.6 rpm. The corresponding rotational frequency of the feeder is $4.6 / 60 \approx 0.077$. But the rotor has eight pockets, so for each revolution, eight strokes of solid feeding occurred. So, the frequency of the feeder would be $0.077 * 8 = 0.62$ Hz. Similar to the case of gas flow only, the magnitude of power was increased as the velocity of the air increases for the fixed mass flow rate of solid.

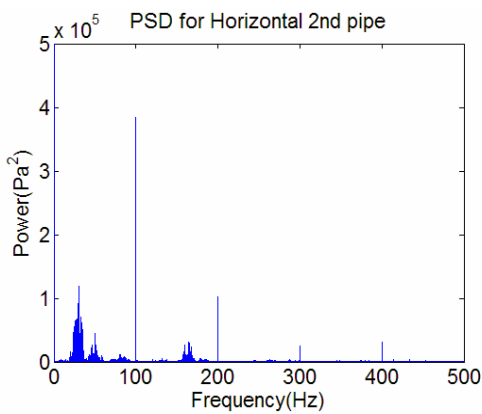
For the lower horizontal and the vertical section, a few power concentrations were observed. Among them, the magnitudes of the two power concentrations were much higher than the others. Those concentrations occurred around 5 Hz - 10 Hz and around 25 Hz. As the mass flow rate of solid increases, the smaller power concentrations diminish, while the major two concentrations behave randomly (sometimes the power increases and sometimes it decreases). On the upper horizontal section, when the blower frequency is fixed, the magnitude of power peaks decreased as the solid loading ratio increases. Also, compared to the other sections, the power peak due to the blower is dramatically reduced. On this section, since this section is far -



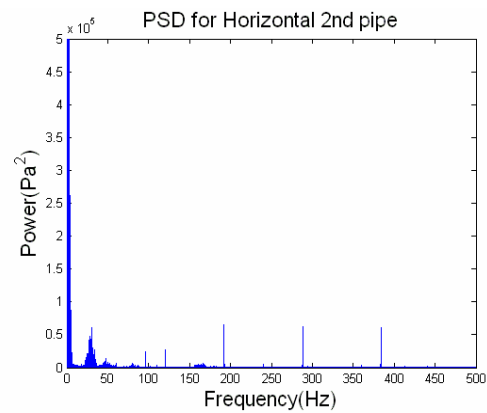
Lower horizontal section (Gas only)



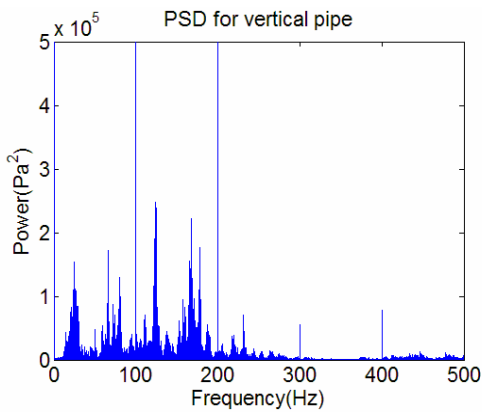
Lower horizontal section ($\mu = 1.4$)



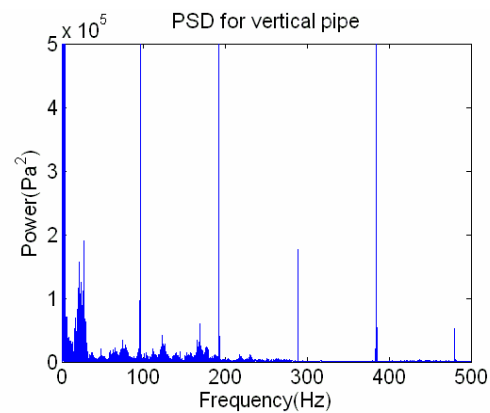
Upper horizontal section (Gas only)



Upper horizontal section ($\mu = 1.4$)



Vertical section (Gas only)



Vertical section ($\mu = 1.4$)

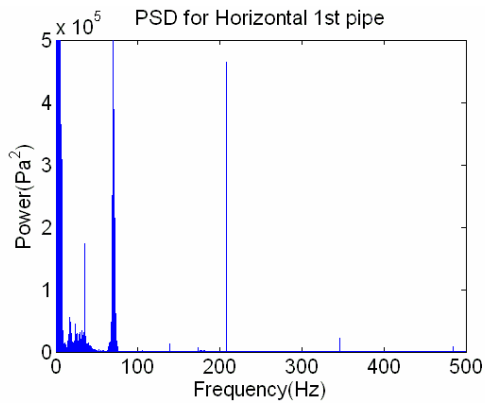
Figure 28 PSD graphs for different sections along the pipe with blower frequency = 100 Hz, air only (left graphs) and solid loading ratio, $\mu = 1.4$ (right graphs), polyester

from the entrance of the air and solid, the effect of the blower and feeder is smaller than the other sections. Furthermore, the particles in the pipe hitting each other and hitting the air would also decrease the effect of the blower and feeder.

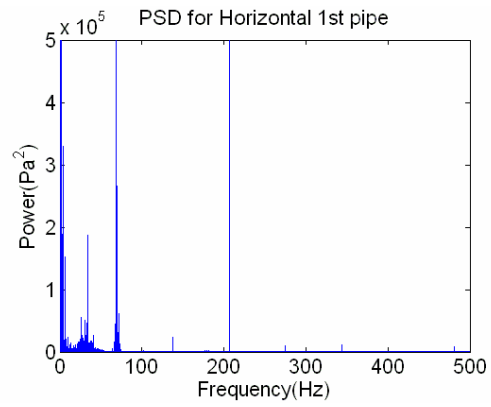
When the solid loading ratio increases, another power peak was observed right before or after the power peak due to the blower. This shows that the blower frequency was affected by feeder behavior. The type of feeder used for this research is a drop through rotary feeder, so the pellets are not dropped continuously. The feed rate was pulsatile.

The Figure 29 shows the PSD graph for polyester and polystyrene with the similar loading conditions. As seen on Figure 29, the general behavior of the power spectrum is probably due to the gas – particle interaction look similar. For the range of frequency, magnitude of power for polyester was slightly higher than the one for polystyrene.

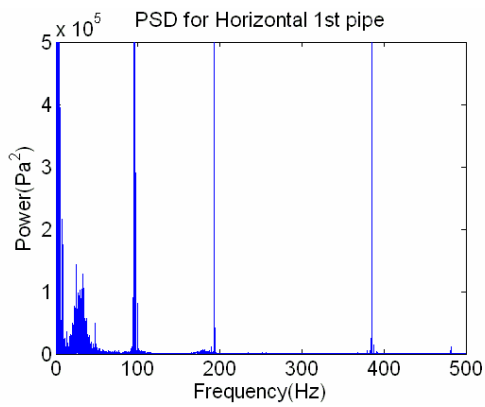
The PSD graph for polyolefin was illustrated on Figure 30. As mentioned before, this material has very low density, it is a lighter material compared to the other two polymers. Feeding problems prevented a wide range of feed rates to be studied. Also, the operational velocity of the air to transport this material was lower than the other two materials. One notes from Figure 30 that the PSD signal for the polyolefin was less than the polyester and polystyrene, and this is most likely due to the particle behavior.



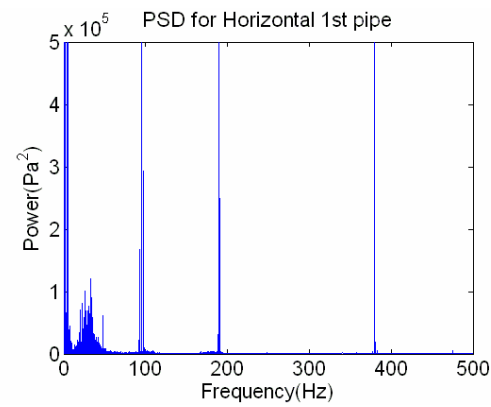
Blower = 72 Hz, $\mu = 4.3$



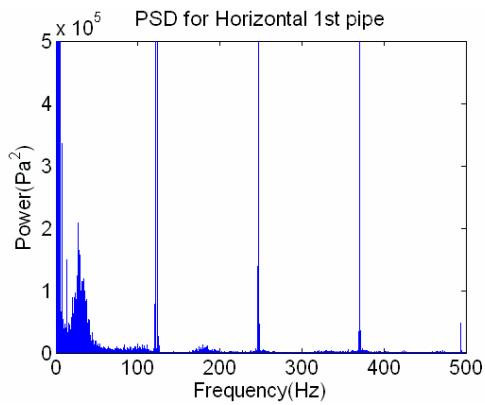
Blower = 72 Hz, $\mu = 4.2$



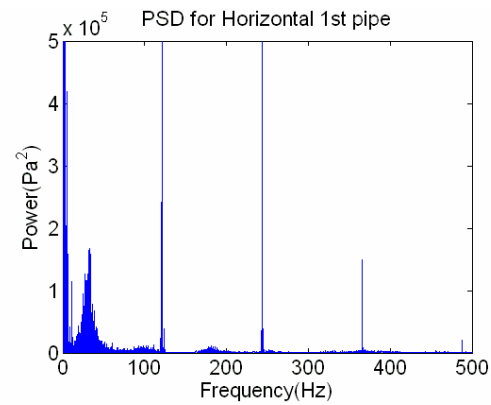
Blower = 100 Hz, $\mu = 3.6$



Blower = 100 Hz, $\mu = 3.6$

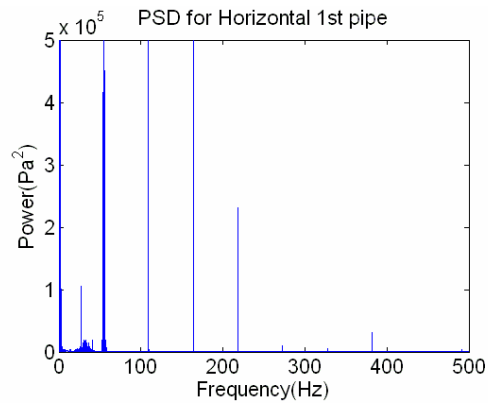


Blower = 128 Hz, $\mu = 2.7$

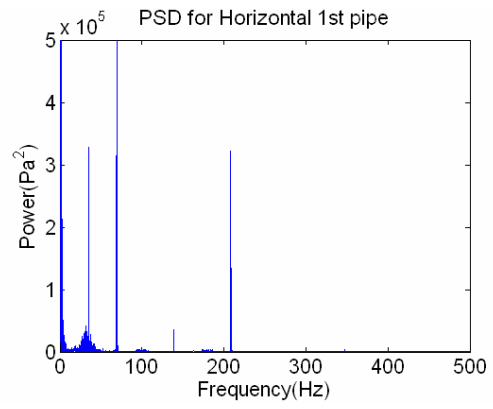


Blower = 128 Hz, $\mu = 2.6$

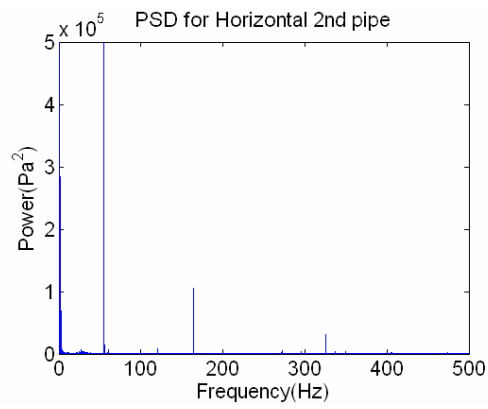
Figure 29 Comparison of PSD graph of polyester (left) to polystyrene (right) for the differential pressure measured on the lower horizontal section



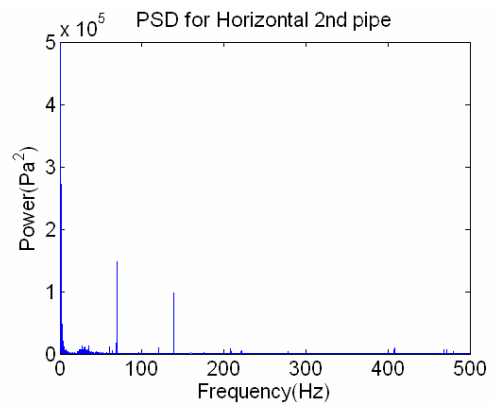
Lower horizontal



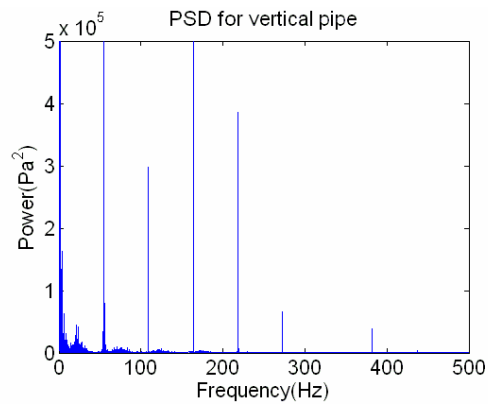
Lower horizontal



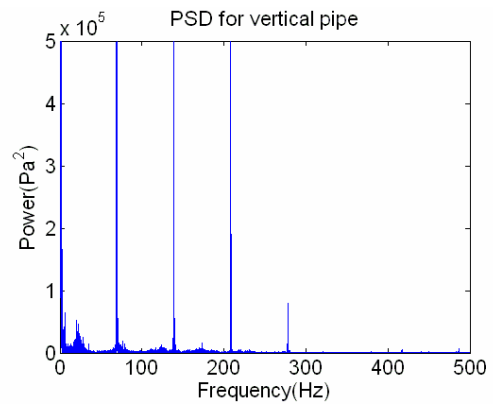
Upper Horizontal



Upper Horizontal



Vertical



Vertical

Figure 30 PSD graph of polyolefin for Blower = 56.7 Hz, $\mu = 2.3$ (Left), Blower = 74.3 Hz, $\mu = 1.0$ (Right)

4.3 RESCALED RANGE ANALYSIS AND HURST'S EXPONENT

The relationship between R/S and Hurst exponent was shown in the equation (17). The Hurst's exponent can be determined from this equation

$$H = \frac{\log(R/S)}{\log(a\tau)} \quad (21)$$

where, a is equal to 0.5 (taken by Hurst). The values of R/S are logarithmically plotted as a function of τ in Figure 31. A linear fit of these terms provides the value of H from the slope of the plot.

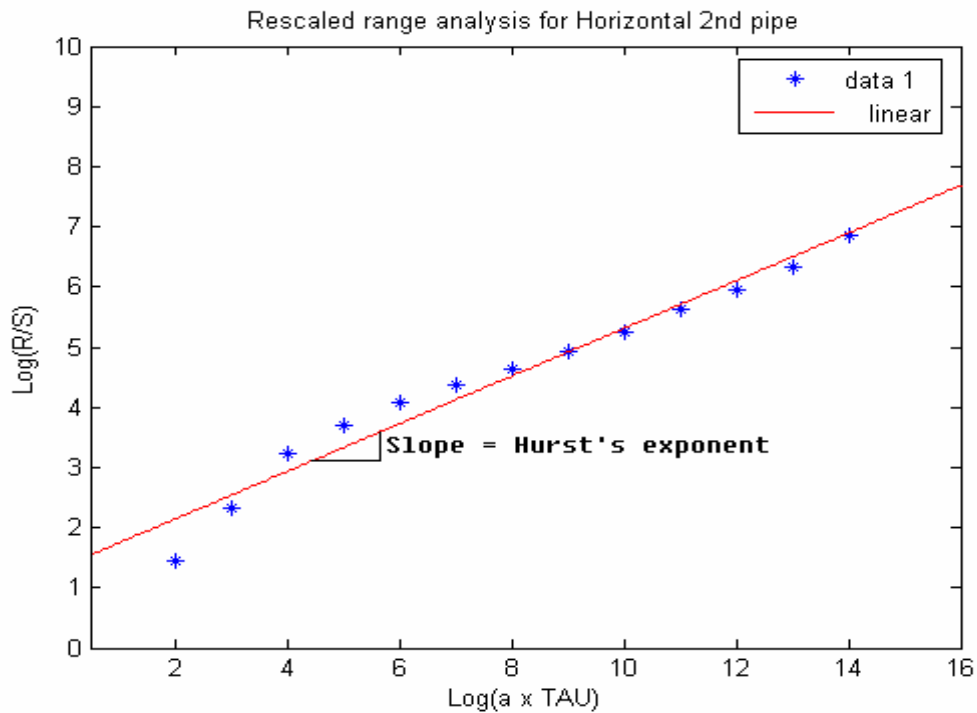


Figure 31 Relationship between R/S, τ , and Hurst's exponent

4.3.1 Gas flow only

For the case of gas flow only, the Hurst exponent was less than 0.5 which indicates anti-persistence in the analysis. The behavior for this case is shown in Figure 32. One can show that the value of Hurst's exponents for all three sections of piping should not be affected by the blower's frequency. Cabrejos⁽³⁾ showed that the Hurst's exponent indicates the flow regime in horizontal pneumatic conveying. The value of the exponent for upper horizontal section is higher than the other two sections and it is closest to 0.5 but does not change much as the gas velocity increases indicating a uniform, steady flow.

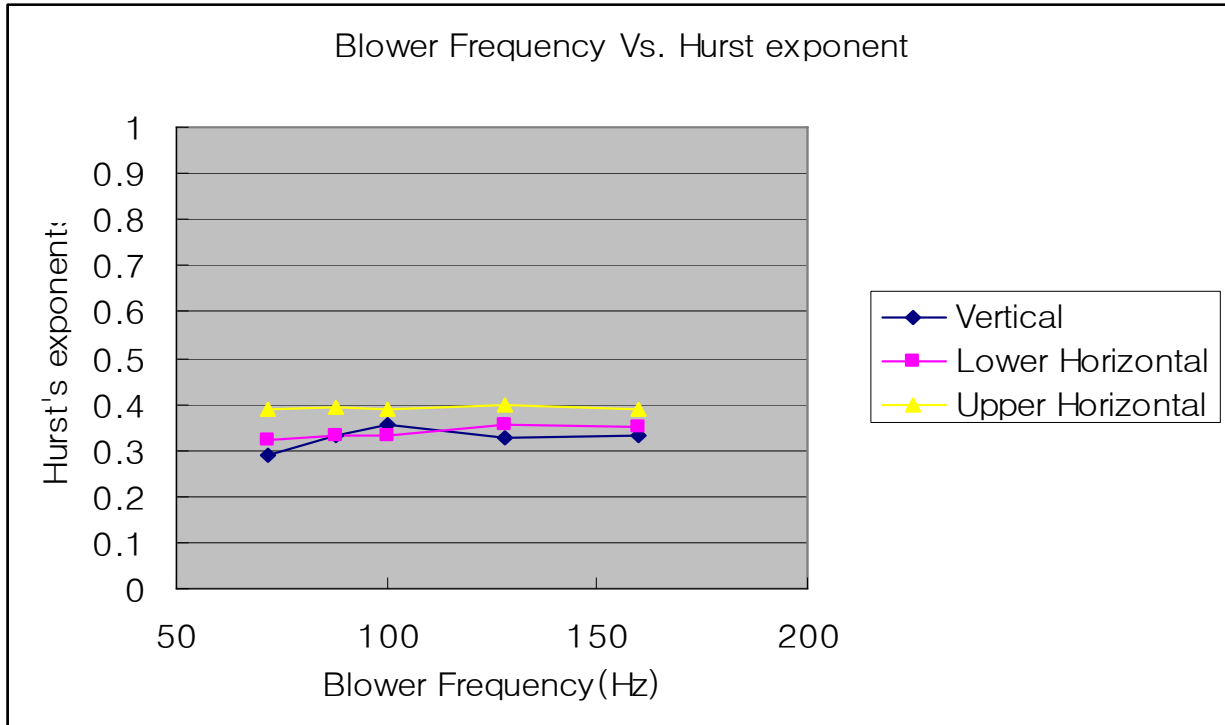


Figure 32 Hurst's exponents for different measurement locations and different blower frequencies, gas flow only

4.3.2 Effect of solid loading

When the solid loading ratio is not zero, the Hurst's exponent was higher than 0.5, this means that it has a persistence behavior, indicating that the same trend of data recorded from the past times will be expected to the future times.

Figure 33 and 34 illustrates the Hurst's exponents for polyester, polystyrene and polyolefin with different system configuration (different air velocity and solid loading ratio). When these figures are compared to flow patterns observed, one can understand that the Hurst's exponent is closely related to the flow pattern.

As a result, when the flow was homogeneous or homogeneous-pulsating flow, the Hurst's exponent increased as the solid loading ratio was increased. On the other hand, when the dominant flow pattern was pulsating flow, such as pulsating and pulsating-homogeneous flow, the Hurst's exponent decreased as the solid loading ratio was increased. For the case of two phase homogeneous flow, the Hurst's exponent increased when the solid loading ratio was increased. Also, it was found that the transition between one flow pattern and another occurs at the lower solid loading ratio, as the air velocity increased.

For polyester, the Hurst's exponent for the lower horizontal section (Figure 33 top left graph) decreased as the solid loading ratio increased. A pulsating flow was observed at the lower solid loading ratio ($\mu = 1.5 - 5.5$ for blower frequency = 72Hz, $\mu = 1.4 - 5.0$ for blower frequency = 88 Hz, and $\mu = 0.8 - 4.6$ for blower frequency = 100 Hz). When the solid loading was high ($\mu = 6.3 - 7.6$ for blower frequency = 72 Hz, and $\mu = 5.6 - 6.0$ for blower frequency = 88 Hz), a pulsating-homogeneous flow was observed.

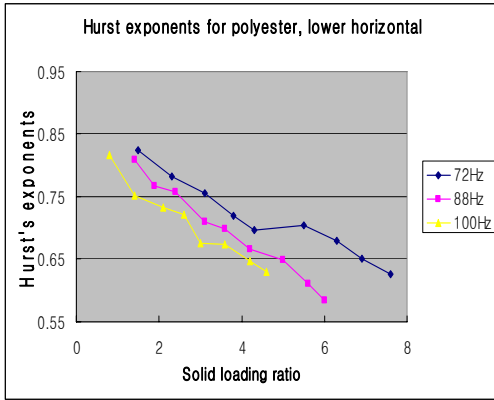
At the upper horizontal section of the pipe (Figure 33 middle left graph), the flow pattern was pulsating flow. As the solid loading ratio increased the flow becomes homogeneous-

pulsating, pulsating-homogeneous flow, homogeneous flow, and finally, two phase homogeneous flow was observed at the highest solid loading ratio. Note that at the blower frequency of 100 Hz, the two phase homogeneous flow pattern was not observed since the maximum solid loading ratio at this air velocity was too low to compare to the other blower frequency, but one may expect two phase homogeneous flow pattern when the solid loading ratio increased.

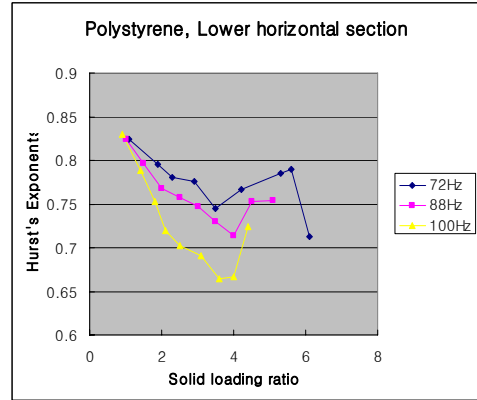
For polystyrene, in the lower horizontal section, pulsating flow was observed at the beginning and it becomes homogeneous-pulsating flow, homogeneous flow and two phase homogeneous flow at the blower frequency of 72 Hz, but for 88 Hz and 100 Hz, this pattern was not observed since the maximum solid loading ratio was low.

At the upper horizontal section, the flow pattern changed from pulsating flow, homogeneous pulsating flow, pulsating-homogeneous flow and homogeneous flow as the solid loading ratio increases. Also, two phase homogeneous flow was observed at the blower frequency of 72 Hz.

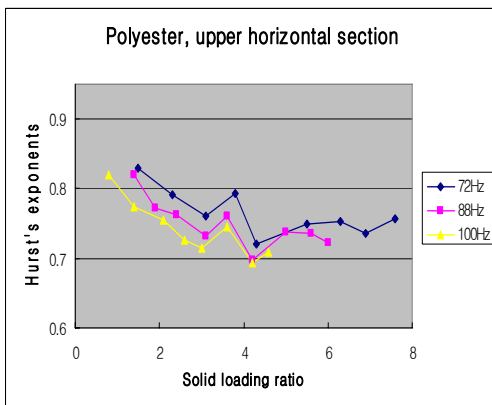
Since the number of data collected was limited due to the material properties of polyolefin, it is more difficult to explain the tendency of its Hurst's exponent values, but in general, the Hurst's exponent decreased when the solid loading ratio increased at the lower horizontal section and vertical section while it decreased and increased again at the upper horizontal section.



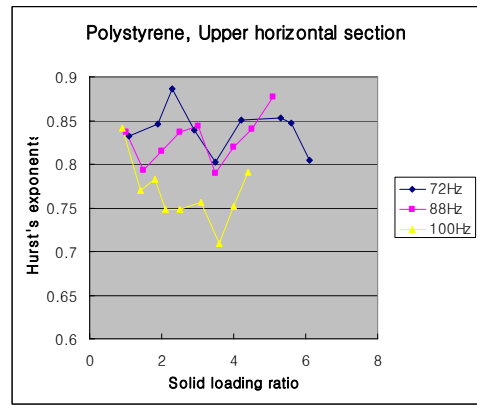
Lower horizontal section



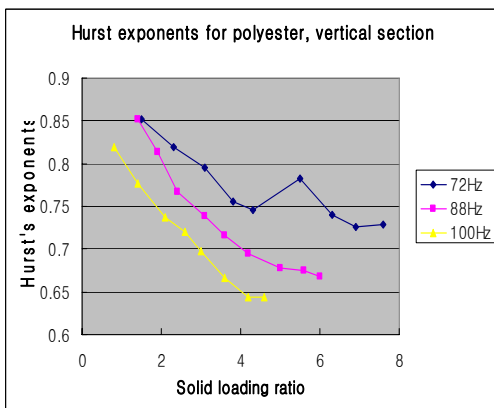
Lower Horizontal section



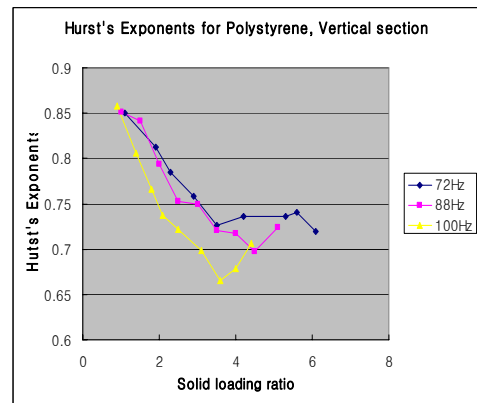
Upper horizontal section



Upper Horizontal section

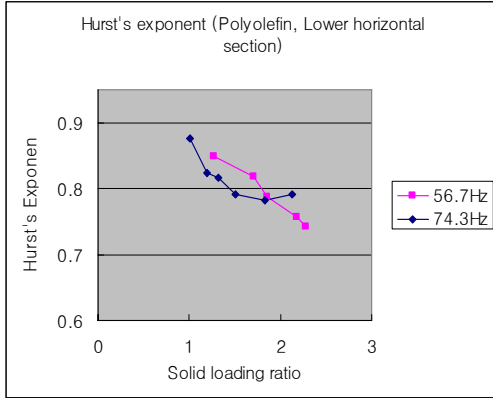


Vertical section

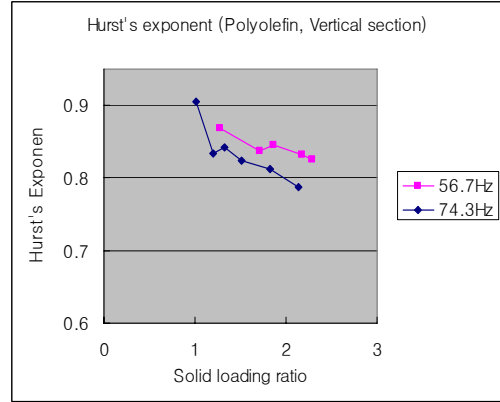


Vertical Section

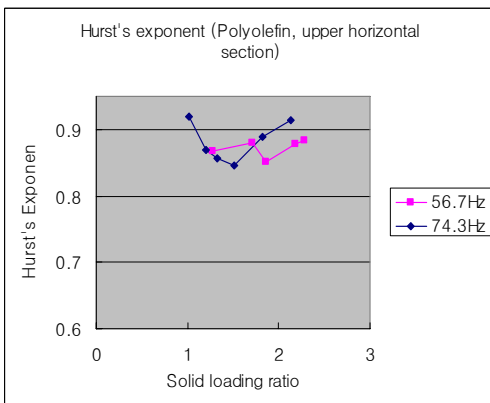
Figure 33 Hurst Exponents for polyester (left) and polystyrene (right) with different solid loading ratio



Lower horizontal



Vertical



Upper Horizontal

Figure 34 Hurst Exponents for polyolefin with different solid loading ratio and different measurement locations

4.4 FRACTAL DIMENSION ANALYSIS

The fractal dimensions for a phase space diagram have been determined by the box counting method. Since the phase space diagrams were expressed in two dimensional space, the relationship between Hurst's exponent and fractal dimension ($D = 2 - H$) does not exactly match. This is because the Hurst's exponents were determined from one dimensional time series differential pressure data. Figures 35, 36, and illustrate the fractal dimension of the different polymers measured at the vertical, lower and upper horizontal pipe arrangements respectively.

As the solid loading ratio increases, the fractal dimension seems to decrease slightly or remain the same in the vertical section of the pipe, but in horizontal sections it increases. Specifically in the upper horizontal section of the pipe, the fractal dimension increases more than in the other sections. This means that the shape of the phase space diagram is smoother as the solid loading ratio increases for the upper horizontal section. As mentioned before, this section has the most stable flow, thus increasing the solid loading ratio decreases the signal fluctuation. In the vertical section, however, increasing the solid ratio causes a more fluidized like behavior of flow, thus more signal fluctuations are expected. In the lower horizontal section, one may intuitively think that even though the pressure fluctuation was damped by increasing the solid loading ratio, the gas and particles interact more than the upper horizontal section (in other words this section has a flow developmental process occurring) thus the signal fluctuates more than in upper horizontal section.

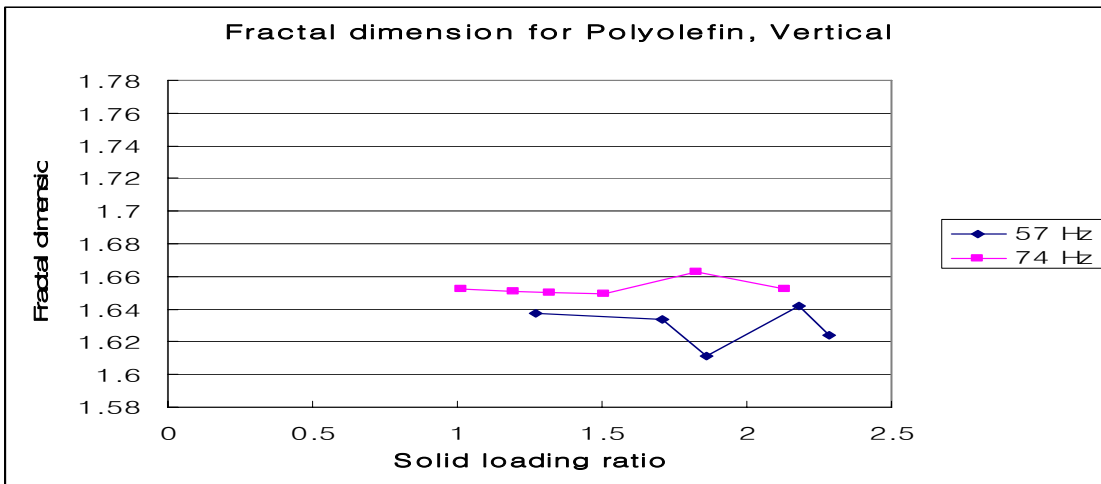
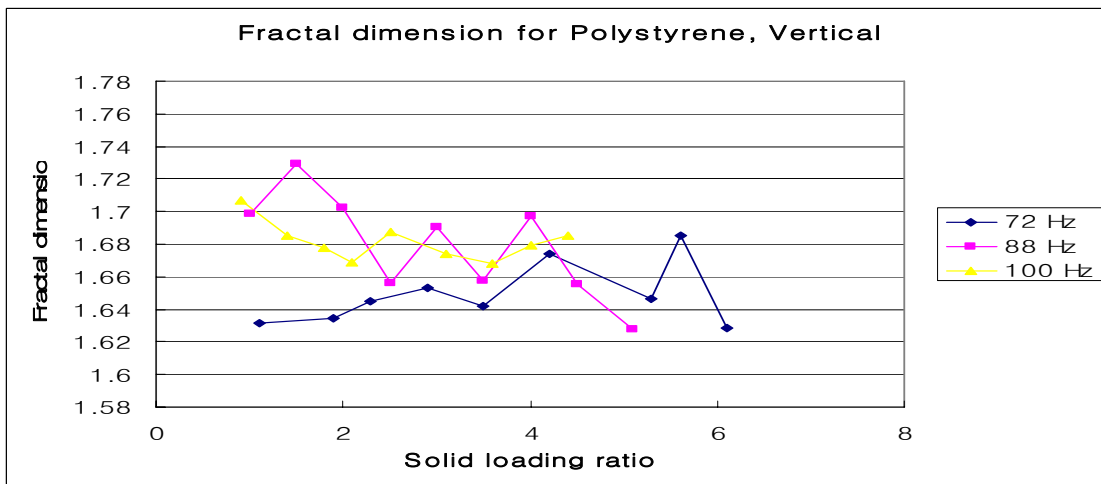
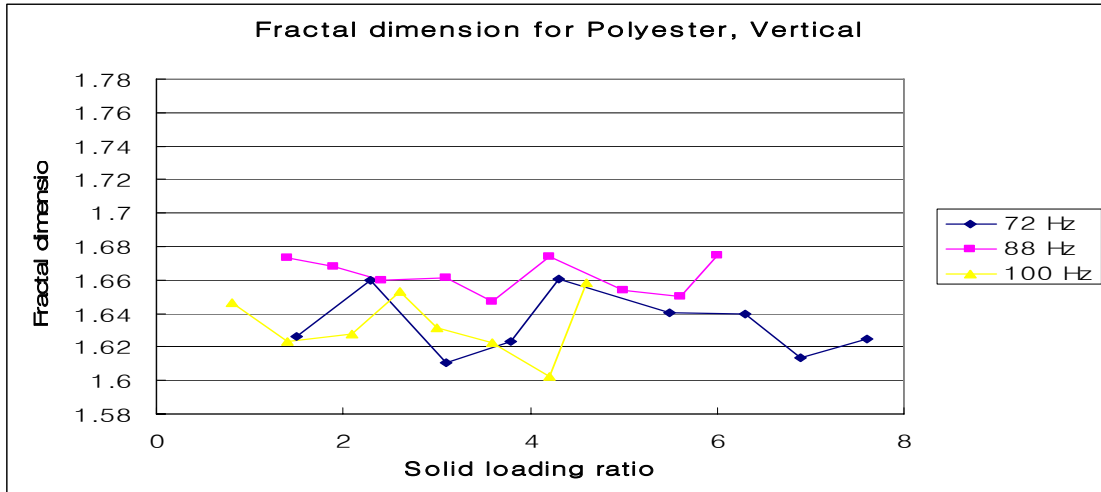


Figure 35 Fractal Dimension for different materials and solid loading ratio measured in the vertical section

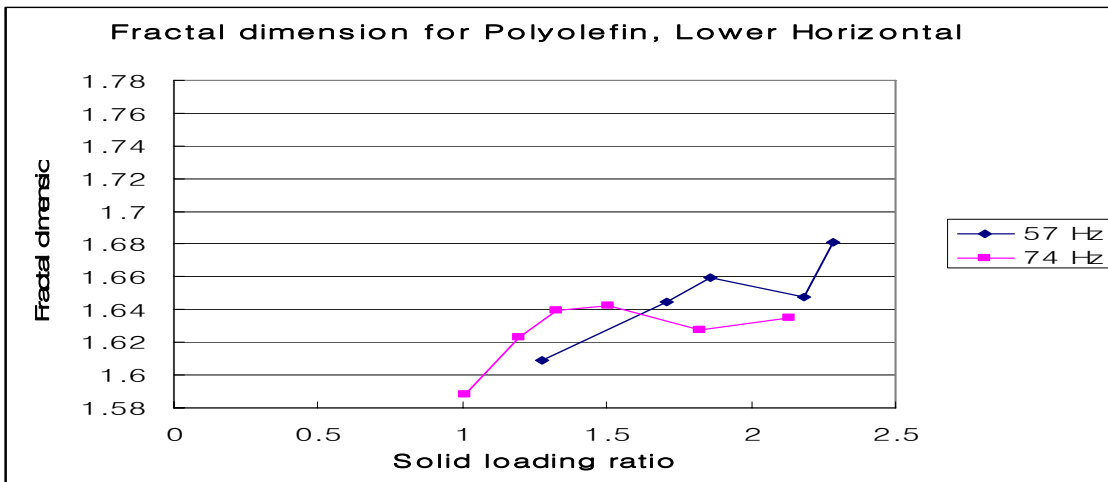
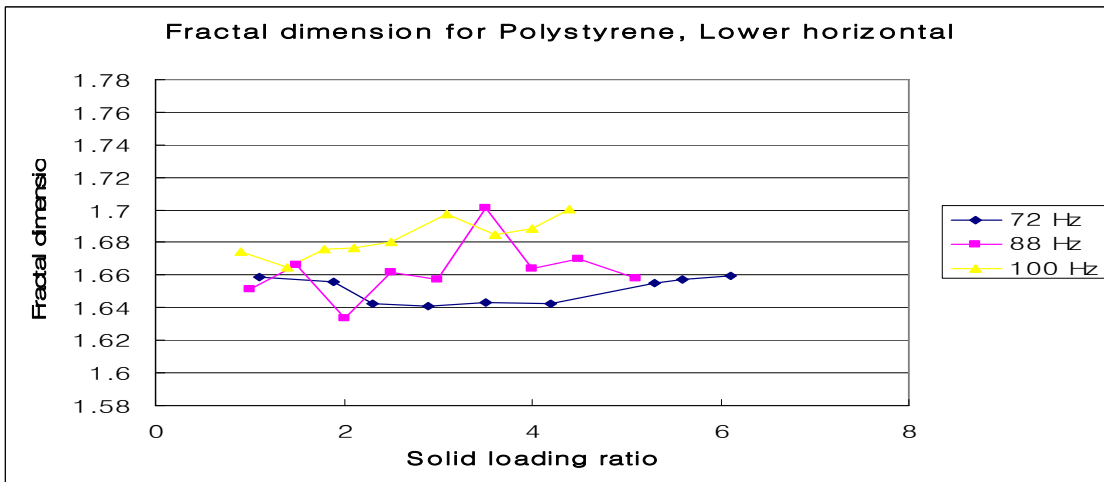
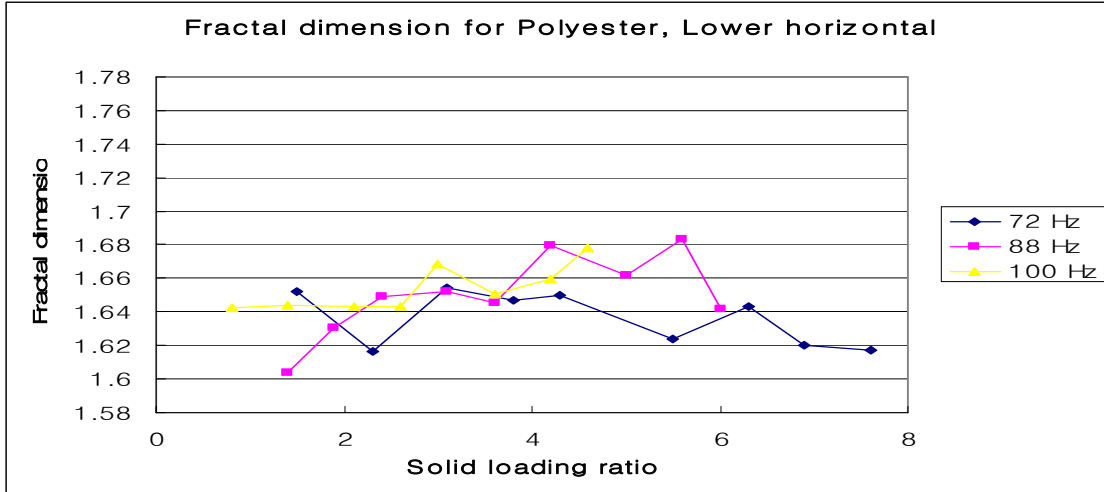


Figure 36 Fractal Dimension for different materials, and solid loading ratio measured in the lower horizontal section

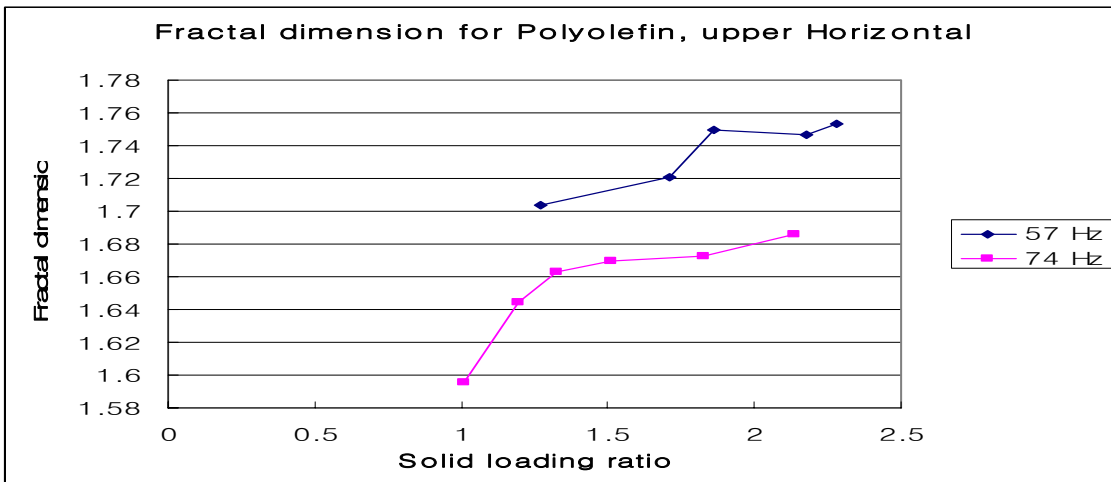
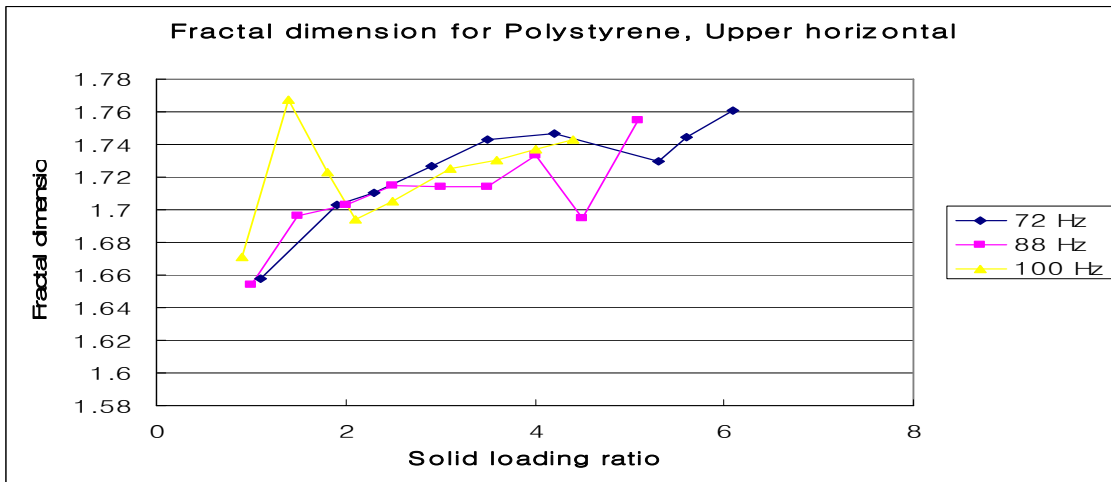
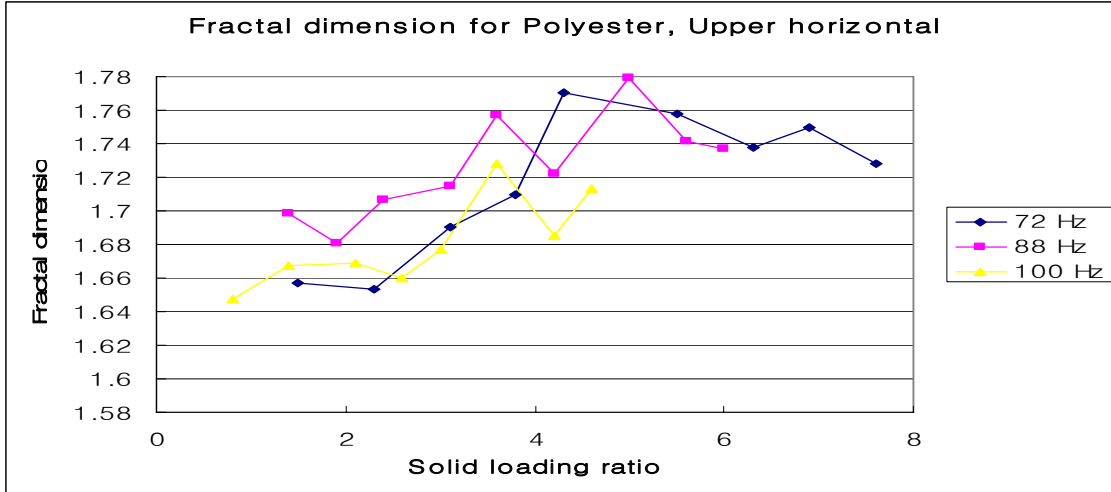


Figure 37 Fractal Dimension for different materials, and solid loading ratio measured in the upper horizontal section

4.5 WAVELET ANALYSIS

By using the wavelet toolbox in MATLAB, the original differential pressure signal has been decomposed into various components. As mentioned before, the Daubechies4 (db4) wavelet was used as the mother wavelet and the signal was decomposed to five scale levels. Other mother wavelets such as Haar (or db1) was evaluated as a mother wavelet for the initial exploration, and similar results were obtained. Figure 38 illustrates the signal decomposition signal.

The horizontal axis in Figure 38 shows the measuring time, which was 65.5 sec since the number of data points collected was 65536 with the sampling frequency of 1 kHz. The vertical axis represents the differential pressure. Graph show the original signal and the various decomposed components to a level of five.

The frequency range of each detailed signal was determined in the following manner. The sampling frequency for collecting data was 1 kHz, as mentioned before. This sampling frequency was more than enough to satisfy the Shannon sampling theorem. The maximum frequency of the data is below 500 Hz. If the maximum frequency of data is up to 500 Hz, then the detail component of the initially decomposed signal has frequency range from 250 Hz to 500 Hz, and the down sampling by a factor of two produces the frequency range of the detail component at level two with a range from 125 Hz to 250 Hz and so on.

The blower frequency for Figure 38 was 88 Hz, and the feeder frequency was approximately 2.1 Hz. In the decomposed signals, the approximation component scale at five (a_5) has similar frequency to the feeder frequency. This means that the a_5 signal contains the component due to the feeder which is dominant. More over, if the signal is further decomposed to more levels, the frequency range of the detail component at level nine (d_9) would be the same

as that of the feeder. This phenomenon can be seen if the signal in the graph is enlarged. Also, the frequency range of the detail component level three (d_3) coincides with that of the blower, which is 88 Hz.

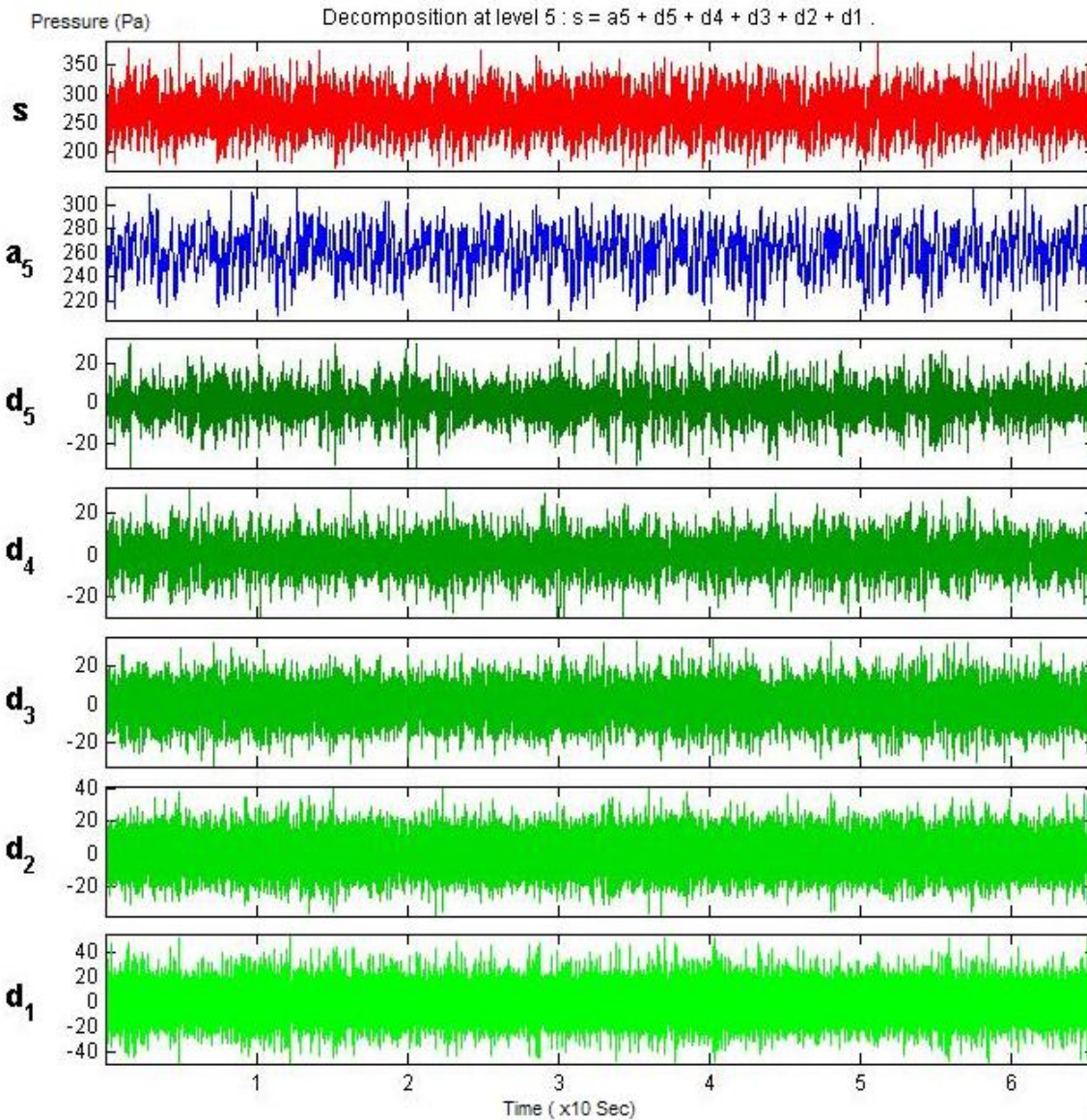


Figure 38 Decomposed signals, Polyester, blower = 88 Hz, $\mu = 6.0$, measured in the upper horizontal section

The detail component at scale level one (d_1), corresponding frequency range of 250 Hz – 500 Hz, seems to represent some of the turbulence signal. It should be noted that the magnitude of the power spectrum for this frequency range is small. The detail components at level two (d_2), four (d_4) and five (d_5) appear to be related to particle movement, and interaction of particles with the turbulence fluctuations. Further study may lead to identify the meaning of each individual detailed signal. One must note that the wavelet analysis is useful but will not produce miracles in understanding the signal components generated.

Figures 39 to 47 show the standard deviations of decomposed signals with different system configurations for different materials. The detailed signal varies when the solid loading ratio increases. When the plots are compared to the PSD figure, it was clearly seen that the magnitude of standard deviation of wavelet coefficients have a direct relationship with the magnitude of power peaks in the PSD graph. In other words, the magnitudes of power in the PSD graph increase or decrease (as the solid loading ratio varies), the standard deviations of the wavelet coefficient vary in the same manner. The wavelet coefficient represents how well the scaled and shifted wavelet matches with the original signal of a particular duration. For a higher standard deviation of the wavelet coefficients, one notes the larger fluctuations of the original signal.

From Figures 39, 40 and 41 one sees that the magnitude of the standard deviation of wavelet coefficients was the highest at the vertical section and the smallest at the upper horizontal section of the pipe. This indicates that the upper horizontal section of the pipe has the most stable flow and the vertical section has the most unstable flow. These results coincide with the results of the other methods of analysis. The signals decreased gradually at the upper horizontal section as the solid loading ratio was increased, but it increased at the lower horizontal

section and in the vertical section showed a mixed behavior. Thus it is conjectured that in the upper horizontal section, the air and particles are well mixed and have a stable flow pattern showing a damping of the variance as particle concentration, loading, increases. In the lower and vertical section, flow development and mixing is still going on with distance from the feeder, so one would expect more gas-particle interactions. The behavior of the standard deviation graph for polystyrene (see Figures 42, 43 and 44) was similar to that of the polyester.

Table 2 Characteristic of decomposed signal for polyester and polystyrene

Signal	Frequency range (Hz)	Represents for
d ₁	250 – 500	Gas turbulence
d ₂	125 - 250	Particle–gas interaction
d ₃	62.5 – 125	Blower
d ₄	31.3 - 62.5	Particle–gas interaction
d ₅	15.7 – 31.3	Particle–gas interaction
a ₅	0 – 15.7	Feeder

Note that in the vertical section, one can see clearly that as the solid loading ratio increases the detailed component at level two signal (d₂), with corresponding frequency range between 125 Hz to 250 Hz, decreases while the detailed component at level five (d₅), with corresponding frequency range of 15 Hz - 30 Hz increases. When the solid loading ratio is increased while the gas velocity is fixed, the individual gas particle interact more with the solid

particles causing momentum transferred from gas to solid. In other words, the gas will be damped while the solid particle movement will become more active (e.g. increased the rotational and translational velocities). Thus, this study conjectures that the detail component at level two (d_2) in the vertical section for polyester and polystyrene may represent the signal due to the air while the detail signal at level five (d_5) may be the one due to the particle movement.

The behavior of polyolefin was different from the other polymer particles studied. See the fast video section. In the lower horizontal section, detail signal at level four (d_4) increases slightly as the solid loading ratio increases while detailed signal at level five (d_5) slightly decreases. In the upper horizontal section, all detailed signals have a slightly decreasing behavior as the solid loading ratio increased. Compared to the other polymers, for both lower and upper horizontal section it is hard to tell if the detail signals are related to the gas particle interaction due to the small increasing solid concentration. It should be noted the range of loading for this polymer is narrow due to the limited feed rates because of operational difficulties. One can see that the detailed signals did not disperse as much in comparison to that of the other polymers. Thus in the lower and upper horizontal section for this polymer, the signal has small fluctuations.

Even though the fast video showed that the polyolefin particles have more random motion, the overall effect appears to be one of providing a more well mixed condition with pressure fluctuation damping.

When the blower rotational frequency was 57 Hz, it was found that the detail signal at level four (d_4) was due to the blower frequency, while for the case of blower rotational frequency of 74 Hz, the detail at level three signal (d_3) was related to the signal due to the blower.

In the vertical section, the detail signals at levels two (d_2) and level three (d_3) or level four (d_4) have different values, but the trend of the plots look similar showing gradually decreasing signals, when the solid loading ratio increases. This phenomenon was observed for both blower rotational frequencies, 57 Hz and 74 Hz. Also, the detail signal at level five (d_5) increases when the solid loading ratio increases. Similar to the other materials, it is conjectured that detail level two (d_2) and three (d_3) for polyolefin at the vertical section is related to gas behavior while detail level five signal (d_5) is related to the particle-gas interaction. Overall, one notes that the vertical section showed larger standard deviations than the horizontal section results.

Table 3. Characteristic of decomposed signal for polyolefin

Signal	Frequency range (Hz)	Represents for
d_1	250 – 500	Gas turbulence
d_2	125 - 250	Particle–gas interaction
d_3	62.5 – 125	Particle–gas interaction (for blower = 57 Hz) Blower (for blower = 74Hz)
d_4	31.3 - 62.5	Blower (for blower = 57Hz) Particle–gas interaction (for blower = 74Hz)
d_5	15.7 – 31.3	Particle–gas interaction
a_5	7.8 – 15.7	Feeder

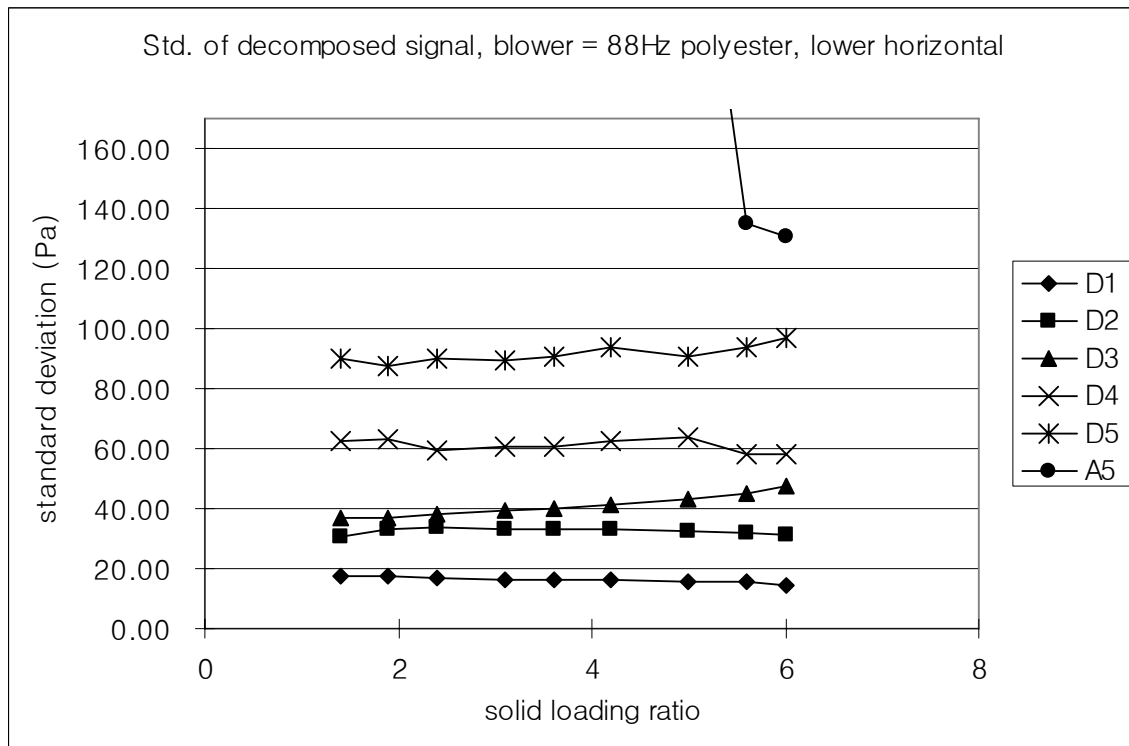
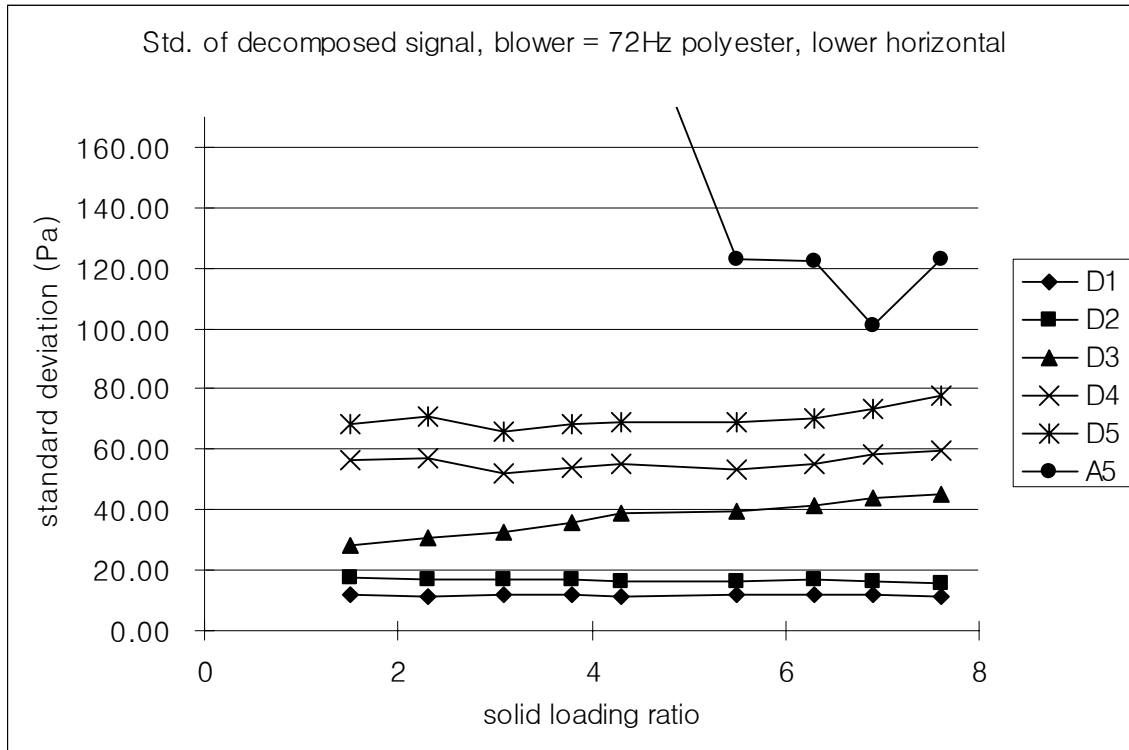


Figure 39 Standard deviation of wavelet coefficient of each decomposed signals, polyester, lower horizontal section, blower = 72 Hz (top), 88 Hz (bottom)

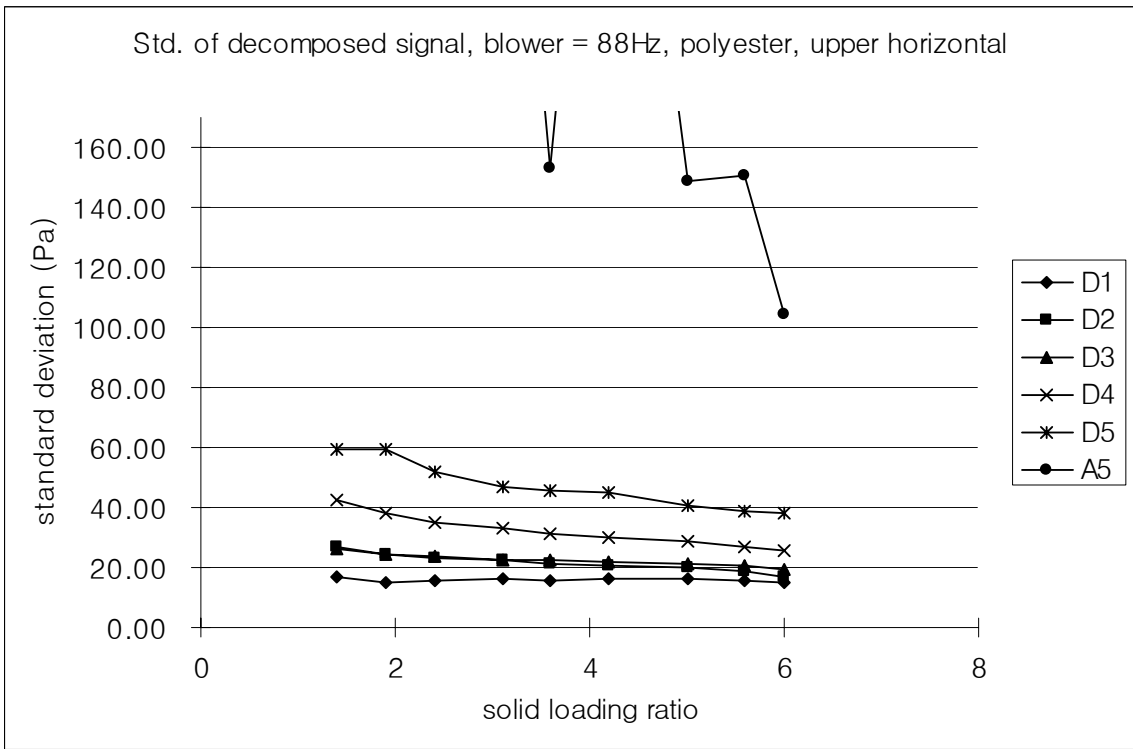
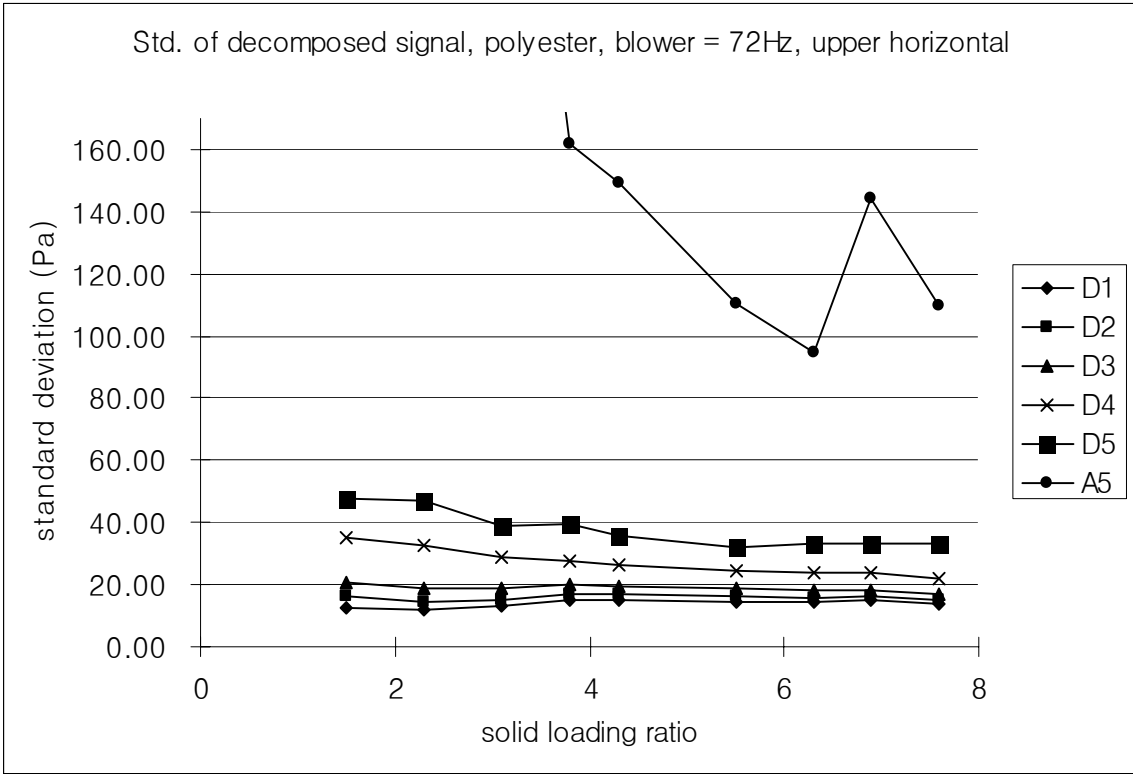


Figure 40 Standard deviation of wavelet coefficient of each decomposed signals, polyester, upper horizontal section, blower = 72 Hz (top), 88 Hz (bottom)

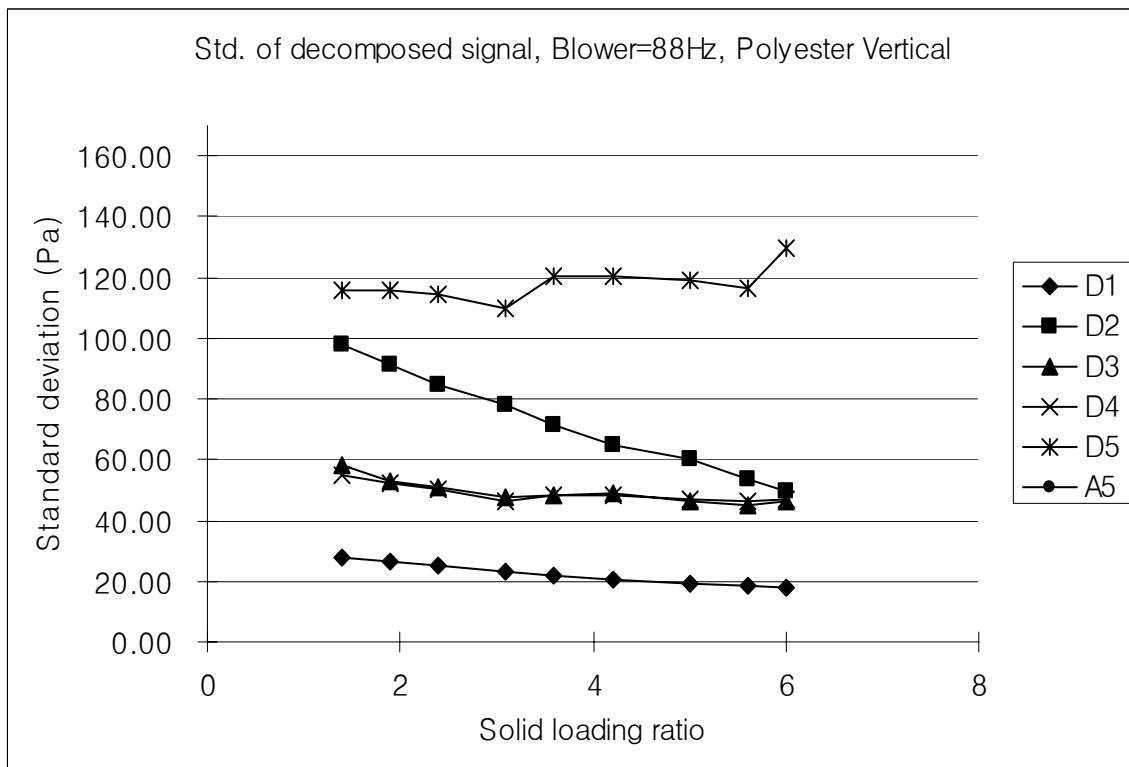
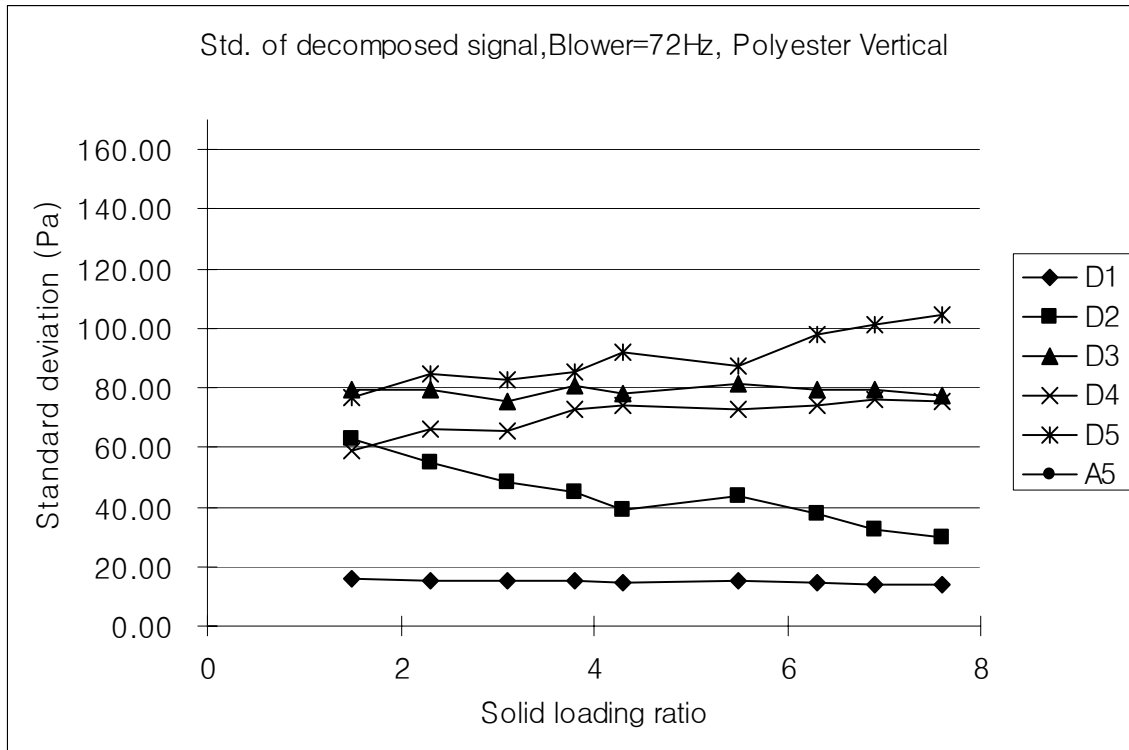


Figure 41 Standard deviation of wavelet coefficient of each decomposed signals, polyester, vertical section, blower = 72 Hz (top), 88 Hz (bottom)

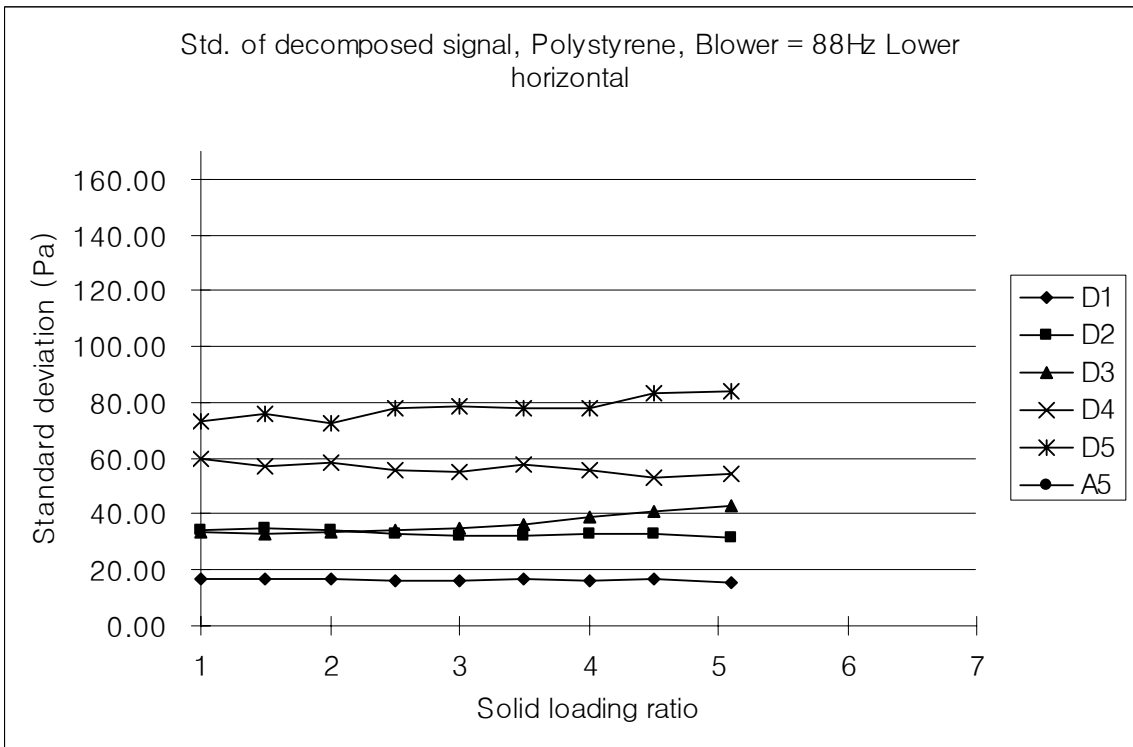
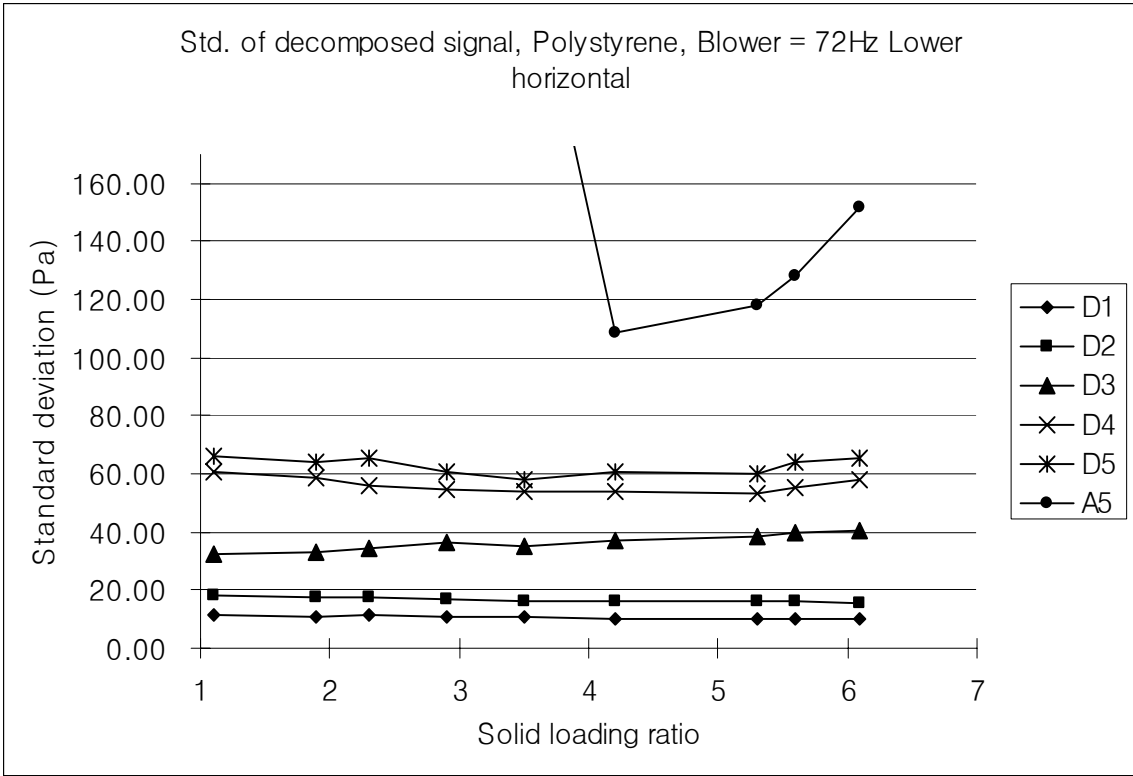


Figure 42 Standard deviation of wavelet coefficient of each decomposed signals, polystyrene, lower horizontal section, blower = 77 Hz (top), 88 Hz (bottom)

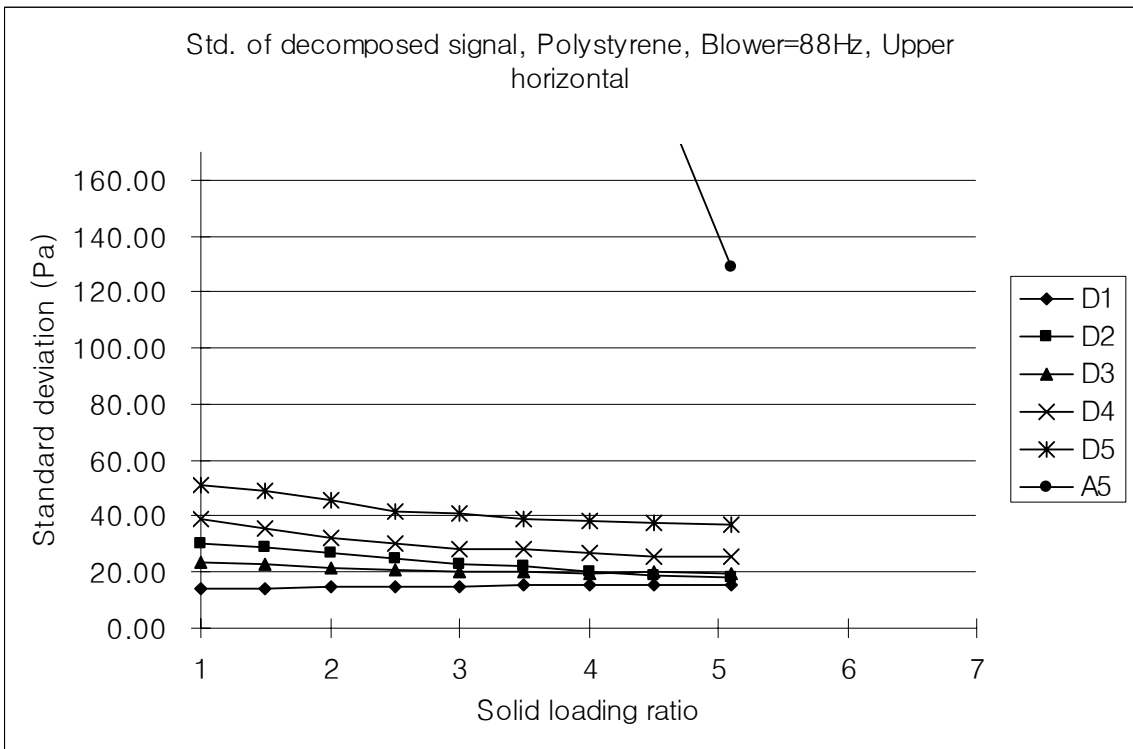
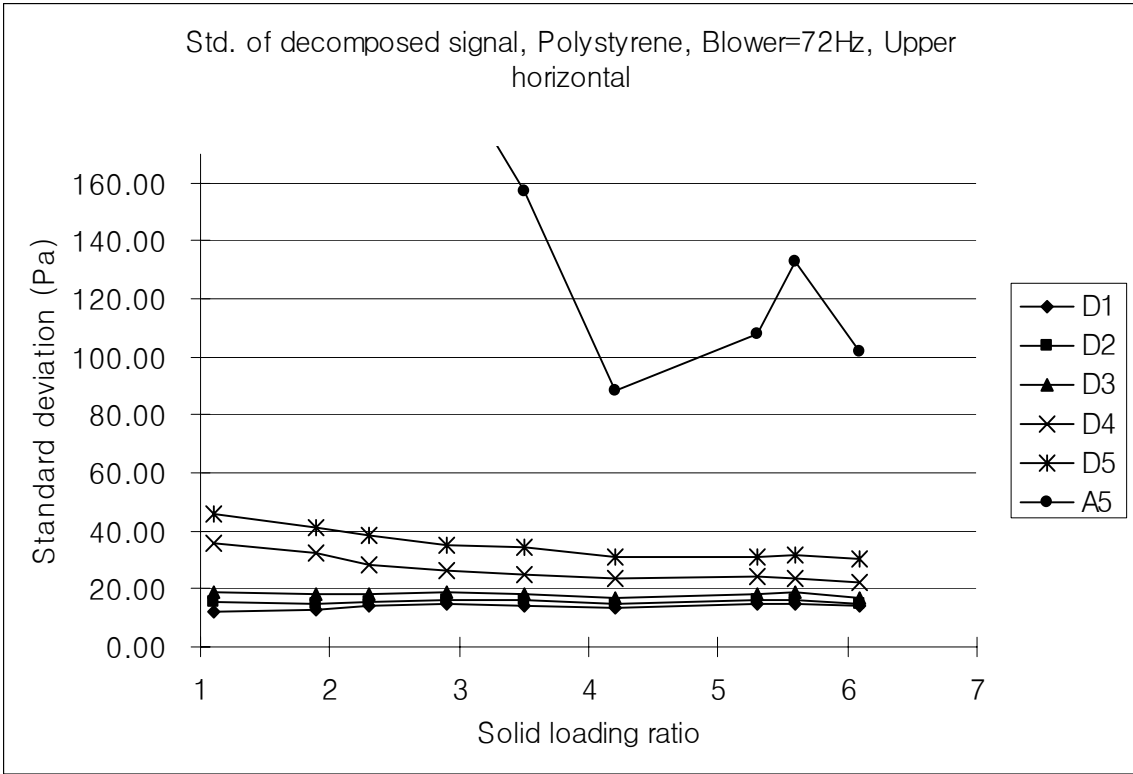


Figure 43 Standard deviation of wavelet coefficient of each decomposed signals, polystyrene, upper horizontal section, blower = 77 Hz (top), 88 Hz (bottom)

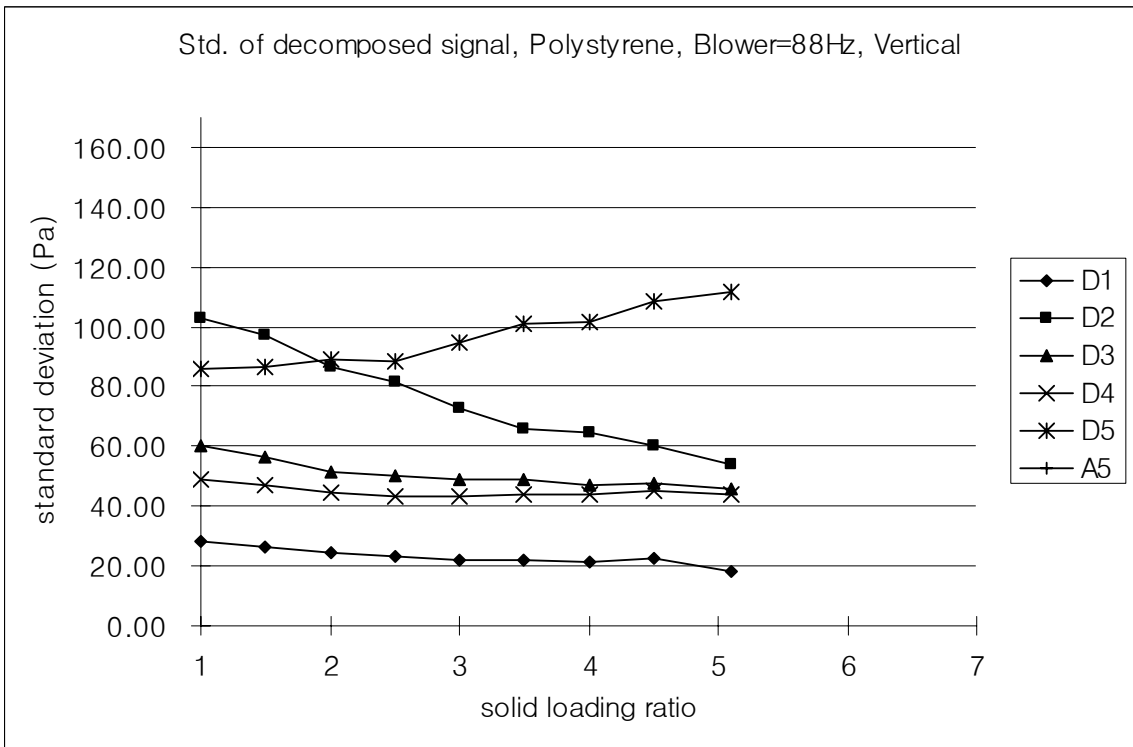
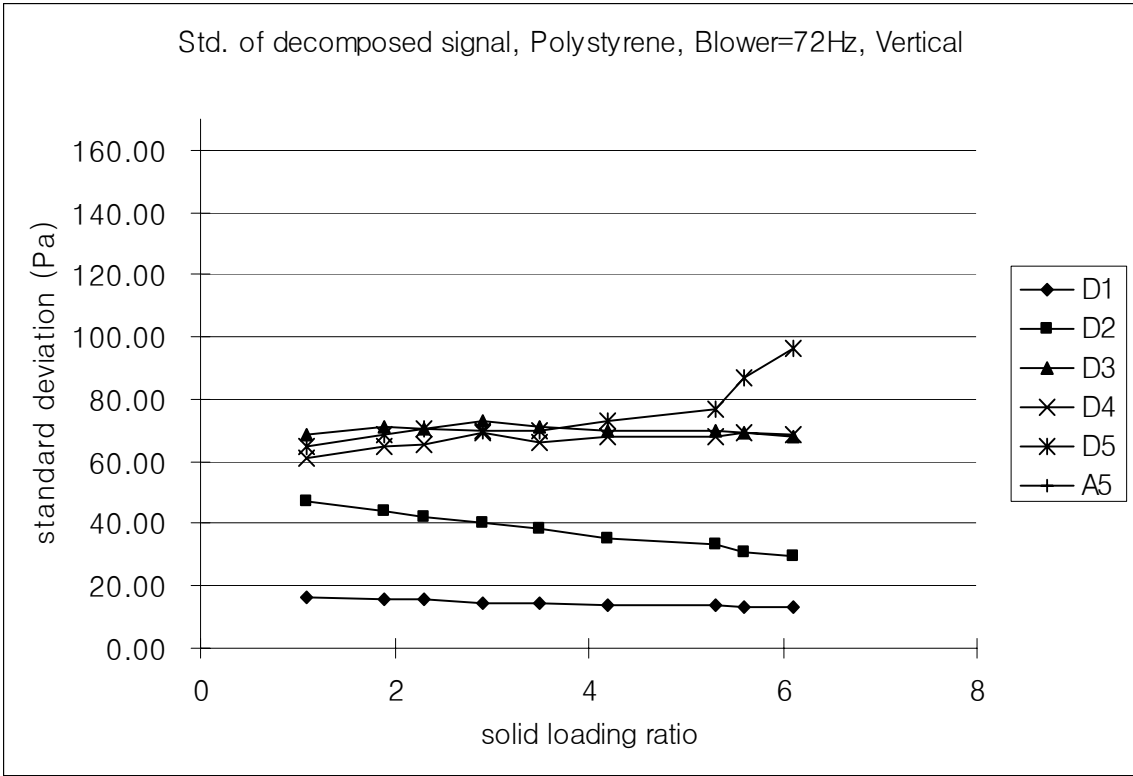


Figure 44 Standard deviation of wavelet coefficient of each decomposed signals, polystyrene, vertical section, blower = 77 Hz (top), 88 Hz (bottom)

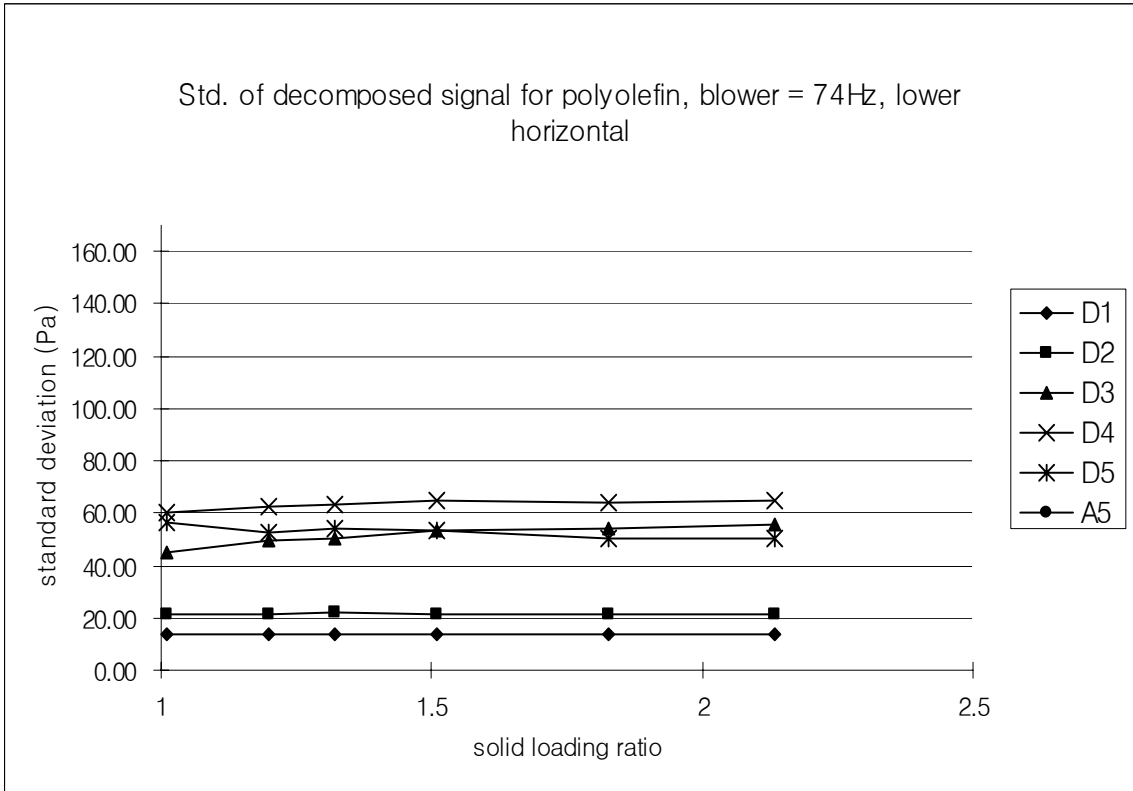
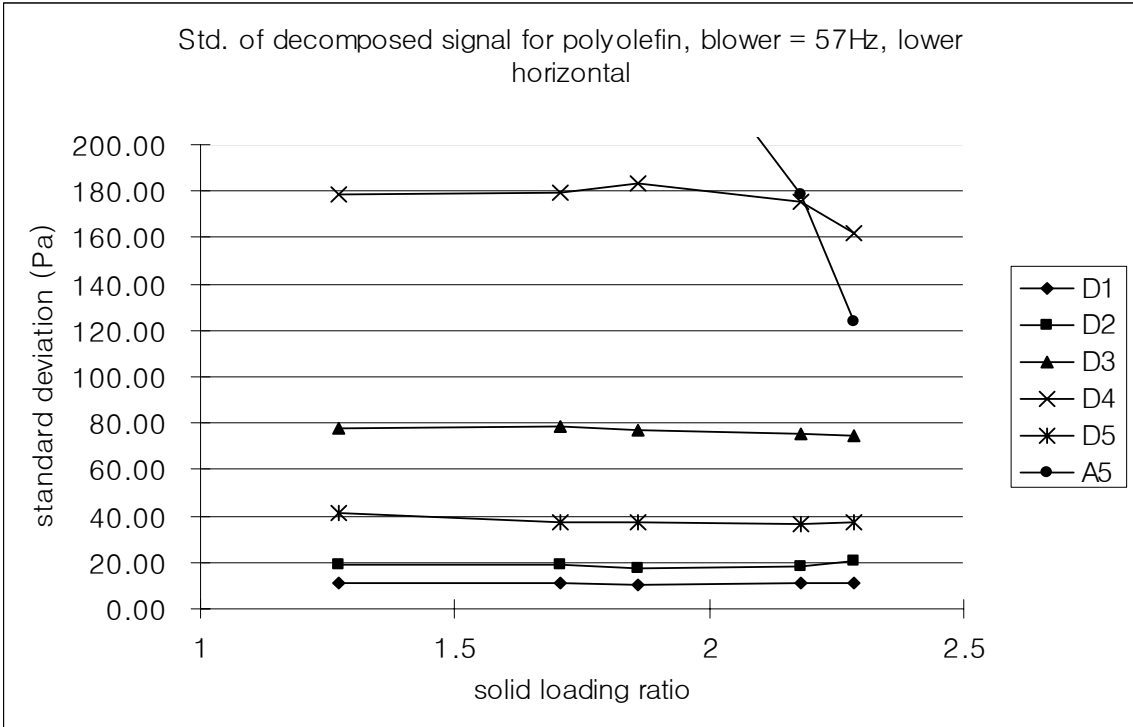


Figure 45 Standard deviation of wavelet coefficient of each decomposed signals, polyolefin, lower horizontal section, blower = 57 Hz (top), 74 Hz (bottom)

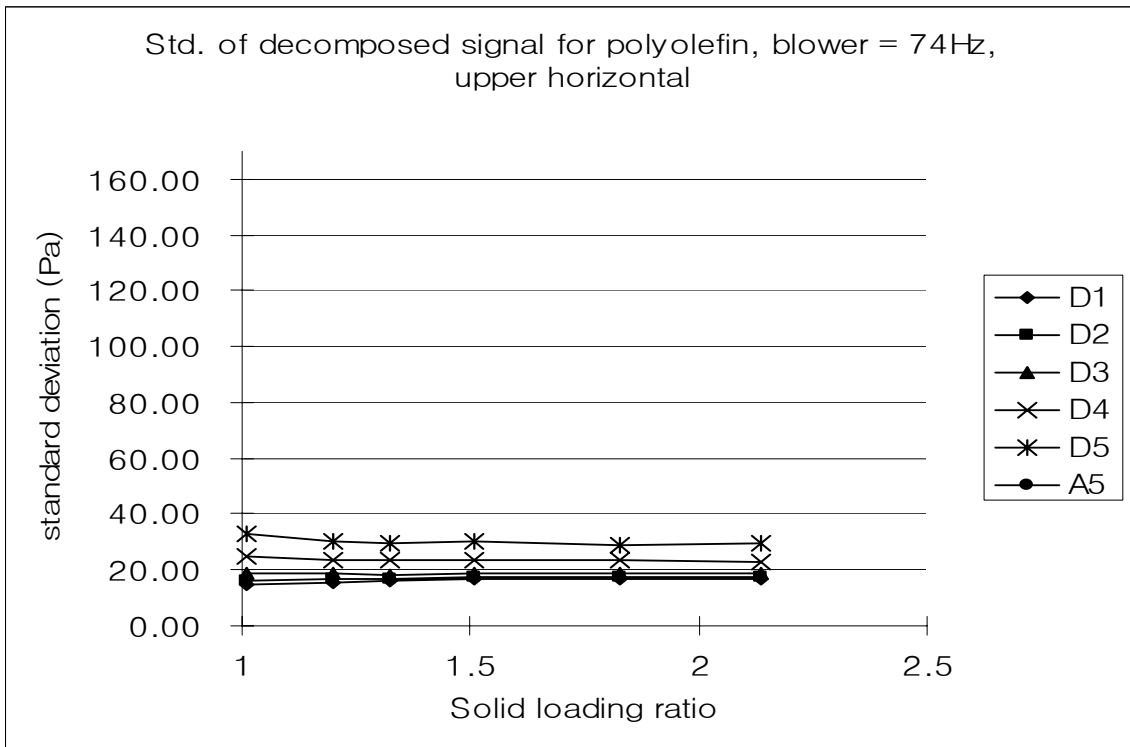
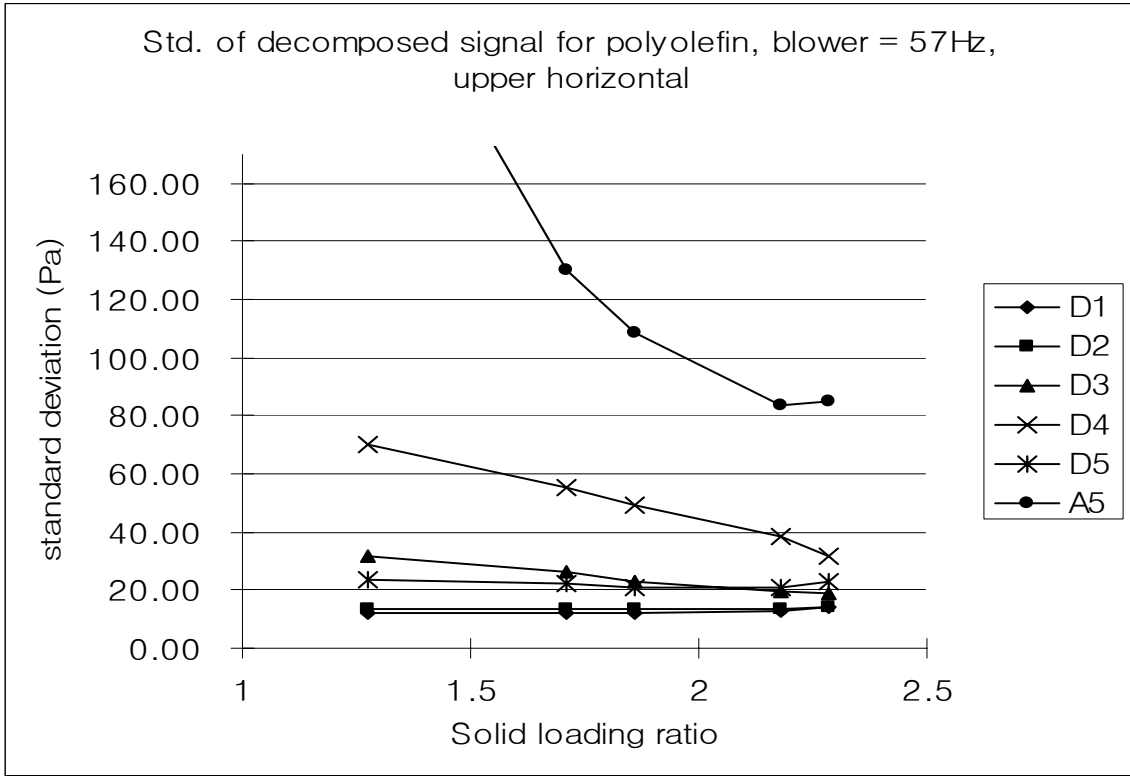


Figure 46 Standard deviation of wavelet coefficient of each decomposed signals, polyolefin, upper horizontal section, blower = 57 Hz (top), 74 Hz (bottom)

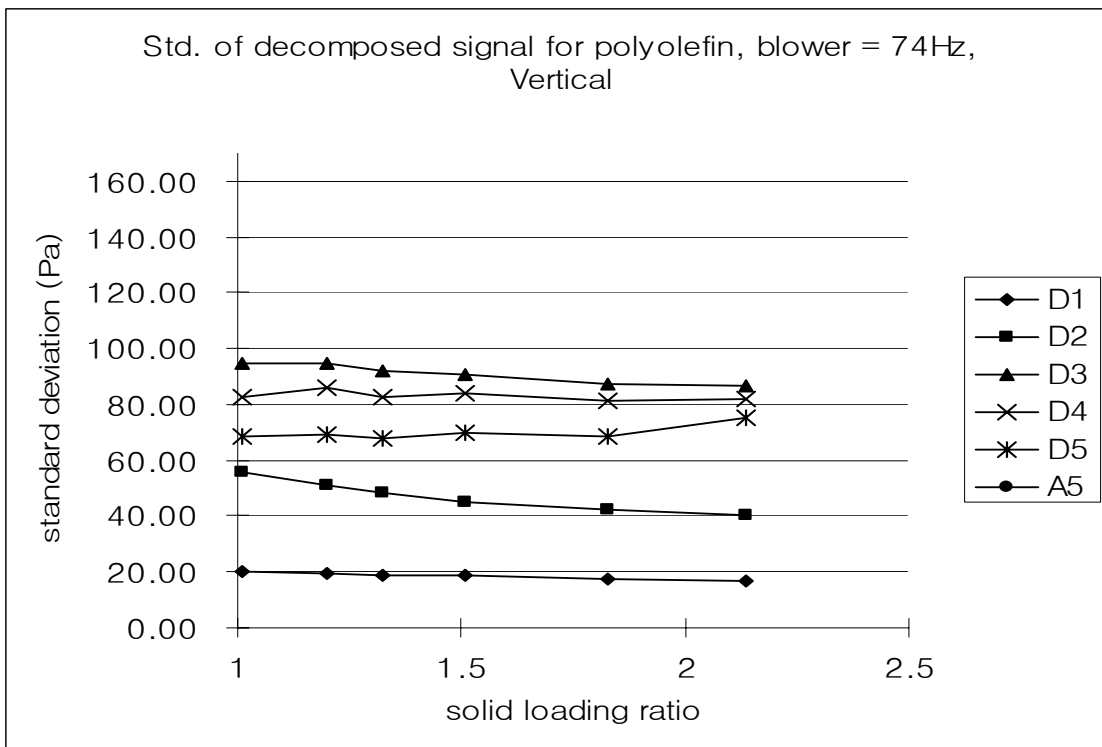
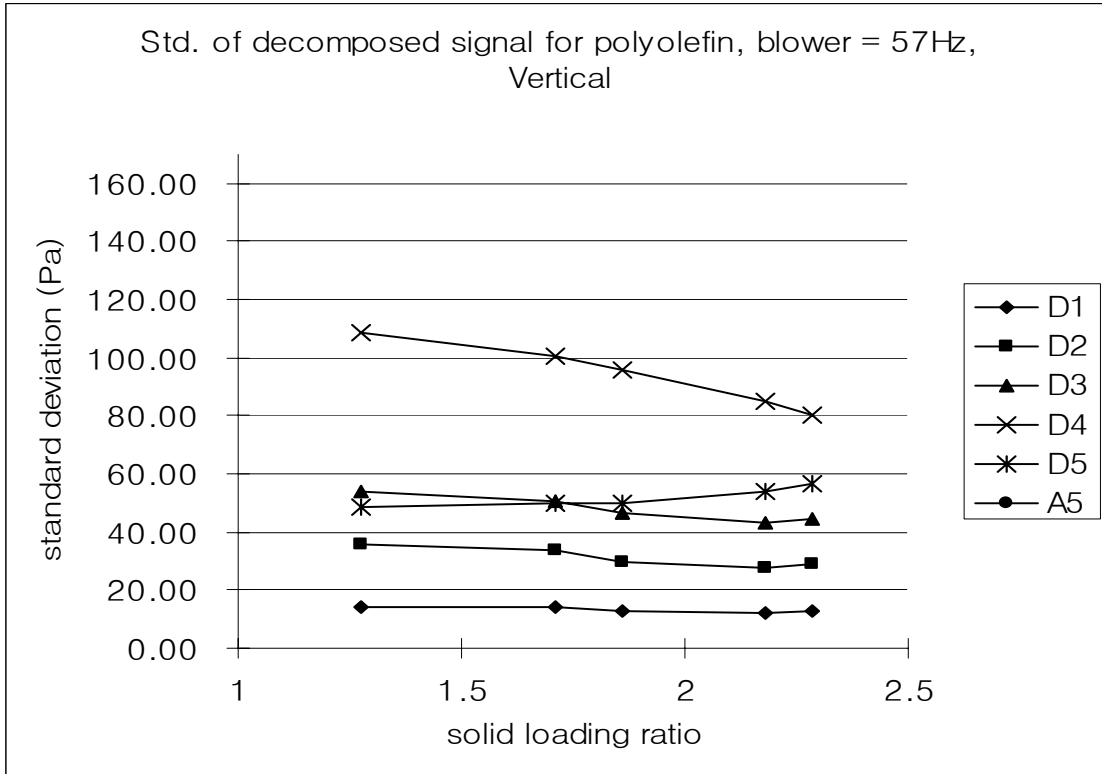


Figure 47 Standard deviation of wavelet coefficient of each decomposed signals, polyolefin, vertical section, Blower = 57 Hz (top), 74 Hz (bottom)

4.6 HIGH SPEED VIDEO OBSERVATION

High speed videos of the flow of polyester and polyolefin transported by air have been taken at the lower horizontal section of the pipe using the Phantom V3.0 High Speed Camera manufactured by Vision Research, Inc. The video has been taken with the speed of 1500 picture per second (PPS) for about 10 second. Larger time intervals were not possible because of storage capacity. The DVD-rom attached to this dissertation contains the video files for both polymer. Figure 48, and 49 illustrate the particle movement for polyester and polyolefin respectively.

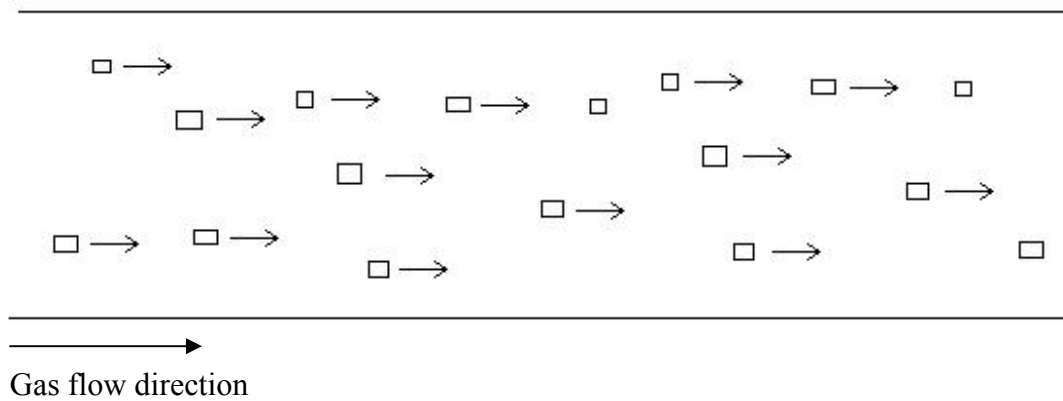


Figure 48 Particle movement behavior, polyester

The polyester, which has higher density, hard surface, and cubical shape moves in a straight manner forward along the flow direction. Rotation and spin were difficult to ascertain from the video. For the case of the polyolefin a different picture was observed.

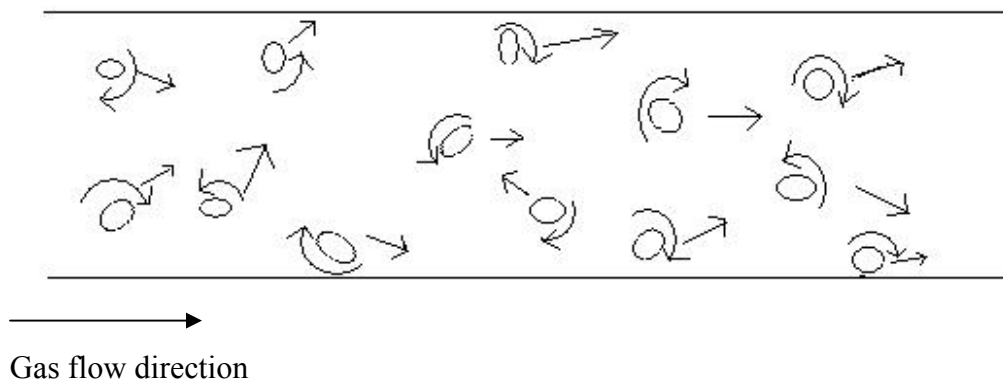


Figure 49 Particle movement behavior, polyolefin

The polyolefin has a low density, is soft (sticky) in nature and is ellipsoid shaped. The polyolefin particles move with considerable rotation and spin. Sometimes, particles were bouncing counter to the gas flow direction. In Figure 49, the straight arrow represents the particle's translational direction and curved arrow represents the particle's rotational direction. As noted, some of the particles even bounce in the adverse direction to the main flow direction. The soft surface appears to be the cause of this unique behavior.

5.0 CONCLUSION

The flow characteristics for different system configurations, materials, and measuring locations have been investigated by different methods of signal analysis. Each of the methods of signal analysis was aimed to help understand the flow characteristics and conditions.

The phase space diagram for the gas flow can exhibit one or two attractor points with a low degree of eccentricity, two attractor points are seen with a high degree of eccentricity. The area of this phase space increases as the velocity of the air increases. The area was generally seen to decrease when the solid loading ratio increases. No clear pattern for this rule could be established other than the high degree of eccentricity when solids are flowing. The fractal dimension analysis with the box counting method has been applied to find a fractal pattern. This pattern appears do not follow the Hurst's exponents but seems to provide a measure of the flow stability.

The result of the power spectrum analysis enables one to find true signal which is the signal due to the flow noise as well as the signal due to the blower and feeder. The magnitude of the power is seen to increase when the velocity of the air increases. In addition, the power decreases when the solid loading ratio increases since the air flow fluctuations appear to be damped by presence of particles. For the same system configuration, the largest power was observed in the vertical section followed by the lower horizontal section. The smallest power peaks were observed for the upper horizontal pipe. This behavior can be attributed to the flow

stability in these configurations. For similar conditions (air velocity and solid loading ratio), the result of power spectral density was similar for the polyester and polystyrene pellets.

The Hurst's exponents from the rescaled range analysis were closely related to flow patterns present. The Hurst exponent has an anti-persistence behavior ($H < 0.5$) for gas flow only, while when the solids are being transported, the exponent became more persistent in behavior ($H > 0.5$). When the flow pattern was homogeneous dominant, the Hurst's exponents increased as the solid loading ratio increased. For pulsating dominant flow pattern, the Hurst's exponents decreased as the solid loading ratio increased.

By applying wavelet analysis, the original differential pressure signal has been decomposed and the signal due to the blower, feeder and the noise signal can be easily detected. Some of decomposed signal contains important information due to the gas, the particles, and the interaction between the gas and particles. It is conjectured that the standard deviation of wavelet coefficient decreases as the solid loading ratio increases. This behavior may indicate that the signal is related to the gas fluctuations while the increasing standard deviation of wavelet coefficient graph may represent the solid particle interactions. The polyester and polystyrene polymer particles behaved in like this manner while the polyolefin showed considerable random particle behavior after viewing the details of the high speed video recording. The wavelet analysis of the polyolefin showed a more well mixed particle-gas interaction behavior.

6.0 FUTURE WORK

So far, the differential pressure for the dilute phase pneumatic conveying has been analyzed and there are many unknown factors that one would like to know in this field of study. Some of these factors for future work are suggested as follows:

One may obtain interesting results by plotting non-dimensional numbers such as the Reynolds number and Froude number for the various conditions studied. The Reynolds number represents that the ratio of inertial force to the viscous force while the Froude number represents that the ratio of inertial force to the gravitational force. Thus when analyzing the differential pressure data by different methods, instead of using the velocity of the air or solid loading ratio as a changing parameter using these non-dimensionless numbers for the flow conditions may give further insight to the process..

To develop the fractal dimension analysis, it would be useful to de-noise signal before plotting the phase space diagram since it is difficult to determine the correct fractal dimension when noise exists.

For the wavelet transform analysis, among the decomposed signal, only a few signals due to the blower and feeder were identified clearly. Each of the rest of detailed signal is related to gas, gas – particle, and particle - particle interaction, but could not be identified directly. By taking high speed video camera clips one may determine these other interactions.

The number of particles that have been transported were large, thus it was difficult to analyze the individual particle's behavior by numerical method, because the calculation time would be too long. It would be worthwhile to try to simulate this pneumatic conveying system with a small number of particles and compare the result with the experimental findings.

BIBLIOGRAPHY

1. G. E. Klinzing, R. D. Marcus, F. Rizk, and L. S. Leung, Pneumatic conveying of solids, a theoretical and practical approach. 2nd ed. New York: Chapman & Hall, 1997. pp. 2,8.
2. Tim Singer, “You too, can select a pneumatic conveying system”
<http://www.powderandbulk.com/pb_services/ask_joe_archive/select_pneumatic_conveying_system.htm> (4 December 2006)
3. F. J. Cabrejos. Experimental investigation on the fully developed pipe flow of dilute gas – solids suspensions. Pittsburgh: University of Pittsburgh press, 1994. pp 157-208, 210.
4. S. V. Dhodapkar and George E. Klinzing. “Pressure fluctuation in pneumatic conveying systems powder technology.” Vol 74 (1993): pp. 179-195.
5. unknown author. “Hurst and Rescaled Range Analysis”,
<<http://www.xplore-stat.de/tutorials/xfghtmlnode99.html>> (25 April 2006)
6. Vikram K. Yeragani, K. Srinivasan, S. Vempati, R. Pohl and R. Balon. “Fractal dimension of heart rate time series: an effective measure of automic function, Journal of applied Physiology.” Vol 75, No. 6 (1993): pp. 2429-2438.
7. Francisco J. Cabrejos, and George E. Klinzing. “Characterization of dilute gas-solids flows using the rescaled range analysis. Powder technology” Vol 84 (1995), pp. 139-156.
8. Jinqiang Ren, Qiming Mao, Jinghai Li, and Weigang Lin., “Wavelet analysis of dynamic behavior in fluidized beds, Chemical Engineering Science” Vol. 56, (2001), pp. 981-988.
9. Xuesong Lu, and Hongzhong Li., “Wavelet analysis of pressure fluctuation signals in a bubbling fluidized bed, Chemical Engineering Journal” Vol. 75, (1999), pp. 113-119
10. “ACFM Vs. SCFM Vs ICFM, Series of white technical papers from Squire-cogswell”
<<http://www.ohiomedical.com/pdfs/11-icfm.pdf>> (4 December 2006)
11. Robert W. Fox. and Alan T. McDonald. Introduction to fluid mechanics. 6th ed. New York: John Wiley & Sons, Inc.,2003. pp. 239-240.

12. D. Geldart, "Types of gas fluidization, Powder technology" Vol. 7, (1973), pp. 285-292.
13. Martin Rodes, "Fluidization of particles by fluids" 2001
<<http://www.erpt.org/012Q/rhod-04.htm>> (4 December 2006)
14. George G. Chase, "Class note of solid."
<<http://www.engineering.uakron.edu/~chem/fclty/chase/Solids/SolidsNotes5%20Fluidization.pdf>> (4 December 2006)
15. Luis Gabino Sanchez Varela. Characterization of bulk solid for dense phase pneumatic conveying, Pittsburgh:University of Pittsburgh press, 1998. pp. 184-185.
16. Shrikant V. Dhodapkar. Flow pattern classification in gas-solid suspension, Pittsburgh: University of Pittsburgh press, 1991. pp. 43.
17. Wikipedia, The free encyclopedia. "Phase space" October 2006,
<http://en.wikipedia.org/wiki/Phase_space> (4 December 2006)
18. Unknown author, "Glossary of terms used in time series analysis of cardiovascular"
<<http://www.cbi.dongnocchi.it/glossary/PowerSpectralDensity.html>>
(4 December 2006)
19. Khan, Ashfaq, Digital signal processing fundamentals, Da Vinch Engineering Press, 2005, pp. 69-100.
20. P. Vanouplines "Rescaled range analysis and the fractal dimension of pi"
19 November 1995, University Library, Free University Brussels,
<<http://ftp.vub.ac.be/~pvouplin/pi/rswhat.htm>> (4 December 2006)
21. Alexandros Leontitsis "rsana.m"
<<http://www.mathworks.com/matlabcentral/fileexchange/loadFile.do?objectId=4325&objectType=file>> (4 December 2006)
22. C. Sidney Burrus, Ramesh A. Gopinath, and Haitao Guo, Introduction to wavelets and wavelet transforms, A primer, New Jersey: Prantice hall, pp. 1.
23. Wikipedia the Free Encyclopedia, "Fast wavelet transform" 16 November 2006
<http://en.wikipedia.org/wiki/Fast_wavelet_transform> (4 December 2006)